Novel mathematical model for laser speckle contrast: effect of temporal and spatial correlation in speckle contrast

por el

M. en C. Julio César Juárez Ramírez

Tesis sometida como requisito parcial para obtener el grado de

DOCTORADO EN CIENCIAS EN LA ESPECIALIDAD DE ÓPTICA

en el

Instituto Nacional de Astrofísica, Óptica y Electrónica

Supervisada por:
Dr. Julio César Ramírez San Juan
INAOE

Febrero 2024
Tonantzintla, Puebla

Acknowledgments

Quiero agradecer a mis papás por la educación y los valores que me inculcaron. Su apoyo, orientación y consejos me han guiado desde niño.

Quiero agradecer a mi esposa por todo su apoyo e ideas durante todo este tiempo.

A mi hija por motivarme y resolver misterios juntos.

A mis hermanos, a mi familia, a mi asesor y a mis maestros.

Sinceramente, gracias. Nunca estuve solo, todos colaboraron.

Resumen

En este trabajo, se estudia el patrón de moteado generado por una fuente de luz coherente, más conocido como *speckle*. Este patrón de interferencia es aleatorio y se produce debido a la interacción de la luz con superficies que presentan rugosidades de un tamaño similar al de la longitud de onda.

El patrón de speckle contiene información sobre la luz y el objeto que lo genera, mostrando una alta sensibilidad a cambios pequeños. En el caso de que el objeto que genere el patrón de speckle tenga algún tipo de dinámica, esta se reflejará en el propio patrón de speckle. Por lo tanto, al estudiar el movimiento del patrón de speckle, es posible inferir el movimiento en la superficie o el interior de la muestra.

Existen varías técnicas para realizar este análisis, una de ellas es la formación de imágenes de contraste de speckle laser, (en inglés, *laser speckle contrast imaging*). El cual tiene aplicaciones en múltiples áreas de la ingeniería y la medicina como, por ejemplo; oftalmología, neurología, dermatología, entre otros. Por lo que un modelo matemático confiable capaz de describir correctamente las mediciones experimentales es muy necesario.

La teoría fue desarrollada por Fercher y Briers, en el año de 1981 y desde entonces el modelo matemático se ha ido mejorando, para una descripción cada vez más exacta de las mediciones experimentales. Los modelos matemáticos actuales funcionan muy bien al momento de describir el contraste para dinámicas rápidas, por ejemplo, la dinámica del flujo sanguíneo. Sin embargo, hay una gran discrepancia al momento de medir dinámicas lentas, como podría ser el crecimiento de bacterias, hongos, semillas o el cambio estructural de diversos objetos, como la oxidación o degradación de alimentos, el secado de pintura entre otras.

En este trabajo se desarrolla un nuevo modelo matemático para el contraste de speckle considerando tanto el formalismo espacial como el temporal que sea aplicable tanto a dinámicas lentas como rápidas.

Para ello, se considera la correlación de los datos vecinos, pixeles adyacentes en el formalismo espacial, e imágenes adyacentes para el formalismo temporal.

Nuestra propuesta tanto para el régimen espacial como para el temporal coincide con los modelos matemáticos previos para dinámicas rápidas y además se ajusta muy bien a datos experimentales y simulados para dinámicas lentas, obteniendo así un modelo más robusto, aplicable tanto para dinámicas lentas como rápidas.

Summary

In this work, speckle patterns generated by coherent light are studied, commonly known as speckle, which is used in laser speckle contrast imaging with multiple application areas of engineering and medicine, for instance, ophthalmology, neurology, dermatology, among others. Therefore, a trustworthy mathematical model capable of describing the experimental measurements correctly is of vital importance.

Fercher and Briers developed the theory in 1981. Since then, the mathematical model has been continuously improved to provide an increasingly accurate description of experimental measurements. The current mathematical models work well in describing fast dynamics, such as blood flow dynamics. However, there is a discrepancy with the experimental data when describing slow dynamics, such as bacteria or fungus colony growth, seed growth, or structural changes like oxidation or degradation of food, paint drying, among others.

In this work a novel mathematical model is developed for speckle contrast, both temporal and spatial contrast applicable to slow as well fast dynamics.

To achieve this, we consider correlations between neighboring data, using adjacent pixels for spatial contrast and adjacent frames for temporal contrast.

Our proposal for temporal and spatial contrast match with the current mathematical models for fast dynamics. Furthermore, our proposal fits experimental and simulated data as well for slow dynamics getting a more robust model applicable both slow and fast dynamics.

Index

Speckle pattern and its properties

Interference pattern:

Speckle pattern is an interference phenomenon consisting of a set of bright and dark grains, resembling salt-and-pepper noise, commonly known simply as speckle. It occurs when light interacts with any kind of material that has wavelength-sized roughness, such as walls, sheets of paper, skin, leaves, optical diffusers, etc.

When light illuminates matter, photons interact with the molecules, and during each interaction, a fraction of light is absorbed, while another fraction of light is reflected in almost random direction. The number of interactions depends on the density and thickness of the material, as well as the energy of the light source. Some photons may undergo hundreds of interactions with various molecules in the material before being either absorbed or exiting the medium through reflection or transmission. Each interaction acts as if it were a distinct light source with different intensity (amplitude) and phase. The interference of all these virtual light sources generates a complex interference pattern composed of bright and dark grains, known as the speckle pattern.

In Figure 1, a schematic representation of the interaction between light and matter is shown. A ray of light is represented by a large gray arrow which is illuminating a sample of the material. Different photons took different paths, depicted in different colors for simplicity of tracking, although there is no consideration of a change in the wavelength (color) of the photons in this representation.

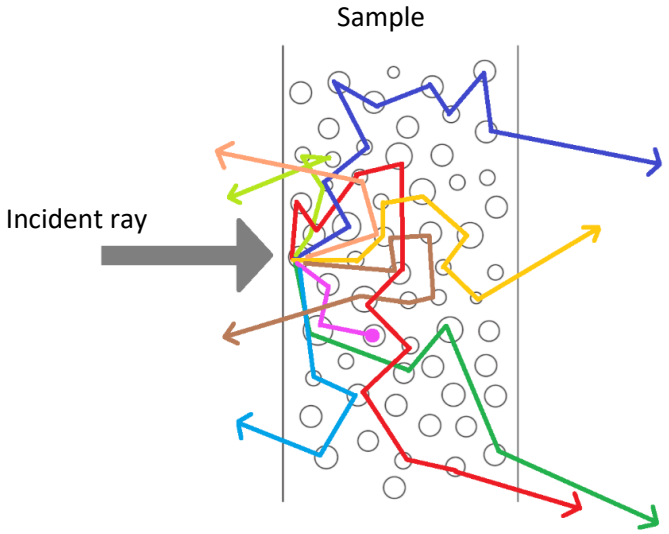

Figure 1. A schematic representation of light interacting with molecules in a scattering medium.

Light interacting with the sample may be reflected within the sample in any direction. A fraction of the light will pass through (represented by blue, yellow, dark green and red rays on Figure 1) generating the speckle pattern on *transmission*. Another fraction of the light will be absorbed (indicated by pink ray on Figure 1) and a fraction of the light will be reflected back (indicated by coral, light green, brown and cyan rays on Figure 1) generating the speckle pattern on reflection.

Considering that the transmission pattern is the light that passes through and the reflection pattern is the light that reflect back, it is easy to think that the transmission is the negative picture of the transmission, in other words, the grains that are bright in transmission are dark in reflection and vice versa. However, this is not the case. The transmission and reflection pattern does not depend on each other but rather on the interaction with the sample. Hence, both patterns contain information about the sample, as well as fringes in Young's interferometer provide information about the slits. The speckle pattern carries details about the sample's density, internal structure, speed of particles within the sample, and other physical properties. However, measuring any of these properties is challenging because the speckle pattern is far more complex than Young's or Michelson's patterns.

A good analogy is to consider a still body of water, such as a pool or lake. When an object, like a rock, is dropped into the water, it generates concentric circular waves. If two identical rocks are dropped into the water, two sets of concentric circular waves are generated, one for each rock. Eventually, these waves meet and interfere with each other, creating taller and deeper waves when combined. In other words, the waves are interfering. *Constructive interference* occurs when the amplitude (the height or depth) of the combined waves is greater than that of the individual waves. *Destructive interference*, on the other hand, happens when the amplitude of the combined waves is smaller than that of the individual waves. If three rocks are dropped on the water, three sets of waves are generated, interfering with each other and creating a more complex interference pattern. However, it is still possible to follow the trace of the waves and predict their behavior. If ten rocks are dropped on the water, the interference pattern becomes much more complex, and it becomes harder to follow the trace of the wave or predict their behavior. Now, let us imagine hundreds or thousands of rocks with different sizes and shapes being dropped at different times. The interference pattern becomes so much more complex that it is almost impossible to follow or predict the behavior of the waves generated by each rock. The interference pattern will rapidly change, exhibiting an almost random distribution of peaks and valleys, where no apparent order can be seen. This interference pattern is equivalent to a speckle pattern. The rocks, in this analogy, represent the interactions between a molecule and a photon, wherein the photons are reflected with different amplitude and phase, ultimately generating the speckle pattern.

In Figure 2 shows an experimental speckle pattern. The pattern was captured by a grayscale camera and is presented in false color to resemble speckle generated with red (laser) light.

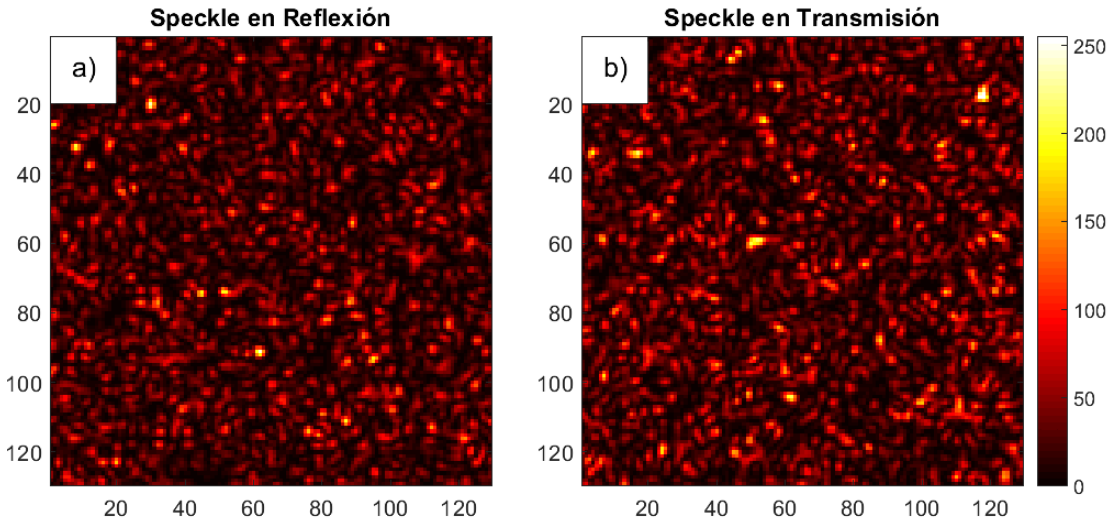

Figure 2. a) Speckle pattern on reflection and b) on transmission of a skin phantom.

Figure 2 may remind the static presented on old TV´s, which is also an interference pattern. Speckle pattern may be observed in various image system, such as satellite radar image [1, 2], holography [3, 4], microscopy image [5, 6, 7], astronomy image [8, 9, 10], ultrasound image [11, 12] (see Figure 3), among others.

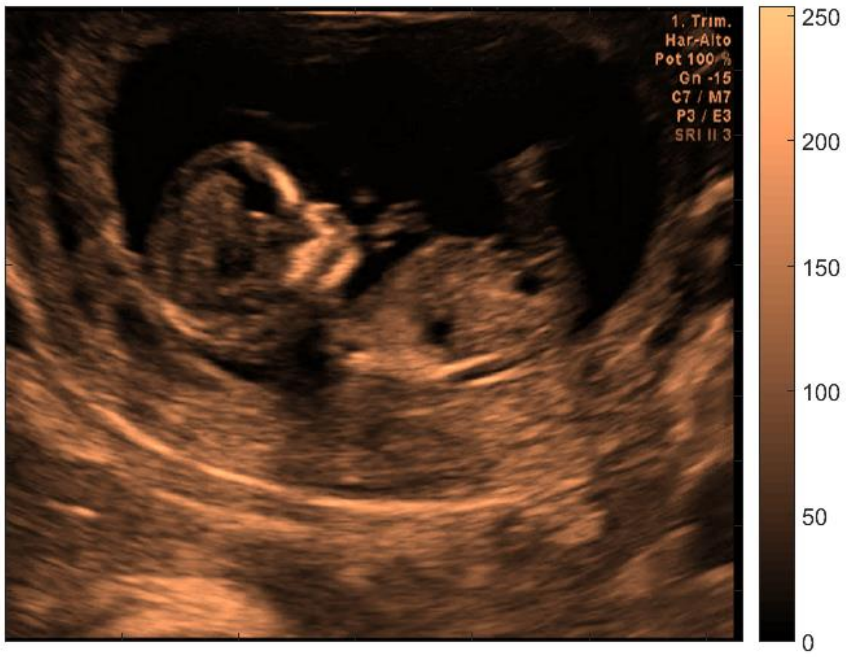

Figure 3. A typical ultrasound image with speckle noise.

Generally, speckle is an unwanted phenomena, frequently considered as *noise* and considerable research is focused on methods to reduce speckle to a minimum level [1, 2, 3, 4, 5, 6, 8, 10, 11]. Nevertheless, as mentioned before, speckle contains information about the sample, and it is possible to recover valuable information or enhance the resolution of the image using speckle [9, 12, 13, 14, 15, 16, 17, 18, 19, 20].

Properties and applications of Speckle:

Speckle size:

The average of a distance between adjacent bright and dark grains is related to the aperture angle and the plane where the speckle is defined. There are two possible scenarios; *objective* speckle (without lens), and *subjective* speckle (with lens) [21] as show Figure 4 and Figure 5 respectively.

For instance, the diameter of a speckle grain σ' for objective speckle generated by illuminating a scattering object with a circular beam of light of diameter D and observed at plane A at a distance L is determined by the relationship;

$$\sigma' \approx 1.2\lambda L/D, \tag{1}$$

where λ is the wavelength of the illumination light.

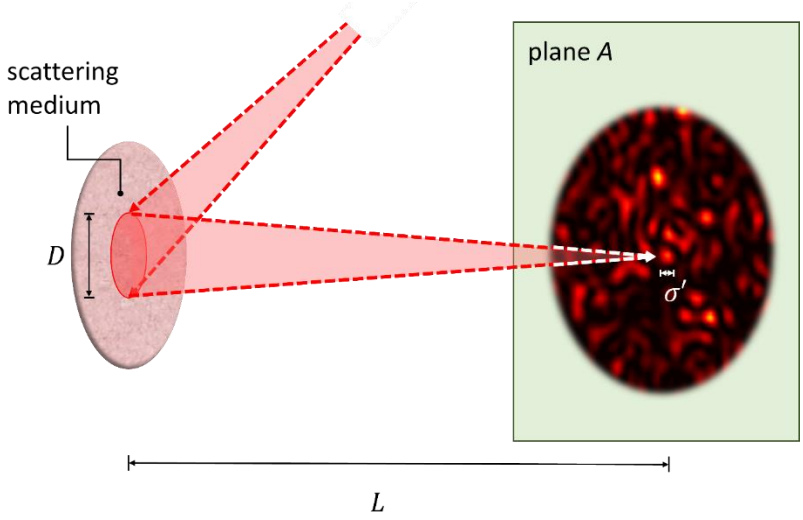

Figure 4. Schematic representation of objective speckle.

The diameter of speckle grain σ for subjective light, i.e., light collected by a lens with a numerical aperture $N.A.$ and focused on the plane A, is determined by the relationship;

$$\sigma \approx 0.6\lambda/N.A., \tag{2}$$

or in terms of magnification M and f-number F of the lens, the diameter σ is;

$$\sigma \approx 1.2(1 + M)\lambda F. \tag{3}$$

Considering the subjective speckle as the scaled image on the surface of the scattering medium, the diameter Σ is;

$$\Sigma \approx 1.2(1 + M)\lambda F/M. \tag{4}$$

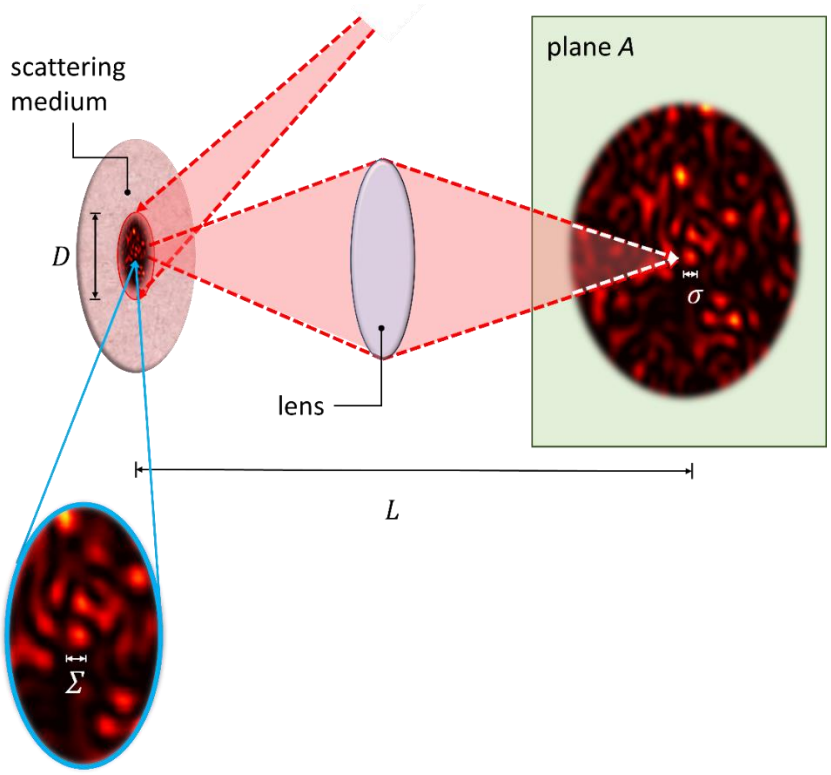

Figure 5. Schematic representation of subjective speckle.

Localness and memory effect

The speckle pattern is different for each object and even more, the speckle pattern changes in the same object if the illumination spot is displaced enough. For instance, consider a sheet of paper illuminated by spot of light of 2 mm of diameter, the speckle obtained there is different to the one obtained 1 cm aside. Even a displacement of a couple of millimeters is enough to get a totally different speckle pattern (see Figure 6 a) and c)). Both patterns may seem identical to the naked eye, but upon meticulous review, it becomes easy to discern the differences. There exists a small neighborhood where the light beam may be displaced over the sample and the speckle remains (almost) constant except for a slight displacement. This phenomenon is known as *memory effect* and was first reported by P. A. Lee, A. D. Stone et. al. in 1988 [22] and verified experimentally by I.

Freund, M. Rosenbluh and S. Feng in 1988 [23]. The range of memory effect is $\Delta x \ll u\lambda/\pi L$ [24], where u is the distance between the source and the scattering medium, L is the thickness of the medium and λ is the wavelength. In Figure 6 shows a schematic representation of the memory effect.

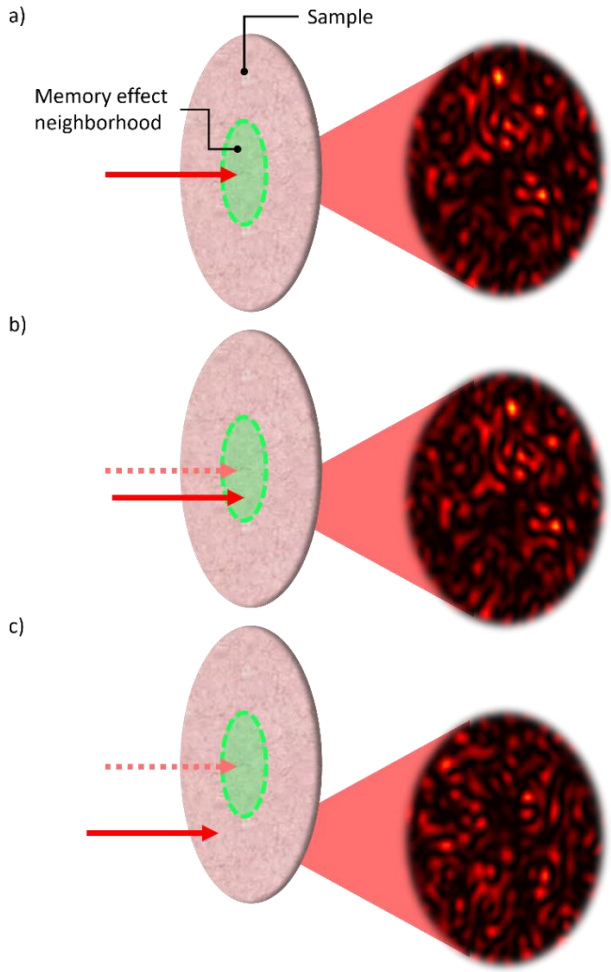

Figure 6. a) Speckle patern on transmission due to beam illuminated an arbitrary position in the sample, b) the beam is displaced within the memory effect neighborhood (green disk) of the original position (marked in dashed line arrow) resulting in similar but slightly displaced speckle compared to the original speckle pattern, c) whereas displacement of the beam outside the memory effect neighborhood leads to a totally different speckle pattern.

Dependency on wavelength and wavefront:

Speckle does not only depend on the sample; it also depends on the incident light. For instance, the number of speckle grains N is giving by $= 2\pi A/\lambda^2$ where λ is the wavelength and A is the area illuminated [25]. This means that different wavelength would produce a different number of speckle grains and, consequently, a different speckle pattern. Furthermore, speckle depends on the wavefront. For instance, a plane wave produces a different speckle pattern than a spherical or cylindrical wave or any other kind of wavefront. Even more, and contrary to intuition, it is possible to manipulate the wavefront in order to choose how the light interact to the matter to redirect the energy to a specific speckle grain. In other words, it is possible to focus light like, just like a lens or

magnifying glass does using any object that produce speckle. The shape or opacity of the object doesn't matter as long as it produces speckle.

. Figure 7 shows a schematic representation of a) speckle generated by a plane wave and b) the focus spot after wavefront shaping.

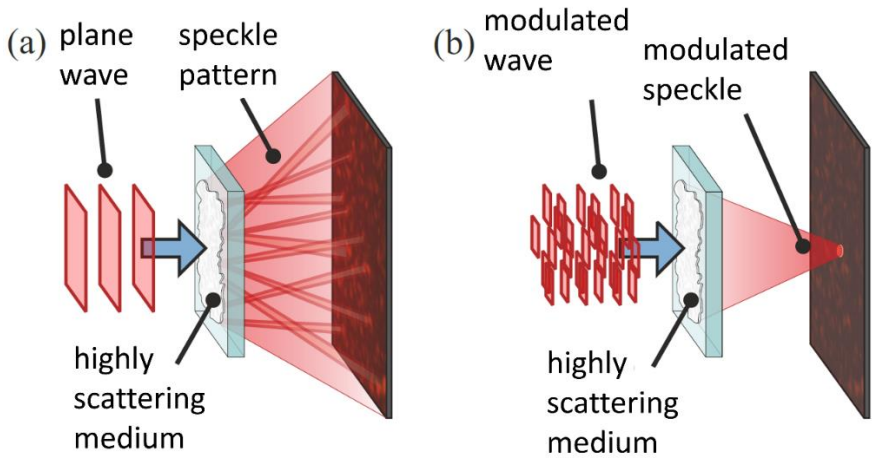

Figure 7. Schematic representation of a) speckle pattern produced by a plane wave and a focus point produced to a modulated wave.

The method of manipulating the wavefront is known as *wavefront shaping* (WFS) and was developed and experimental demonstrated by Mosk, Lagendijk et. al. in 2012 [25]. Figure 8 shows a spot focus through a ceramic plate. The ratio between the final and original intensity in the region of interest (enhancement factor η) is around $\eta = 6.6$ using only 150 pixels on phase, but it is possible to increase the enhancement factor around $\eta = 260$ [26], by increasing the number of iteration and the resolution in phase.

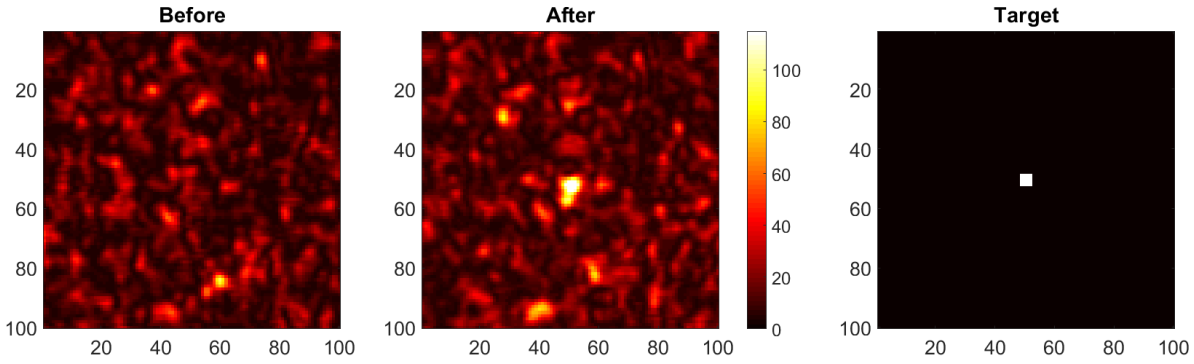

Figure 8. Shows the speckle on reflection of a ceramic plate before and after wavefront shaping, as well the desired image at the end (target).

The region of interest could be more complex than one dot, in fact, it is possible to do wavefront shaping to produce any desired image and position [27].

Uniqueness and unclonable of speckle pattern:

In contrast to well-known interference patterns like Yong or Michelson´s interferometers, speckle pattern is not symmetric, and it is impossible to predict the pattern given a sample object. To predict the pattern accurately, it is necessary to know the exact location of each particle within the sample with a pression smaller than the wavelengths (nanometers) and calculate the interaction, absorption, reflection, etc. of each particle. A change in the position of one particle modifies the speckle pattern. Therefore, each object has a unique speckle pattern that is impossible to replicate. In other words, the speckle pattern is like the fingerprint of the object. To duplicate the speckle pattern, it is necessary to create an object with exact same optical properties, including the exact position of the particles, which is practically impossible.

Due to the uniqueness and unclonable properties of speckle, combined with WFS, A. P. Mosk and P. W. H. Pinkse et. Al. proposed high-security authentication method in 2014 [28], where the speckle pattern works like a *key*. Only the right speckle pattern may unlock the system, for instance, a door or safe cage, or provide access to the bank account, confidential data, etc. The technique proposed by A. P. Mosk and P. W. H. Pinkse is known as quantum secure authentication (QSA).

Dynamic speckle and optical speckle contrast:

Until now, the scattering medium and the particles within it have been considered static. However, If the particles are moving inside the sample, for instance in a liquid, leaf, skin or any other organic tissue, the speckle pattern will move as well. An animation on video is available on our YouTube channel *Nautilus Alfa* in this link or through the QR code in Figure 9. The animation is available to download as .GIF image on the video's description.

Figure 9. QR code for a video in YouTube with a simulation of dynamic speckle.

As shown in the animation (linked to Figure 9), it is possible for the same sample to have a static or quasi-static region where the speckle slowly changes, and a dynamic region where the speckle changes rapidly. For instance, the speckle produced by the skin is quasi-static when there are no significant blood vessels beneath it, in contrast, the skin over a blood vessel change rapidly.

Therefore, when a picture is taken of a dynamic speckle pattern, the picture is not totally sharp, due to the speckle moving during the exposure time, see Figure 10. The faster speckle moves, the more blurred the picture becomes.

Figure 10. Picture inside a train in movement, the seats and the inside of train appear sharps, while the trees outside the train appear blurred. This blurring is caused by the relative movement of the trees during the exposure time.

Therefore, as will be seen in Chapter Two, it is possible to associate the speed of the speckle (of the particles) with the blurriness, more specifically, with the correlation time [29, 30]. The blurriness may be measured with the *optical speckle contrast*, more commonly known as speckle contrast and denoted by K. The speckle contrast of a set of pixels is calculated as;

$$K = \frac{\sigma}{\langle I \rangle}, \tag{5}$$

where, σ is the standard deviation and $\langle I \rangle$ is the mean intensity of the set of pixels. More details of speckle contrast are given on Chapter Two to Four.

In this work, we present a more accurate mathematical model of speckle contrast imaging for both spatial and temporal formalism.

Synthetic speckle (computational simulation)

The algorithm to simulate static speckle is well-known [31]. To simulate a speckle pattern, it is enough to simulate light propagation (using Fourier transform) through a phase object with random phase and a circular aperture. The size of the diameter of the circular aperture d is inversely proportional to the speckle grain size σ [31]. It is not necessary that the circular aperture is centered

on the image due to Fourier's displacement theorem. [31, 32] In Figure 11 is shown a representation of the steps of the synthetic speckle algorithm.

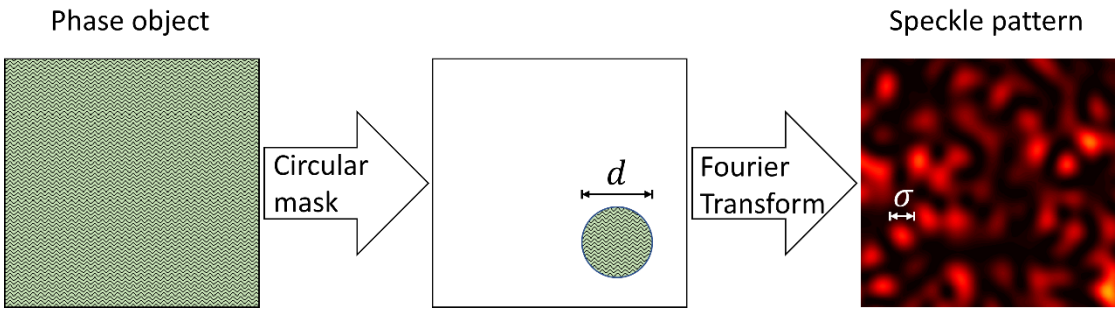

Figure 11. Representation of the steps involved in the algorithm to generate speckle patterns.

The synthetic speckle pattern follows an exponential probability distribution when the phase is distributed between $-\pi$ and π [32].

Figure 12 shows synthetic speckle patterns with different speckle size generated using *MATLAB R2022b*

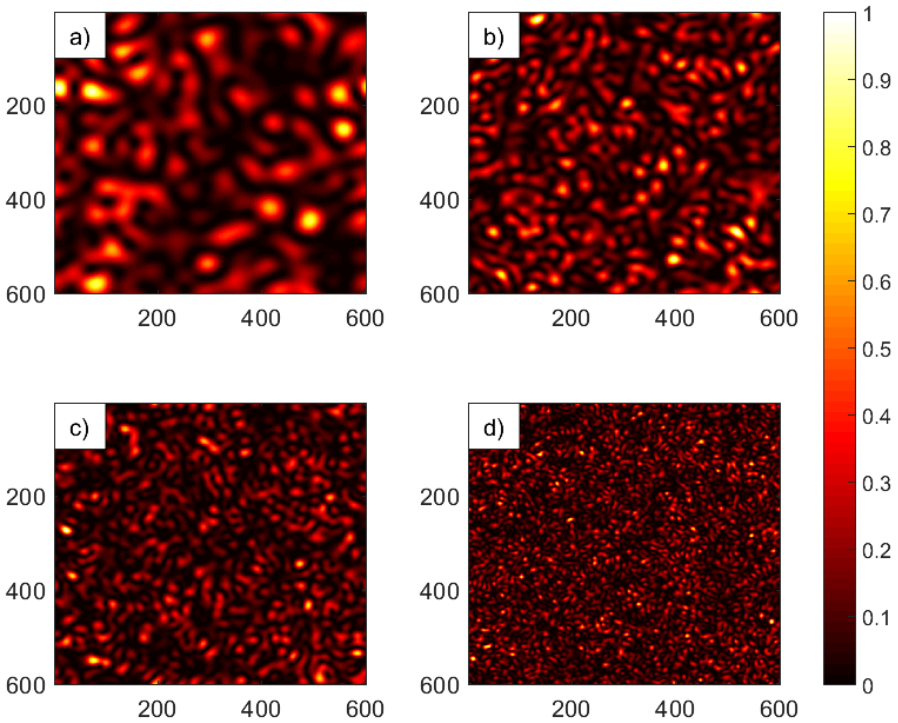

Figure 12. Synthetic speckle patterns of 600x600 pixels with a circular aperture of radius 8, 15, 20 and 40 pixels are shown in images a), b), c) and respectively.

The necessary code to generate the synthetic speckle pattern in *MATLAB R2022b* and *Mathematica 11* is shown on Appendix 1

As mentioned before, we are even able to simulate a dynamic speckle pattern with different dynamic speeds and arbitrary shapes, such as the speckle produced by the skin over blood vessels. You can see the video linked to Figure 9.

Figure 13 shows the speckle simulation of an object with a blood vessels shape. The first column displays a typical speckle frame. In the second column, we present the temporal average of all ten frames. Let us remark there is a slight blurriness in the shape of the simulated object. The third column represents the temporal contrast of the simulation, and in the fourth column we display the simulated object.

Let us note that in first column, it is impossible to discern any information about the blood vessels, such as their position, size, or ramification. However, in the contrast image, it becomes easy to visually identify the simulated object even to the naked eye. More details about temporal contrast are given on Chapter Two and Four.

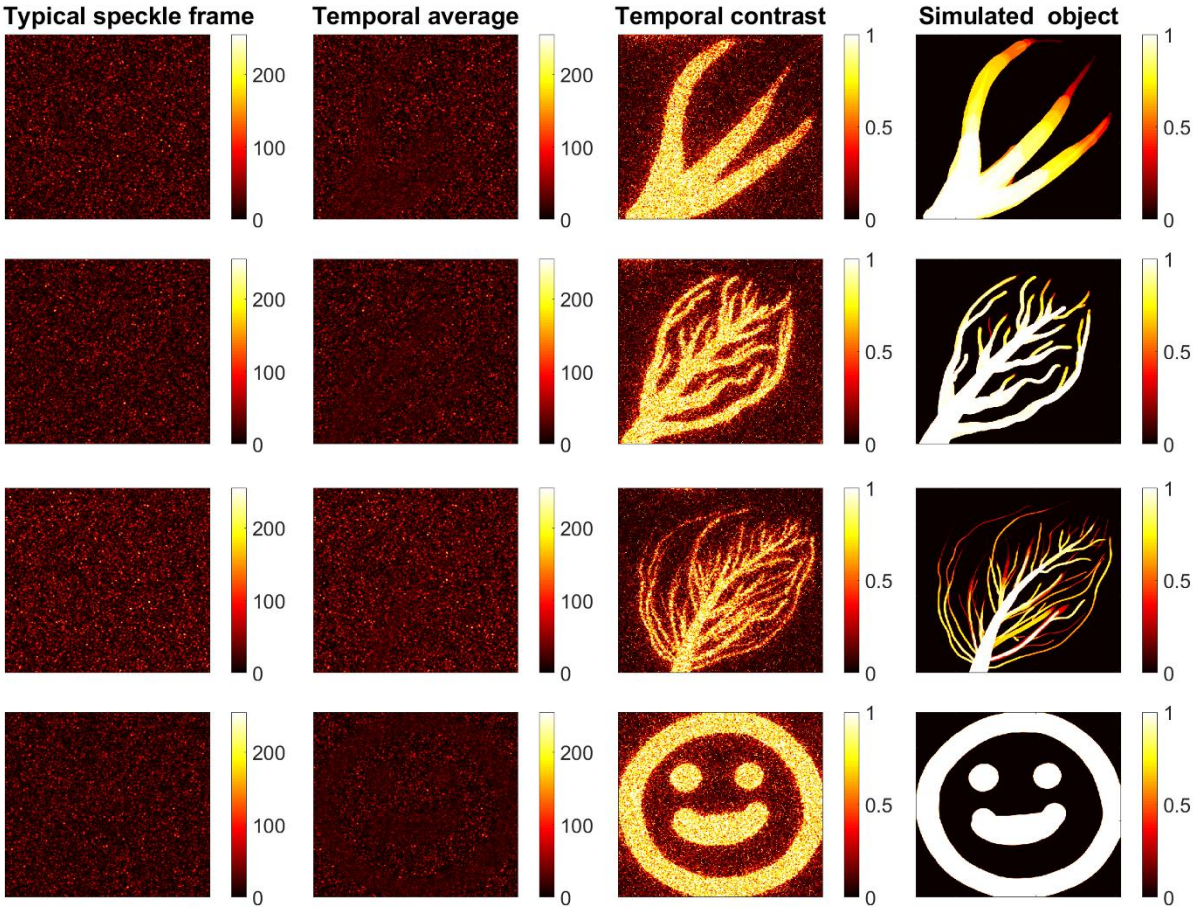

Figure 13. A dynamic speckle simulation of different dynamics with blood vessels shapes or any arbitrary shape (as show on the animation linked to Figure 9). For each simulation, 10 frames were created. The first column displays a typical speckle frame of the simulation, second column shows temporal average of all the ten frames. Third column shows the temporal contrast of the simulation, and the forth column display the simulated object.

References

[1] J. Chen, Y. Kong, D. Zhang, Y. Fu y S. Zhuang, «Two-dimensional phase unwrapping based on U^2-Net in complex noise environment,» *Optics Express,* vol. 31, nº 18, pp. 29792-29812, 2023.

[2] M. Ihmeida y M. Shahzad, «Enhanced Change Detection Performance Based on Deep Despeckling of Synthetic Aperture Radar Images,» *IEEE Access,* vol. 11, pp. 1-14, 2023.

[3] V. Kumar, A. Kumar Dubey, M. Gupta, V. Singh, A. Butola y D. Singh Mehta, «Speckle noise reduction strategies in laser-based projection imaging, fluorescence microscopy, and digital holography with uniform illumination, improved image sharpness, and resolution,» *Optics & laser technology,* vol. 141, 2021.

[4] V. Bianco, P. Memmolo, M. Leo, S. Montresor, C. Distante, M. Paturzo, P. Picart, B. Javidi y P. Ferraro, «Strategies for reducing speckle noise in digital holography,» *Light science & applications,* vol. 7, nº 48, pp. 1-16, 2018.

[5] K. Zhuo, Y. Wang, Y. Ma, S. An, Z. Zalevsky, J. Zheng y P. Gao, «Quantitative Phase Contrast Microscopy with Optimized Partially Coherent Illumination,» *Photonics,* vol. 10, nº 391, pp. 1-9, 2023.

[6] J. Zhao, B. Liang, E. Dobo, M. J. Khan, E. Yang y D. Kang, «Speckle and Shadow Artifacts Reduction in Scattering-Based Light Sheet Microscopy,» de *Biophotonics Congress: Optics in the Life Sciences 2023 (OMA, NTM, BODA, OMP, BRAIN),* , 2023.

[7] S. Morawiec, P. Stremplewski, A. Ajduk, B. F. Kennedy y M. Szkulmowski, «Dynamic full-field optical coherence microscopy of early mammalian oocytes,» de *Multiscale Imaging and Spectroscopy IV;*, San Francisco, 2023.

[8] W. Thompson, C. Marois, C. R. Do Ó, Q. Konopacky, J.-B. Ruffio, J. Wang, A. J. Skemer, R. J. De Rosa y B. Macintosh, «Deep Orbital Search for Additional Planets in the HR 8799 System,» *The astronomical journal,* vol. 165, nº 1, p. 29, 2023.

[9] A. Tokovinin, «Exploring Thousands of Nearby Hierarchical Systems with Gaia and Speckle Interferometry,» *The Astronomical Journal,* vol. 165, nº 4, p. 180, 2023.

[10] J. Kammerer, C. C. Stark, K. J. Ludwick, R. Juanola-Parramon y Bijan Nemati, «Simulating Reflected Light Coronagraphy of Earth-like Exoplanets with a Large IR/O/UV Space Telescope: Impact and Calibration of Smooth Exozodiacal Dust,» *The Astronomical Journal,* vol. 164, nº 6, p. 235, 2022.

[11] Y. Zhou y Y. Fang, «Diagnosis of breast cancer lesion using ultrasound images, elastography, and Ki-67 protein cell proliferation index: Ultrasound images, elastography, and Ki-67 protein in breast cancer,» *Cellular and molecular biology,* vol. 69, nº 4, pp. 16-23, 2023.

[12] D. C. P. a. D. W. Park, «Ultrasound Speckle Decorrelation-Based Blood Flow Measurements,» *Ultrasound in Medicine & Biology,* vol. 49, nº 7, pp. 1491-1498, 2023.

[13] D. D. Patel y D. M. Lipinski, «Validating a low-cost laser speckle contrast imaging system as a quantitative tool for assessing retinal vascular function,» *Scientific Reports,* pp. 1-11, 2020.

[14] A. I. Srienc, Z. L. Kurth-Nelson y E. A. Newman, «Imaging retinal blood flow with laer speckle flowmetry,» *Frontiers in Neuroenergetics,* vol. 2, pp. 128-1 - 128-10, 2010.

[15] B. Choi, N. M. Kang y J. S. Nelson, «Laser speckle imaging for monitoring blood flow dynamics in the in vivo rodent dorsal skin fold model,» *Microvascular Research,* vol. 68, pp. 143-146, 2004.

[16] J. Cracowski, F. Gaillard-Bigot, C. Cracowski, M. Roustit y C. Millet, «Skin microdualysis coupled with laser Speckle Contrast Imaging to assess microvascular reactivity,» *Microvascular Research,* vol. 82, nº 3, pp. 333-338, 2011.

[17] A. K. Dunn, «Laser Speckle Contrast Imaging of Cerebral Blood Flow,» *Annals of Biomedical Engineering,* vol. 40, pp. 367-377, 2012.

[18] G. A. Armitage, K. G. Todd, A. Shuaib y I. R. Winship, «Laser speckle contrast imaging of collateral blood flow during acute ischemic stroke,» *Journal of Cerebral Blood Flow & Metabolism,* vol. 30, pp. 1432-1436, 2010.

[19] F. Nirwana, P. Prajitno y S. Kusama Wijaya, «Correlation of Laser Speckle Image with Metal Surface Changes due to Corrosion Process,» *2019 International Conference on Electrical, Electronics and Information Engineering (ICEEIE),* vol. 6, pp. 244-249, 2019.

[20] P. C. da Silva, C. F. L. Junior, J. A. O. Huguenin, E. A. Ferreira, L. da Silva y S. A. Carvalho, «Investigation of copper and zinc alloy surface exposed to corrosion environment by digital image processing,» *Journal of materials research and technology,* vol. 24, pp. 9743-9753, 2023.

[21] J. Dainty, J. Goodman, G. Parry, T. McKechnie, M. Fançon y A. Ennos, Topics in Applied Physics Laser Speckle and Related Phenomena, Springer-Verlag Berlin Heidelberg GmbH, 1975.

[22] S. Feng, C. Kane, P. A. Lee y A. D. Stone, «Correlations and Fluctuations of Coherent Wave Transmission through Disordered Media,» *Physical Review Letters,* vol. 61, nº 7, pp. 834-837, 1988.

[23] I. Freund, M. Rosenbluh y S. Feng, «Memory Effects in Propagation of Optical Waves through Disordered Media,» *Physical Review Letters,* vol. 61, nº 20, pp. 2328-2332, 1988.

[24] O. Katz, P. Heidmann, M. Fink y S. Gigan, «Non-invasive real-time imaging through scattering layers and around corners via speckle correlations,» *Nature Photonics,* vol. 8, nº 10, pp. 784-790, 2014.

[25] A. P. Mosk, A. Lagendijk, G. Lerosey y M. Fink, «Controlling waves in space and time for imaging and focusing in complex media,» *Nature Photonics,* vol. 6, nº 5, pp. 283-292, 2012.

[26] J. C. Juárez Ramírez, *Método de autentificación óptica utilizando funciones físicas inclonables. Tesis para obtener el grado de maestría.,* Puebla, 2016.

[27] B. Coyotl Ocelotl, R. Porras Aguilar, R. Ramos Garcia y J. C. Ramirez San Juan, «Implementation of focusing and redirecting light through highly scattering media,» *Proceedings of SPIE,* vol. 9660, pp. 96601X-1-96601X-5, 2015.

[28] S. A. Goorden, M. Horstmann, B. Škoric, A. P. Mosk y P. W. H. Pinkse, «Quantum-secure authentication of a physical unclonable key,» *Optica,* vol. 1, nº 6, pp. 421-424, 2014.

[29] K. Basak, M. Manjunatha y P. Krumar Dutta, «Review of laser speckle-based analysis in medical imaging,» *Medical & Biological Engineering & Computing,* vol. 50, pp. 547-558, 2012.

[30] D. D. Duncan, S. J. Kirkpatrick y J. C. Gladish, «What is the proper statistical model for laser speckle flowmetry?,» *Proceedings of SPIE,* vol. 6855, pp. 685502-1-685502-7, 2008.

[31] D. D. Duncan y S. J. Kirkpatrick, «The copula: a tool for simulating speckle dynamics,» *Journal of the Optical Society of America A,* vol. 25, nº 1, pp. 231-237, 2008.

[32] D. D. Duncan, S. J. Kirkpatrick y R. K. Wang, «Statistics of local speckle contrast,» *Journal of the Optical Society of America A,* vol. 25, nº 1, pp. 9-15, 2008.

Coherence and optical contrast

Coherence:

As mentioned in Chapter 1, a speckle pattern is generated when light interacts with almost everything, except by mirrors or mirror-like materials (metals). Then, why is it not usual to see a speckle pattern in our daily life? Where is the speckle produced by sunlight or a bulb light? The speckle and any other interferometry pattern are always present, but they are not visible due to the rapid changes in the interference pattern. These changes occur so fast that we perceive an average of the interferometry pattern, resulting in a blurred interference pattern that appears as homogeneous illumination.

To easily observe an interference pattern like the speckle pattern, it is necessary for the illumination source to be highly *coherent*. There are two types of coherence: *temporal coherence* and *spatial coherence*. In simple words coherence is a measure of how similar two light beams are. Coherence equal to zero means that the light beams are totally different (the light beams are incoherent), and coherence equal to one, means that both light beams are identical to each other (totally coherent). In nature, it does not exist light beams totally incoherent or totally coherent, but rather partially coherence light beams with values between 0 and 1.

Temporal coherence measures how similar the light is to itself but at different moments (displaced in time) but not spatially shifted of itself [1]. For instance, it assesses how similar the light emitted from your bulb light is to the light emitted from the same bulb light in the same place but one second before. A formal definition for temporal coherence, as given by Hecht [2], is: "the temporal interval over which we can reasonably predict the phase of the lightwave at a given point in the space." This interval of time is known as *coherence time*. An *amplitude splitter* experiment, such as the Michelson interferometer, are able to detect and measure temporal coherence.

Similarly, spatial coherence measure how similar the light is when emitting from the same light source (which is larger in dimensions than the wavelength λ) but spatially displaced and not delayed on time of itself [1]. For instance, it assesses how similar the light is when emitting from your light bulb in the center and the light emitting from the same light bulb at the same time but displaced one centimeter to the left. Spatial coherence is related to the neighborhood around a spot in the light source within which the phase can be reasonably predicted. This region is named as *coherence area*. *Wavefront splitter* experiment, such as the Young interferometer, are able to detect and measure spatial coherence.

It is important to distinguish the coherence area from *coherence length* L. Coherence area is the region in space where light is similar to each other, and coherence length is the distance that light can propagate during coherence time.

In simple words, coherence quantifies how easy it is to see an interference pattern. That is the reason why speckle patterns started to be noticed in the 1960s when laser beams became available [3]. However, interference patterns have also been observed with sunlight [2].

As a formal definition, coherence is a property of light that is highly dependent on the quasi-monochromaticity of the light [4]. Coherence refers to the statistical analysis of the variations in phase and amplitude of a wave.

Degree of coherence:

Normalized first-order coherence:

The normalized autocorrelation function also known as the *complex degree of coherence* g_1, is a quantifier of coherence between two points ($\overrightarrow{r_1}$ and $\overrightarrow{r_2}$) in the field at two moments (t_1 and t_2 respectively) [1]. It is given by;

$$g_1(\overrightarrow{r_1}, t_1, \overrightarrow{r_2}, t_2) = \frac{\langle E^*(\overrightarrow{r_1}, t_1) E(\overrightarrow{r_2}, t_2)\rangle}{\sqrt{\langle |E(\overrightarrow{r_1}, t_1)|^2\rangle \langle |E(\overrightarrow{r_2}, t_2)|^2\rangle}}, \tag{1}$$

where $\langle \quad \rangle$ denotes time average. It is possible to interchange time and ensemble average if the process is ergodic [1]. Sometimes, the complex degree of coherence g_1 is also denoted by γ.

Given the definition (equation (1)), let us note some useful properties. For instance, when $\overrightarrow{r_1} = \overrightarrow{r_2}$ and $t_1 = t_2$, the complex degree of coherence is given by;

$$g_1(\overrightarrow{r_1}, t_1, \overrightarrow{r_1}, t_1) = 1. \tag{2}$$

The complex degree of coherence for the same point at the same time is equal to one, meaning, any point in the field is totally coherence with itself when comparing at the same time.

For an arbitrary two points $\overrightarrow{r_1}$ and $\overrightarrow{r_2}$ at arbitrary two moments t_1 and t_2, the absolute value of complex degree of coherence is given by;

$$|g_1(\overrightarrow{r_1}, t_1, \overrightarrow{r_2}, t_2)| \leq 1. \tag{3}$$

Normalized second-order coherence:

Similarly, as the complex degree of coherence g_1, another quantifier of the coherence is the *second-order degree of coherence*, denoted by g_1 and defined by;

$$g_2(\overrightarrow{r_1}, t_1, \overrightarrow{r_2}, t_2) = \frac{\langle E^*(\overrightarrow{r_1}, t_1) E^*(\overrightarrow{r_2}, t_2) E(\overrightarrow{r_1}, t_1) E(\overrightarrow{r_2}, t_2)\rangle}{\langle |E(\overrightarrow{r_1}, t_1)|^2\rangle \langle |E(\overrightarrow{r_2}, t_2)|^2\rangle}. \tag{4}$$

It is possible to rewrite equation (4) in function of the intensity $I(\vec{r}, t) = |E(\vec{r}, t)|^2$ leading to;

$$g_2(\overrightarrow{r_1}, t_1, \overrightarrow{r_2}, t_2) = \frac{\langle I(\overrightarrow{r_1}, t_1) I(\overrightarrow{r_2}, t_2)\rangle}{\langle I(\overrightarrow{r_1}, t_1)\rangle \langle I(\overrightarrow{r_2}, t_2)\rangle.} \quad (5)$$

Sometimes the second-order coherence g_2 is also denoted by Γ.

Siegert relationship:

Mathematically is easier work with the electromagnetic field E instead of the intensity I, however the second-order coherence has a particular importance due to, experimental detectors are sensitive to intensity not electromagnetic field. Therefore, it is quite useful the relation between g_1 and g_2 known as Siegert equation [5]. The original Siegert equation was [6];

$$g_2(\overrightarrow{r_1}, t_1, \overrightarrow{r_2}, t_2) = 1 + \left(g_1(\overrightarrow{r_1}, t_1, \overrightarrow{r_2}, t_2)\right)^2, \quad (6)$$

a modern version of Siegert equation, considering more parameters is;

$$g_2(\overrightarrow{r_1}, t_1, \overrightarrow{r_2}, t_2) = B + \beta\left(g_1(\overrightarrow{r_1}, t_1, \overrightarrow{r_2}, t_2)\right)^2, \quad (7)$$

where β it is a correction factor that depends on optical alignment, detector area, and scattering properties, with $B \approx 1$ is the base line [7].

Distribution:

The analytical expression for speckle contrast changes depending on the velocity distribution (g_1 and g_2) of the scatterers. In 1984, Goodman presented a negative exponential distribution [8] that represents an ideal speckle pattern. Considering ideal monochromatic and polarized light, the mean intensity $\langle I\rangle$ and the standard deviation σ are identical, leading to a speckle contrast equal to unity. The speckle pattern that achieves these properties is known as “fully developed speckle”. It is assumed that for a physical distribution, the standard deviation is less than the average intensity, and therefore, the contrast is bounded between 0 and 1. However, as we will see in the section *speckle contrast properties* this is not strictly true.

Correlation time

Given a coherence light, such as a laser beam, its properties such as intensity and phase are considered constant during an interval of time known as the correlation time. This can be precisely defined in terms of g_1, for instance, Mandel's definition;

$$\tau_c = \int_{-\infty}^{\infty} |g_1|^2 \mathrm{d}\, t, \tag{8}$$

where for Lorentzian distribution, which accurately describes the distribution for Brownian motion [9, 10];

$$|g_1| = \exp\left(-\frac{|t|}{\tau_c}\right). \tag{9}$$

For the Gaussian distribution, which describes laminar flow [10], Ramirez-San-Juan et. al. proposed;

$$|g_1| = \exp\left(-\frac{\pi t^2}{2\tau_c^2}\right), \tag{10}$$

an expression that indeed satisfies Mendel's definition (8), unlike the one used by Briers et. al. [5].

Many studies use the Lorentzian distribution to describe blood flow due to the simplicity of the equations. However, blood flow is inherently laminar, and such flow is more accurately described by a Gaussian distribution.

However, Duncan, Kirkpatrick and Wang [9] suggest that complex motion, such as blood flow, can be described as a combination of two stochastically independent processes: Lorentzian and Gaussian distributions. Unfortunately, there is no analytic expression for the Voigt distribution, so numerical approximations must be used [11]. The Voigt expression [12] is given by the integral;

$$V(x) = \int_{-\infty}^{\infty} L(x-\xi)G(\xi)\mathrm{d}\,\xi = \frac{w_L/w_G}{\pi^{3/2}} \int_{-\infty}^{\infty} \frac{\exp(-(\xi/w_G)^2)}{(x-\xi)^2 + w_L^2} \mathrm{d}\xi, \tag{11}$$

where w_L and w_G represent the widths of the Lorentzian and Gaussian profiles, respectively.

Speckle contrast:

Brief history:

Laser speckle imaging (LSI) is a technique developed by Fercher and Biers [13] in 1981 for determining blood flow. It is based on *optical speckle contrast*, often referred to as *speckle contrast*. LSI requires only a laser (coherent light), camera, and a computer for processing. Therefore, the technique is low-cost and easy to configure and operate. Moreover, it is a minimally invasive method, as it eliminates the need for dyes or any chemicals before, during, or after the imaging process.Laser illumination during picture acquisition, typically lasting only seconds or less, is the sole requirement. Due to these advantages, various fields have rapidly adopted LSI for research

purposes. For instance, applications extend to dentistry [14, 15], ophthalmology [16, 17] , dermatology [18, 19] , neurobiology [20, 21] , neuroscience [22, 23] , it can be used to measure blood flow [24, 25], monitoring capillary blood flow [26], or intraoperative assessment [27] among others biological applications. the technique has also found utility in studying slow dynamics within the realm of engineering. For instance, it has been employed to investigate degradation processes of metal surfaces resulting from corrosion [28, 29] as well as to characterize drying patterns during paint application [30, 31].

Following the mathematical approach described by Fercher and Briers in 1981 [13] to measure the speckle contrast K using a statistical analysis of a time-average speckle pattern starts by considering that the spatial variance σ^2 as;

$$\sigma^2 = \frac{1}{T}\int_0^T C_t^{(2)}(\tau)d\tau, \tag{12}$$

where, T is the exposure time and $C_t^{(2)}$ is the autocovariance of the temporal fluctuation in the intensity of a single speckle.

Considering the Siegert relationship for gaussian statistics;

$$g_2(\tau) = 1 + |g_1(\tau)|^2. \tag{13}$$

Where $g_1(\tau)$ and $g_2(\tau)$ are the normalized first and second-order autocorrelation function respectively, (representing autocorrelation in the field and intensity, respectively), and τ represents the interval of time it is considered in the calculation. Considering stationarity, we follow the definition of various correlation function;

$$g_2(\tau) = 1 + \frac{C_t^{(2)}}{\langle I\rangle_t^2}, \tag{14}$$

where $\langle \quad \rangle_t$ is defined as the time average.

From equation (13) and (14), it follows that $C_t^{(2)} = \langle I\rangle_t^2|g_1(\tau)|^2$. For the case of a Lorentzian spectrum, $g_1(\tau) = e^{-|\tau|/\tau_c}$, where τ_c is the correlation time. Substituting this into equation (12);

$$\sigma^2 = \frac{1}{T}\int_0^T \langle I\rangle_t^2|g_1(\tau)|^2 d\tau = \frac{\langle I\rangle_t^2}{T}\int_0^T e^{-|\tau|/\tau_c}d\tau, \tag{15}$$

Solving the integral in equation (15) gives;

$$\sigma^2 = \frac{\langle I\rangle_t^2\tau_c}{2T}\left(1 - e^{-2T/\tau_c}\right), \tag{16}$$

Dividing by the term $\langle I\rangle_t^2$, it gets;

$$\frac{\sigma^2}{\langle I\rangle_t^2} = \frac{\tau_c}{2T}\left(1 - e^{-2T/\tau_c}\right). \tag{17}$$

The contrast K is defined as $K = \sigma/\langle I\rangle_t$;

$$K = \frac{\sigma}{\langle I\rangle} = \left(\frac{\tau_c}{2T}\left\{1 - e^{-\frac{2T}{\tau_c}}\right\}\right)^{1/2}, \tag{18}$$

Since then, the model has undergone several modifications, incorporating additional factors to enhance the accuracy of the mathematical model in comparison to experimental data. For instance, Lemieux and Durian in 1999 [32] used a robust Siegert equation, adding a correction factor β, instead of considering equation (13)

$$g_2(\tau) = 1 + \beta|g_1(\tau)|^2, \tag{19}$$

The factor β depends on the camera pixel size and speckle grain size [33]. Although efforts have been made to measure β experimentally [34], the methods employed are intricate and not practical for real-world applications.

Additionally, Bandyopadhyay et al. [34] identified a mistake in Fercher and Briers derivation in equation (15), considering the variance as a single integral of $g_1(\tau)$ over the time window $0 < \tau < T$. Instead, the correct calculation of the variance involves a doble integral of $g_1(t_1 - t_2)$ for two different times in the time window $0 < t_1, t_2 < T$, where $\tau = t_1 - t_2$. Taking into account this, and considering equation (19) as Siegert relation, equation (15) it is rewritten as;

$$\sigma^2 = \frac{1}{T^2}\int_0^T \int_0^T \beta\langle I\rangle_t^2 |g_1(t_1 - t_2)|^2 dt_1\, dt_2. \tag{20}$$

Considering the change of variable $\tau = t_1 - t_2$ and $\tau_2 = \frac{1}{2}(t_1 + t_2)$, the double integral in equation (20) is reduced to;

$$\sigma^2 = \frac{\beta\langle I\rangle_t^2}{T}\int_0^T 2\left(1 - \frac{\tau}{T}\right)|g_1(\tau)|^2 d\tau. \tag{21}$$

Solving the integral for $g_1(\tau) = e^{-|\tau|/\tau_c}$;

$$\sigma^2 = \frac{\langle I\rangle_t^2 \tau_c^2}{2T^2}\left(e^{-2T/\,\tau_c} - 1 + \frac{2T}{\tau}\right). \tag{22}$$

Dividing by $\langle I\rangle_t^2$ obtains an expression for K^2;

$$K^2 = \frac{\sigma^2}{\langle I\rangle_t^2} = \frac{\tau_c^2}{2T^2}\left(e^{-2T/\,\tau_c} - 1 + \frac{2T}{\tau}\right). \tag{23}$$

Defining x as $x = T/\tau_c$, equation (23) is rewritten as;

$$K^2 = \beta \frac{e^{-2x} - 1 + 2x}{2x^2}. \tag{24}$$

Subsequently, several groups [34, 35, 32, 22] demonstrated the necessity of considering not only the fraction of light ρ that interacts with dynamic scatterers, but also the fraction of light $(1-\rho)$ from stationary scatterers.

In 2014, Ramirez-San-Juan et al. further advanced the model by treating pixels not as mere points, but as spatial regions with width and height, essentially accounting for the physical dimensions of the pixels [5]. Consequently, equation (24) change to;

$$K = \alpha^{1/2}\beta^{1/2}(M)\left[\rho^2 \frac{e^{-2x} - 1 + 2x}{2x^2} + 4\rho(1-\rho)\frac{e^{-x} - 1 + x}{x^2} + (1-\rho)^2\right]^{1/2} + K_n, \tag{25}$$

where, M represents the ratio between the pixel area and the correlation area, K_n is a noise term, α is a normalization (proportionality) factor that accommodates effects such as polarization. The term $\beta^{1/2}(M)$ is given by;

$$\beta^{1/2}(M) = \sqrt{1/M}\,\mathrm{erf}\left(\sqrt{\pi M}\right) - (1/(\pi M))(1 - e^{-\pi M}). \tag{26}$$

Equation (25) is not the final expression to model the speckle contrast. Like any other mathematical model, various researchers have been striving to improve its accuracy in fitting experimental data. In this work, we present a mathematical model that better predicts experimental data.

Computational contrast calculation:

Mathematically, given a set of N numbers $\{x_i \in \mathbb{R}\}$ such that $i \in \{1,2,\dots,N\}$, the speckle contrast is defined as the ratio between the standard deviation σ and the mean value of the set $\langle x \rangle$ [13]

$$K = \frac{\sigma}{\langle x \rangle}, \tag{27}$$

where:

$$\sigma = \sqrt{\frac{1}{N-1}\sum_{i=1}^{N}(\langle x \rangle - x_i)^2}, \tag{28}$$

and

$$\langle x \rangle = \frac{1}{N}\sum_{i=1}^{N} x_i. \tag{29}$$

Therefore, when given an experimental speckle photograph, it becomes possible to compute the speckle contrast by considering a set of pixels. Depending on our focus, this set of pixels could encompass all the pixels within a sliding window using a single image (spatial contrast) or the corresponding position across a sequence of images (temporal contrast). Both spatial contrast and temporal contrast have their advantages and limitations. Further elaboration on these distinct contrast types is provided in this Chapter and Chapter 3 and 4.

Speckle contrast properties:

Contrast under scalar operations.

Let us define σ_x and $\langle x \rangle$ as the standard deviation and mean value, respectively, of a set of N numbers $\{x_i \in \mathbb{R}\}$. Given a scalar $a \in \mathbb{R}$ it is possible to define new sets as follows.

Scalar multiplication: Considering the new set $\{y_i = ax_i\}$, it can be shown that $\sigma_y = a\sigma_x$ and $\langle y \rangle = a\,\langle x \rangle$, therefore;

$$K_y = \frac{a\sigma_x}{a\langle x \rangle} = K_x, \tag{30}$$

in other words, the contrast is invariant under scalar multiplication.

Scalar addition: Considering the new set $\{z_i = x_i + a\}$, it can be shown that $\sigma_z = \sigma_x$ and $\langle z \rangle = \langle x \rangle + a$, therefore;

$$K_z = \frac{\sigma_x}{\langle x \rangle + a} = \frac{\sigma_x K_x}{\sigma_x + aK_x}, \tag{31}$$

in other words, the contrast is not invariant under scalar addition but the standard deviation is.

A particular mathematical case

Let us consider a rather odd case: a set of N numbers$\{x_i \in \mathbb{R}\}$ where;

$$x_i = \begin{cases} 0 & i > u \\ a & i \leq u \end{cases} \tag{32}$$

and $1 \leq u \leq N$, and $a \in \mathbb{R}$ is an arbitrary scalar. This describes a set where there are at most two distinct values (0 and a) throughout the entire set. Therefore;

$$\langle x \rangle = \frac{au}{N}, \tag{33}$$

and

$$\sigma = \frac{x}{\sqrt{N}} \sqrt{\frac{u(N-u)}{N-1}}, \tag{34}$$

therefore,

$$K = \sqrt{\frac{N}{u} \cdot \frac{N-u}{N-1}}. \tag{35}$$

From equation (35), the speckle contrast is zero when there is only one value in the whole set ($u = N$). As important remark from equation (35) that the maximum speckle contrast value is $K = \sqrt{N} > 1$, which occurs when $u = 1$. In other words, this happens when all the pixels are zero except for one pixel..

Of course, this is a mathematical scenario. Physically, it's nearly impossible for a speckle pattern to have only two possible values or for all pixels except one to be zero. Nevertheless, when recording a speckle pattern with a camera, it's quite possible that the majority of pixels are close to zero, resulting in a contrast greater than one ($K > 1$). In fact, it's common to experimentally observe a contrast greater than one, and is common to normalize the contrast in order to avoid contrast greater than one.

Speckle contrast algorithms:

Spatial contrast.

This algorithm requires a single frame of speckle and a *sliding window* of $\sqrt{N} \times \sqrt{N}$ pixels (without loss of generality let us consider $\sqrt{N}$ as an odd number). A square region in the image (a virtual construct) is centered on one pixel of the speckle image and is slid over all the pixels of the speckle image. At each position of the sliding window, the mean $\langle I \rangle$ and the standard deviation σ of the pixels within of the sliding window are calculated. The contrast $K = \sigma / \langle I \rangle$ (eq. (27)) for each position of the sliding window is wrote in a new image, called the contrast image (see Figure 1).

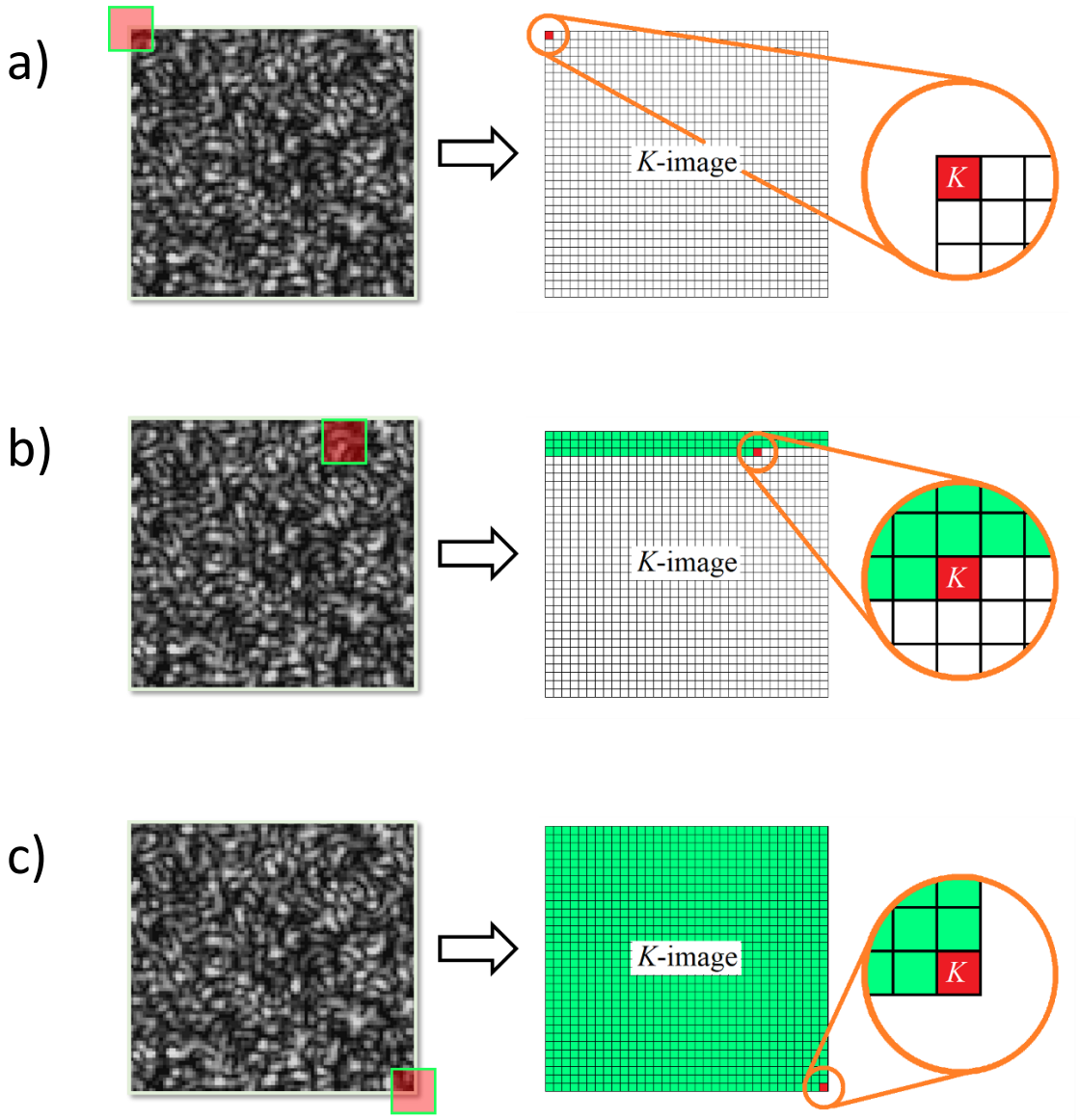

Figure 1. Schematic representation of the spatial contrast algorithm; a) A sliding window (indicated by a red square with green edges) is centered on the first pixel. The contrast is calculated for all pixels within the sliding window, and the calculated contrast value is written onto the contrast image K represented as a green pixel. *The sliding window then moves, and the process is repeated for each position in the speckle image, b) The sliding window is shown centered on another pixel, and the progression of the contrast image is depicted as green pixels. c) The contrast image is completed as the contrast is calculated for windows centered on each pixel in the image.*

In Figure 1, a schematic representation of the spatial contrast algorithm is presented; Figure 1a; the sliding window is centered on the top left corner of the speckle image starting the calculation and writing the first contrast value onto the contrast image (pixel colored in green for visualization). Figure 1b; after some iterations, the sliding window has moved down some rows, and the contrast image now contains multiple contrast values, represented on color green. Figure 1c; the algorithm ends when the sliding window has covered all pixels of the speckle image, resulting in the completion of the contrast image.

Since all the pixels in the speckle image within the sliding window are used to calculate one pixel of the contrast image, the spatial resolution is reduced inversely to the size of the sliding window. However, because only one frame is necessary to calculate the spatial contrast, the temporal resolution of the contrast image remains the same as the temporal resolution of the speckle image.

The spatial contrast algorithm encounters an issue with the edges of the speckle image. If the sliding window is centered on the pixels at the edges, it is possible that a portion of the sliding window extends beyond the image boundaries (see Figure 1a and Figure 1c), resulting in a reduction of the actual pixels within the window. One way to mitigate this problem is by avoiding the centering of the sliding window on the edges of the speckle image, which, however, reduces the effective usable region of the speckle image.

The spatial contrast algorithm is presented in the Appendix 1 for both *MATLAB* and *Mathematica.* In Figure 2 a) displays a raw speckle frame, and b) shows the spatial contrast image generated using the MATLAB code shown in the Appendix 1.

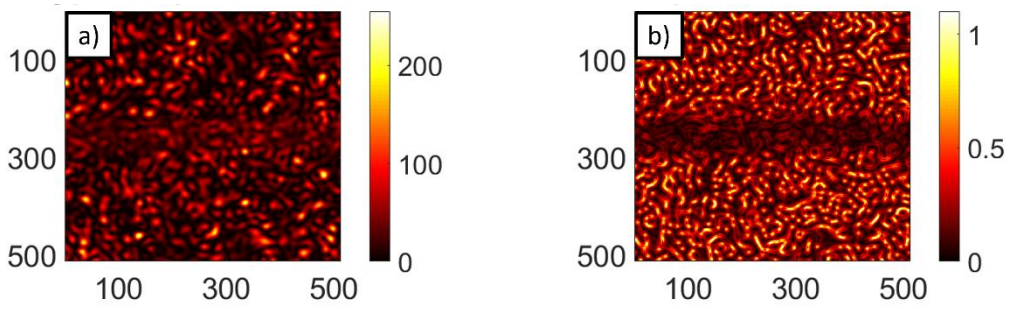

Figure 2. a) Raw speckle frame; b) Spatial contrast image generated MATLAB.

Temporal contrast.

Requires a set of L frames of speckle pattern with an exposure time T and a delay between frames δ. For temporal contrast algorithm For the temporal contrast algorithm, a sliding window is not necessary, but rather a sliding pixel. For each pixel of the speckle picture, the mean $\langle I \rangle$ and the standard deviation σ are calculated across all speckle pictures (see Figure 3). The contrast, $K = \sigma / \langle I \rangle$ (eq. (27)), for each pixel is written to a new image, the contrast image (see Figure 1).

Figure 3 provides a schematic representation of the temporal contrast algorithm. In Figure 3a, the pixel in the top-left corner of the speckle image is selected across all frames, and the first contrast value is written onto the contrast image. After some iteration, in Figure 3b, the contrast image already contains some contrast values, represented in green. In Figure 1c, the algorithm concludes when the contrast is calculated for each pixel in the speckle image, completing the contrast image.

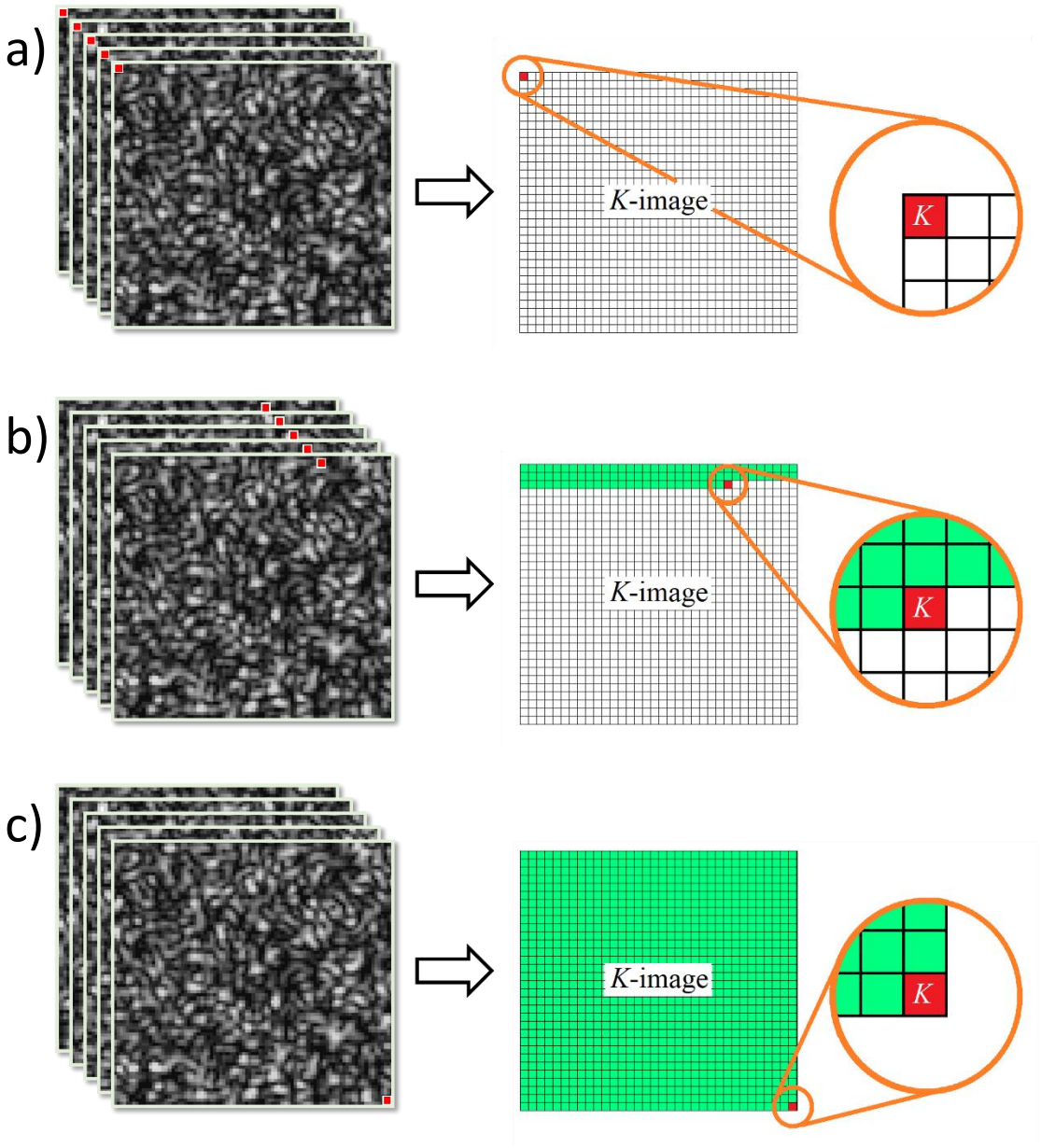

Figure 3. Schematic representation of the temporal contrast algorithm: a) the first pixel is selected (colored in red) over a set of L pictures to calculate the contrast of that pixel set. The contrast is written on the contrast image K. This process is repeated for each position on the speckle image, b) shows the set of pixel chosen on the picture and how the progress on the contrast image is, c) the contrast image is complete when the contrast is calculate for each pixel on the pictures.

The temporal contrast algorithm, takes the same pixel in all the speckle frames, resulting in a reduction in temporal resolution, his is because the information acquired over several frames is averaged and treated as a single frame with a longer exposure time. However, since each pixel in the contrast image requires one pixel from the raw speckle frames, the spatial resolution of the contrast image remains the same as the spatial resolution of the speckle image.

The temporal contrast algorithm is presented in the Appendix 1 for both *MATLAB* and *Mathematica.* In Figure 4 a) displays a raw speckle frame, and b) shows the temporal contrast image generated using the MATLAB code shown in the Appendix 1.

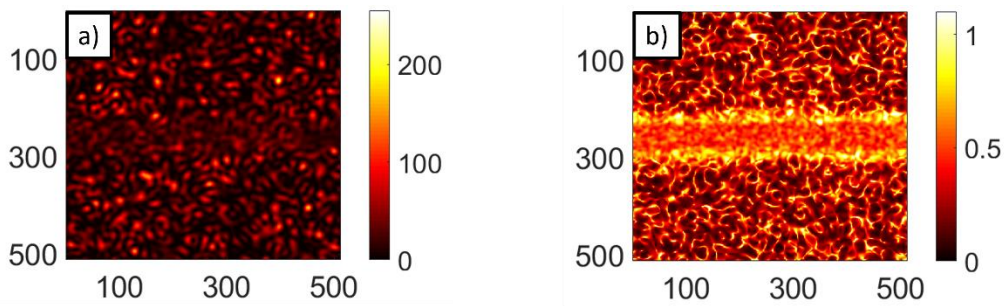

Figure 4. a) Raw speckle frame; b) Spatial contrast image generated MATLAB.

Comparison of temporal and spatial contrast.

Spatial contrast has the advantage of requiring only one frame, making it easier and reducing possible noise due to movement in an in vivo experiment compared to taking a set of photographs (temporal contrast). The temporal resolution of the contrast image and the speckle raw image remains constant; however, the spatial resolution is reduced in the contrast image. Meanwhile the sliding window is larger, there are more pixels within it for a better statistics, the spatial resolution is reduced because the information within the sliding window is reduced to a single pixel in the contrast image.

Temporal contrast has the advantage that the spatial resolution is not reduced in the contrast image. Each pixel on the speckle images corresponds to one pixel in the contrast image. However, the temporal resolution is reduced, due to requires a set of L pictures. The period of time the data is collected extends from T (the exposure time of one picture) to at least $L \cdot T$, which represents the exposure time of L frames without considering any delay between frames.

In Figure 5 and Figure 6 it is showing the compassion of the spatial and temporal contrast. Figure 5 shows the contrast of synthetic (simulated) speckle pattern using the spatial and temporal algorithm.

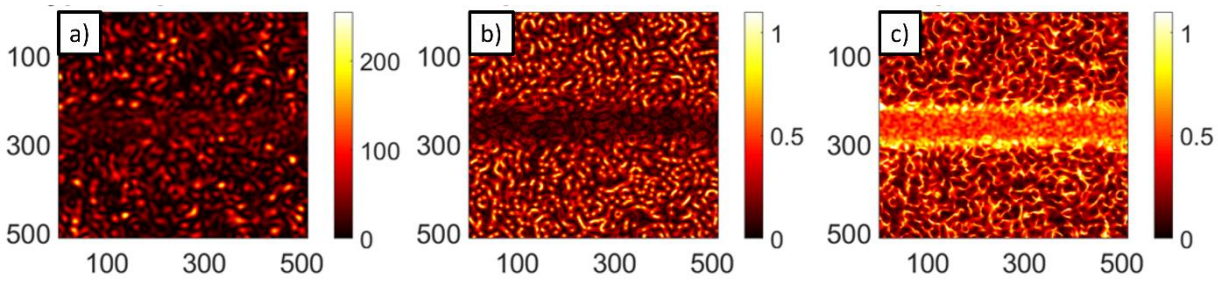

Figure 5. A comparison of spatial and temporal contrast of a simulation of a blood vessel of 25 speckle frames. Left to right, a typical speckle frame of the set. The spatial contrast of the first frame using a sliding window of 3 pixels. The temporal contrast considering 25 frames.

Figure 6 shows the spatial and temporal contrast from a healthy *Candida tropicalis* colony (approximately 2 mm in diameter) over a hot plate at 31° C, which is illuminated with a linearly polarized laser light (He-Ne 633 nm) spatially filtered. The speckle is recorded on reflection through a polarized beam splitter to avoid specular reflection. The experiment was conducted in collaboration with David Loaiza T.

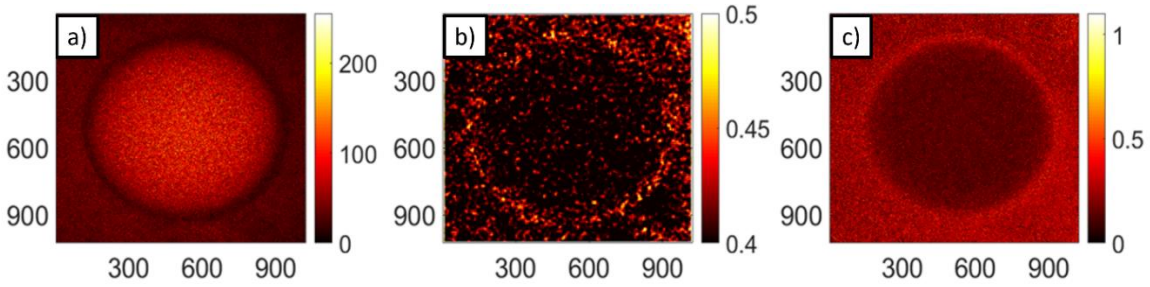

Figure 6. A comparison of spatial and temporal contrast of the speckle on reflection of a candida tropicalis of 48 hours in a petri dish with agar. Left to right, a typical speckle frame of the set. The spatial contrast of the first frame using a sliding window of 3 pixels. The temporal contrast considering 25 frames.

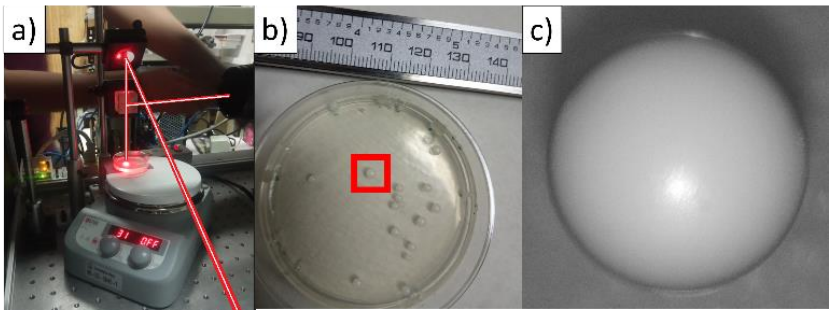

Figure 7. a) experimental setup of the candida experiment, b) Petri dish with candida tropicalis of 48 hours, c) photograph in white light as a reference.

Experimentally, it is easy to note that the value of the contrast (for either temporal or spatial algorithms) strongly depends on some important parameters that may be chosen by the user, such as; the number of frames, exposure time, correlation time, size of the speckle frame, speckle grain size and pixel size. And some other parameters depend on the sample, such as the velocity of the sample dynamics.

Depends on the sample, experimental setup, and goals of the experiment, the suitable algorithm (temporal or spatial) may be chosen.

In the following chapters, a novel mathematical model is presented to describe optical contrast, taking into account the sliding window, spatial correlation between neighboring pixels, exposure and correlation time, as well as the number of frames and temporal correlations between frames. As will be shown in the following chapters, our proposal matches the previous model when there is no correlation. Additionally, in contrast to previous models, our proposal fits experimental data when there are correlations between frames or pixels.

References

[1] J. W. Goodman, Statistical Optics, Wiley-Interscience Publication, 2000.

[2] E. Hecht, Óptica, Madrid: Addison Wesley Iberoamericana, 2000.

[3] J. W. Goodman, Speckle Phenomena in Optics: Theory and Applications, Robert & Company, 2007.

[4] I. V. Hertel and C.-P. Schulz, Atoms, Molecules and Optical Physics 2, Springer-Verlag Berlin Heidelberg, 2015.

[5] J. Ramirez-San-Juan, R. Ramos-Garcia, G. Maartinez-Niconoff and B. Choi, "Simple correction factor for laser speckle imaging of flow dynamics," *Optics Letters,* vol. 39, no. 3, pp. 678-681, 2014.

[6] A. Siegert and Massachusetts Institute of Technology, "On the Fluctuations in Signals Returned by Many Independently Moving Scatterers," Radiation Laboratory, Massachusetts Institute of Technology, 1943.

[7] J. Stetefeld, S. McKenna and T. Patel, "Dynamic light scattering: a practical guide and applications," *Biophysical Reviews,* vol. 8, pp. 409-427, 2016.

[8] J. Dainty, Laser speckle and related phenomena, Springer-Verlag, 1984.

[9] D. D. Duncan, S. J. Kirkpatrick and R. K. Wang, "Statistics of local speckle contrast," *Journal of the Optical Society of America A,* vol. 25, no. 1, pp. 9-15, 2008.

[10] D. D. Duncan, S. J. Kirkpatrick and J. C. Gladish, "What is the proper statistical model for laser speckle flowmetry?," *Proceedings of SPIE,* vol. 6855, pp. 685502-1-685502-7, 2008.

[11] F. G. Smith, D. L. Shumaker and J. S. Accetta, Atmospheric Propagation of Radiation, The Infrared & Electro-Optical Systems Handbook, Volume 2., Infrared Info. Analysis Ctr & SPIE Optical Engineering Press, 1993.

[12] G. Pagnini and F. Mainardi, "Evolution equations for the probabilistic generalization of the Voigt profile function," *Journal of COmputational and Applied Mathematics,* vol. 223, pp. 1590-1595, 2010.

[13] A. Fercher and J. Briers, "Flow visualization by means of single-exposure speckle photography," *Optics communications,* vol. 37, no. 5, pp. 326-330, 1981.

[14] T. Sato, M. Miyazaki, A. Rikuta and K. Kobayashi, "Application of the Laser Speckle-Correlation Method for Determining the Shrinkage Vector of a Light-cured Resin," *Denntal Materials Journal,* vol. 23, no. 3, pp. 284-290, 2004.

[15] C. Stoianovici, P. Wilder-Smith and B. Choi, "Assessment of Pulpal Vitality Using Laser Speckle Imaging," *Laser in Surgery and Medicine,* vol. 43, no. 8, pp. 833-837, 2011.

[16] D. D. Patel and D. M. Lipinski, "Validating a low-cost laser speckle contrast imaging system as a quantitative tool for assessing retinal vascular function," *Scientific Reports,* pp. 1-11, 2020.

[17] A. I. Srienc, Z. L. Kurth-Nelson and E. A. Newman, "Imaging retinal blood flow with laer speckle flowmetry," *Frontiers in Neuroenergetics,* vol. 2, pp. 128-1 - 128-10, 2010.

[18] B. Choi, N. M. Kang and J. S. Nelson, "Laser speckle imaging for monitoring blood flow dynamics in the in vivo rodent dorsal skin fold model," *Microvascular Research,* vol. 68, pp. 143-146, 2004.

[19] J. Cracowski, F. Gaillard-Bigot, C. Cracowski, M. Roustit and C. Millet, "Skin microdualysis coupled with laser Speckle Contrast Imaging to assess microvascular reactivity," *Microvascular Research,* vol. 82, no. 3, pp. 333-338, 2011.

[20] A. K. Dunn, "Laser Speckle Contrast Imaging of Cerebral Blood Flow," *Annals of Biomedical Engineering,* vol. 40, pp. 367-377, 2012.

[21] G. A. Armitage, K. G. Todd, A. Shuaib and I. R. Winship, "Laser speckle contrast imaging of collateral blood flow during acute ischemic stroke," *Journal of Cerebral Blood Flow & Metabolism,* vol. 30, pp. 1432-1436, 2010.

[22] D. A. Boas and A. K. Dunn, "Laser speckle contrast imaging in biomedical optics," *Journal of biomedical optics,* vol. 15, no. 1, p. 011109, 2010.

[23] J. Senarathna, A. Rege, N. Li and N. V. Thakor, "Laser Speckle Contrast Imaging: Theory, Instrumentation and Applications," *IEEE Reviews in Biomedical Engineering,* vol. 6, pp. 99-110, 2013.

[24] J. D. Briers and S. Webster, "Laser Speckle Contrast Analysis (LASCA): A Nonscanning, Full-field Technique For Monitoring Capillary Blood Flow," *Journal of Biomedical Optics,* vol. 1, no. 2, pp. 174-179, 1996.

[25] J. D. Briers, "Laser speckle contrast imaging for measuring blood flow," *Optica Applicata,* vol. 37, no. 1-2, pp. 139-152, 2007.

[26] J. D. Briers and S. Webster, "Laser Speckle Contrast Analysis (LASCA): A Nonscanning, Full-field Technique For Monitoring Capillary Blood Flow," *JOURNAL OF BIOMEDICAL OPTICS,* vol. 1, no. 2, pp. 174-179, 1996.

[27] E. A. Mannoh, G. Thomas, C. C. Solórzano and A. Mahadevan-Jansen, "Intraoperative assessment of parathyroid viability using laser speckle contrast imaging," *Scientific reports,* vol. 7, pp. 1-11, 2017.

[28] F. Nirwana, P. Prajitno and S. Kusama Wijaya, "Correlation of Laser Speckle Image with Metal Surface Changes due to Corrosion Process," *2019 International Conference on Electrical, Electronics and Information Engineering (ICEEIE),* vol. 6, pp. 244-249, 2019.

[29] P. C. da Silva, C. F. L. Junior, J. A. O. Huguenin, E. A. Ferreira, L. da Silva and S. A. Carvalho, "Investigation of copper and zinc alloy surface exposed to corrosion environment by digital image processing," *Journal of materials research and technology,* vol. 24, pp. 9743-9753, 2023.

[30] G. Dwivedi, V. Kumari, N. Barak, A. Anand, A. K. Sharma and G. Sheoran, "Multimodal optical device to study dynamics of drying process," *Optics and Lasers in Engineering,* vol. 169, p. 107726, 2023.

[31] S. Szalai, B. F. Szívós, D. Kurhan, A. Németh, M. Sysyn and S. Fischer, "Optimization of Surface Preparation and Painting Processes for Railway and Automotive Steel Sheets," *Infrastructures,* vol. 8, no. 2, pp. 1-26, 2023.

[32] P.-A. Lemieux and D. J. Durian, "Investigating non-Gaussian scattering processes by using nth-order intensity correlation functions," *Journal of the Optical Society of America A,* vol. 16, no. 7, pp. 1651-1664, 1999.

[33] D. Briers, D. D. Duncan, E. R. Hirst, S. J. Kirkpatrick, M. Larsson, W. Steenbergen, T. Stromberg and O. B. Thompson, "Laser speckle contrast imaging: theoretical and practical limitations," *Journal of Biomedical Optics,* vol. 18, no. 6, pp. 1 - 10, 2013.

[34] R. Bandyopadhyay, A. S. Gittings, S. S. Suh, P. K. Dixon and D. J. Durian, "Speckle-visibility spectroscopy: A tool to study time-varying dynamics," *Review of Scientific Instruments,* vol. 76, no. 9, p. 093110, 2005.

[35] A. B. Parthasarathy, W. J. Tom, A. Gopal, X. Zhang and A. K. Dunn, "Robust flow measurement with multi-exposure speckle imaging," *Optics Express,* vol. 16, no. 3, pp. 1975-1989, 2008.

Improved spatial speckle contrast model for tissue blood flow imaging: Effects of spatial correlation among neighboring camera pixels

Abstract

Significance: Speckle contrast analysis is the basis of Laser Speckle Imaging (LSI), a simple, inexpensive, non-invasive technique used in various fields of medicine and engineering. A common application of LSI is the measurement of tissue blood flow. Accurate measurement of speckle contrast is essential to correctly measure blood flow. Variables such as speckle grain size and camera pixel size affect the speckle pattern and thus the speckle contrast.

Aim: We studied the effects of spatial correlation among adjacent camera pixels on the resulting speckle contrast values.

Approach: We derived a new model that accounts for the potential correlation of intensity values in the common experimental situation where the speckle grain size is larger than the camera pixel size. In vitro phantom experiments were performed to test the model.

Results: Our spatial correlation model predicts that speckle contrast first increases, then decreases as the speckle grain size increases relative to the pixel size. This decreasing trend opposes what is observed with a standard speckle contrast model that does not consider spatial correlation. Experimental data are in good agreement with the predictions of our spatial correlation model.

Conclusions: We present a spatial correlation model that provides a more accurate measurement of speckle contrast, which should lead to improved accuracy in tissue blood flow measurements. The associated correlation factors only need to be calculated once, and open-source software is provided to assist with the calculation.

Introduction

A speckle pattern is created when coherent light is reflected from a rough surface or transmitted through a scattering media. This pattern is made up of regions with high and low intensity and

This chapter has been published as: Julio Cesar Juarez-Ramirez, Beatriz Coyotl-Ocelotl, Bernard Choi, Ruben Ramos-Garcia, Teresita Spezzia-Mazzocco, Julio C. Ramirez-San-Juan, "Improved spatial speckle contrast model for tissue blood flow imaging: effects of spatial correlation among neighboring camera pixels," J. Biomed. Opt. 28(12) 125002 (5 December 2023) https://doi.org/10.1117/1.JBO.28.12.125002

depends on the distribution of scatterers. Static scatterers create a static speckle pattern, while dynamic scatterers create a dynamic speckle pattern. Speckle patterns appear in images collected with many detection systems, including radar [1, 2], microscopy [3, 4, 5], astronomy [6, 7, 8], and ultrasound [9, 10]. Biological samples produce speckle patterns with different dynamics in different regions, such as those associated with blood vessels. Regions rich in blood vessels, like skin, are of particular interest to monitor skin lesions, such as wounds, ulcers, and tumors. It has also been used to assess the efficacy of various treatments, such as topical creams and laser therapy. Additionally, speckle pattern imaging (SPI) can be used to study the effects of aging and diseases, such as diabetes, on skin microcirculation. When recorded by a camera with finite exposure time, dynamic speckle patterns are blurred, and this local blurring is related to the movement of scatterers, such as blood flow, and can be measured as speckle contrast (K).

Speckle contrast analysis is the basis of Laser Speckle Contrast Imaging (LSCI), a low-cost, noninvasive technique used in different areas of medicine such as dentistry [11, 12], ophthalmology [13, 14], dermatology [15, 16], neurobiology [17, 18], and neuroscience [19, 20]. Common uses of LSCI are to measure blood flow [48, 49] and perform intraoperative assessment of tissue perfusion [23].

For LSCI, the propagation of coherent light through scattering media produces a speckle pattern captured with a digital camera. If the medium contains moving scatterers, the speckle pattern fluctuates proportionally to the scatterers' speed. If the exposure time is longer than the correlation time of the backscattered light, the speckle visibility will be reduced. In 1981, Fercher and Briers first measured blood flow speed using LSCI [24] and derived the following expression for the contrast K:

$$K = \frac{\sigma}{\langle I \rangle} = \left(\frac{\tau_c}{2T} \left\{ 1 - e^{-\frac{2T}{\tau_c}} \right\} \right)^{1/2}, \quad (1)$$

where T is the camera exposure time, τ_c is the correlation time of the backscattered light from the sample, σ is the standard deviation and $\langle I \rangle$ the average intensity.

Since this seminal paper, the LSCI technique has evolved and therefore the contrast calculation too. For example, Lemieux and Durian [25] added a correction factor β (which depends on the ratio of the pixel and speckle grain size) to the Siegert relation that links the intensity dynamics associated with scatterer motion with the electric field dynamics [26], resulting in $g_2(\tau) = 1 + \beta|g_1(\tau)|^2$, where $g_1(\tau)$ is the electric field autocorrelation function and $g_2(\tau)$ is the intensity autocorrelation function. In 2005, Bandyopadhyay et al. [27] corrected an over simplification on the derivation of equation (1), applying a double integral of $\tau = t_1 - t_2$, obtaining:

$$K^2 = \beta \frac{e^{-2x} - 1 + 2x}{2x^2}, \tag{2}$$

where $x = T/\tau_c$. This expression still considers only the light scattered from dynamic scatterers and dimensionless pixels. Several groups [19, 25, 27, 28] have since demonstrated the necessity of considering speckle not only from dynamic scatterers but also stationary scatterers. Static scatterers affect the Siegert relation [25] and thus the contrast, resulting in a revised form of g_2:

$$g_2(\tau) = 1 + A\beta|g_1(\tau)|^2 + B\beta|g_1(\tau)|, \tag{3}$$

where $A = \frac{I_f^2}{(I_f+I_s)^2}$, $B = \frac{2I_fI_s}{(I_f+I_s)^2}$, and I_s and I_f represent the contributions from the static and dynamical scattered light, respectively.

$$K = \beta^{1/2}\left[\rho^2 \frac{e^{-2x} - 1 + 2x}{2x^2} + 4\rho(1-\rho)\frac{e^{-x} - 1 + x}{x^2} + (1-\rho)^2\right]^{1/2} + C_n, \tag{4}$$

where $\rho = \frac{I_f}{(I_f+I_s)}$ is the fraction of the fluctuating component of light that interacts with dynamic scatterers, and C_n is an offset term that considers the noise contribution to the measurement.

In reference [27] the authors proposed a technique to measure β experimentally. Accounting for the finite size of the camera pixels [29] led to an analytical expression for β, assuming Gaussian illumination:

$$\beta^{1/2}(M) = \sqrt{1/M}\,\mathrm{erf}\left(\sqrt{\pi M}\right) - (1/(\pi M))(1 - e^{-\pi M}), \tag{5}$$

where M is the ratio between the pixel area and the speckle area (i.e., the speckle grain size). $\beta^{1/2}(M)$ effectively corresponds to the spatial contrast with a sliding window of one pixel size. Equation (5) describes the effect of pixel and speckle sizes on the theoretical calculation of speckle contrast. However, it does not consider the likely correlation among neighboring pixels.

With the derivation of the equations above, the correlation between neighboring pixels is neglected, and hence are valid only for small speckle area compared to the pixel area ($M \geq 1$). When the speckle area is larger than the pixel area ($M < 1$), these models do not fit experimental data well. Here, we present a mathematical model that considers correlations between neighboring pixels to improve the agreement between theoretical and experimental contrast measurements for any size of speckle and pixel areas ($M > 0$).

Theory

Spatial correlation model

Several computational algorithms [30, 31] exist to calculate the speckle contrast from a single raw speckle image or set of images. Application of spatial statistics [24, 32] to a single image is probably the most common approach. This analysis typically implements a sliding square window to calculate the local speckle contrast as the standard deviation of pixel intensities divided by the mean intensity. However, the process of the sliding window is not taken into in the current theoretical model (any of the above mentioned models), which can lead to an inaccurate contrast calculation, and therefore to an inaccurate blood flow calculation. Indeed, it is necessary to consider not only the contribution of the physical size of the camera´s pixel (autocorrelation) but also the effect of the size of the sliding window to improve the accuracy of β and therefore of the contrast.

Skipetrov et. al. [33] employed a sliding window of 3×3 pixels. In this work, we expand on their analysis to extend it to a sliding window of any size to measure an accurate blood flow speed. We show that the mathematical model considering the statistical analysis of the sliding window agrees well with experimental data.

We assume a speckle pattern $I(\vec{r})$ recorded by a digital camera, where $\vec{r} = x\hat{\imath} + y\hat{\jmath}$ is the position vector on the CCD image. Here, we consider a sliding window of $\sqrt{N} \times \sqrt{N}$ pixels, with N being an odd number. We define the speckle spot size as comprising a subregion of $(2p + 1) \times (2p + 1)$ pixels in size, where $p \in \mathbb{Z}^+$ and $2p + 1 \leq \sqrt{N}$. Within this subregion, the pixels are assumed to be spatially correlated. Figure 1 (a) shows a schematic representation of the sliding window (pink rectangles) and one possible example of a correlation subregion (blue triangles).

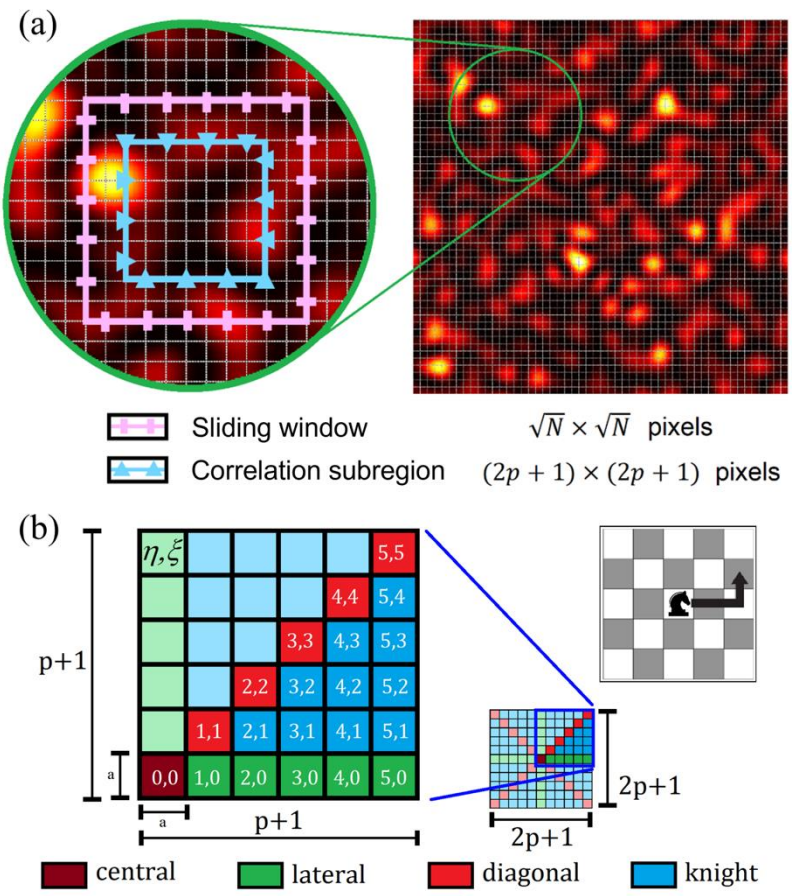

Figure 1. (a) Schematic representation of the sliding window of ($\sqrt{N} \times \sqrt{N}$) pixels (pink) and the correlation subregion of $(2p+1)^2$ (blue). In this example, the sliding window of size $\sqrt{N} = 11$, and correlation subregion of size $2p+1 = 7$ is shown. (b) Schematic representation of the correlation region of $(2p+1)^2$ pixels, with a close-up view of the first quadrant, and a chess board showing the movement of a knight. Some pixels are labeled with their coordinates, and they are colored according to their type (see text for details).

Figure 1 (b) shows the corresponding coordinates (η, ξ) for each pixel of the sliding window, where $\eta, \xi \in \left\{0, \pm 1, \pm 2 \dots, \pm \frac{\sqrt{N}-1}{2}\right\}$ and a correlation subregion containing different types of correlations: central, lateral, diagonal and knight-type. It is important to mention that all pixels within the subregion are correlated and all of them are considered on calculations. However, due to symmetry, many of the correlations are repeated several times. For example, since the lateral pixels $(0, \eta)$, $(\eta, 0)$, $(0, -\eta)$ and $(-\eta, 0)$ are all at the same distance from the central pixel of the sliding window, they are equally correlated with the central pixel, and therefore this correlation value is repeated four times.

Considering a pixel with area a^2, the analytic expression for the speckle contrast calculated over an arbitrary sliding window size of $\sqrt{N} \times \sqrt{N}$ pixels, and hence an arbitrary correlation subregion of $(2p+1) \times (2p+1)$ pixels, may be written as (details can be found in appendix 2):

$$K_s^2(N,p) = \frac{1}{\mu_{0,0}} - \frac{1}{N(N-1)}\left(4\sum_{\eta=1}^{p}\left(\sqrt{N}-\eta\right)\sqrt{N}\,\frac{1}{\mu_{\eta,0}} + 4\sum_{\eta=1}^{p}\left(\sqrt{N}-\eta\right)^2\frac{1}{\mu_{\eta,\eta}} + 8\sum_{\xi=1}^{p-1}\sum_{\eta=\xi+1}^{p}\left(\sqrt{N}-\eta\right)\left(\sqrt{N}-\xi\right)\frac{1}{\mu_{\eta,\xi}}\right), \quad (6)$$

where each summation inside the parentheses stands for a diagonal, lateral, or knight-type correlation, respectively. As described in appendix 2, equation (6) is valid for $p \geq 2$, i.e., a 5×5 subregion. For $p = 1$, there is no knight correlation, and thus the double summation does not exist. For $p = 0$, there is no lateral, diagonal or knight-type correlation, and thus the terms in parentheses equal zero. Here, we consider only $p \geq 2$. $1/\mu_{\eta,\xi}$ is the correlation factor of the pixel with coordinates (η, ξ) and with the central pixel $(0,0)$ of the sliding window, given by:

$$\frac{1}{\mu_{\eta,\xi}} = \frac{1}{a^4}\int_{a(2\xi-1)/2}^{a(2\xi+1)/2}\int_{a(2\eta-1)/2}^{a(2\eta+1)/2}\int_{-a/2}^{a/2}\int_{-a/2}^{a/2} {g_1}^2(x-x', y-y')\,\mathrm{d}x\,\mathrm{d}y\mathrm{d}x'\,\mathrm{d}y', \quad (7)$$

where g_1 is a first-order correlation function. At this point, we have not considered the correlation function $\left({g_1}^2(\vec{r}-\vec{r}')\right)$; this will be the topic of the next section. The factor β in equation (4) corresponds to the spatial contrast $K_s^2(N,p)$ (i.e, $\beta = K_s^2(N,p)$) for any window size, while equation (5), $K_s^2(N,p)$ takes into account not only the finite dimension of the pixel but its possible spatial correlation.

Table 1 shows expressions for the spatial contrast using equation (6) for the first four different dimensions of the sliding window.

Table 1. Expressions for equation (6) for sliding window sizes of 1×1 *(i.e., autocorrelation),* $3 \times 3, 5$ *x* 5*, and* 7×7 *pixels.*

$K_s^2(1^2,0)$	$\frac{1}{\mu_{0,0}}$
$K_s^2(3^2,1)$	$\frac{1}{\mu_{0,0}} + \left(-\frac{1}{3}\frac{1}{\mu_{1,0}}\right) + \left(-\frac{2}{9}\frac{1}{\mu_{1,1}}\right)$
$K_s^2(5^2,2)$	$\frac{1}{\mu_{0,0}} + \left(-\frac{2}{15}\frac{1}{\mu_{1,0}} - \frac{1}{10}\frac{1}{\mu_{2,0}}\right) + \left(-\frac{8}{75}\frac{1}{\mu_{1,1}} - \frac{3}{50}\frac{1}{\mu_{2,2}}\right) + \left(-\frac{4}{25}\frac{1}{\mu_{2,1}}\right)$
$K_s^2(7^2,3)$	$\frac{1}{\mu_{0,0}} + \left(-\frac{1}{14}\frac{1}{\mu_{1,0}} - \frac{5}{84}\frac{1}{\mu_{2,0}} - \frac{1}{21}\frac{1}{\mu_{3,0}}\right) + \left(-\frac{3}{49}\frac{1}{\mu_{1,1}} - \frac{25}{588}\frac{1}{\mu_{2,2}} - \frac{4}{147}\frac{1}{\mu_{3,3}}\right) + \left(-\frac{5}{49}\frac{1}{\mu_{2,1}} - \frac{4}{49}\frac{1}{\mu_{3,1}} - \frac{10}{147}\frac{1}{\mu_{3,2}}\right)$

As it seen in Table 1, the contribution of each lateral, diagonal and knight correlation decreases with increasing subregion size.

Gaussian velocity distribution function

For a Gaussian-shaped laser beam, the spatial correlation function also is Gaussian in shape.

Analytical solutions

The Gaussian correlation function ${g_1}^2(\vec{r}-\vec{r}') = exp\left[-\frac{\pi}{2}\frac{(x-x\prime)^2+(y-y\prime)^2}{A_c}\right]$ [33, 34] may be written using a change of variables $w = x - x'$, $\bar{w} = (x + x')/2$, $u = y - y'$, and $\bar{u} = (y + y')/2$:

$$g_1(w,u) = \exp\left[-\frac{\pi}{2}\frac{(w^2+u^2)}{A_c}\right], \tag{8}$$

where A_c is the correlation area (i.e., speckle size) For a speckle area with radius b:

$$g_1^2(w,u) = \left(\exp\left[-\frac{\pi}{2}\frac{(w^2+u^2)}{\pi\, b^2}\right]\right)^2 = \exp[-(w^2+u^2)/b^2], \tag{9}$$

Substituting equation (9) into (7), we obtain:

$$\begin{aligned}\frac{1}{\mu_{\eta,\xi}} = \frac{1}{4\pi^2M^2} \times \Big(& e^{-\pi M(\eta-1)^2} - 2e^{-\pi M\eta^2} + e^{-\pi M(\eta+1)^2} \\ & + \pi\sqrt{M}\big((\eta-1)erf\big[\sqrt{\pi M}(\eta-1)\big] - 2\eta Erf\big[\sqrt{\pi M}\eta\big] + (\eta \\ & + 1)erf\big[\sqrt{\pi M}(\eta+1)\big]\big)\Big) \\ & \times \Big(e^{-\pi M(\xi-1)^2} - 2e^{-\pi M\xi^2} + e^{-\pi M(\xi+1)^2} \\ & + \pi\sqrt{M}\big((\xi-1)erf\big[\sqrt{\pi M}(\xi-1)\big] - 2\xi erf(\sqrt{\pi M}\xi) + (\xi \\ & + 1)erf\big[\sqrt{\pi M}(\xi+1)\big]\big)\Big).\end{aligned} \tag{10}$$

where $M = a^2/\pi b^2$ is the ratio of the pixel area and the speckle area. Equation (10) provides an expression for speckle contrast that is similar to that described in section 4.6 of reference. [35].

Equations (6) and (10) are programmed and available in MATLAB and Mathematica, see Code, Data, and Materials Availability.

One particular case is when $p = 0$ (i.e., autocorrelation), corresponding to a spatial correlation subregion of only a single pixel. For this case, we obtain the well-established analytic expression for spatial speckle contrast [29]:

$$K_s^2(N, p=0) = \frac{1}{\mu_{0,0}} = \frac{1}{\pi^2M^2}\left(-1 + e^{-\pi M} + \pi\sqrt{M}erf\left[\sqrt{\pi M}\right]\right)^2. \tag{11}$$

Equation (11) is identical to the correction factor β (see equation (5)) proposed in references [19] and [25].

Table 2 shows the first $1/\mu_{\eta,\xi}$ factors needed to calculate the speckle contrast for 1×1, 3×3, 5×5 and 7×7 sliding windows.

Table 2 Correlation factors calculated using equation (10) needed to calculate the speckle contrast of a 7×7 sliding window.

central	
$\frac{1}{\mu_{0,0}}$	$\frac{1}{M^2\pi^2}\left(-1+e^{-M\pi}+\sqrt{M}\pi\mathrm{erf}\left(\sqrt{M}\sqrt{\pi}\right)\right)^2$
lateral	
$\frac{1}{\mu_{1,0}}$	$\frac{1}{2M^2\pi^2}\left(-1+e^{-M\pi}+\sqrt{M}\pi\mathrm{erf}\left(\sqrt{M}\sqrt{\pi}\right)\right)\left(1+e^{-4M\pi}-2e^{-M\pi}-2\sqrt{M}\pi\left(\mathrm{erf}\left(\sqrt{M}\sqrt{\pi}\right)-\mathrm{erf}\left(2\sqrt{M}\sqrt{\pi}\right)\right)\right)$
$\frac{1}{\mu_{2,0}}$	$\frac{1}{2M^2\pi^2}(-1+e^{-M\pi}+\sqrt{M}\pi\mathrm{erf}(\sqrt{M}\sqrt{\pi}))(e^{-9M\pi}-2e^{-4M\pi}+e^{-M\pi}+\sqrt{M}\pi(\mathrm{erf}(\sqrt{M}\sqrt{\pi})-4\mathrm{erf}(2\sqrt{M}\sqrt{\pi})+3\mathrm{erf}(3\sqrt{M}\sqrt{\pi})))$
$\frac{1}{\mu_{3,0}}$	$\frac{1}{2M^2\pi^2}\left(-1+e^{-M\pi}+\sqrt{M}\pi\mathrm{erf}\left(\sqrt{M}\sqrt{\pi}\right)\right)\left(e^{-16M\pi}-2e^{-9M\pi}+e^{-4M\pi}+2\sqrt{M}\pi\left(\mathrm{erf}\left(2\sqrt{M}\sqrt{\pi}\right)-3\mathrm{erf}\left(3\sqrt{M}\sqrt{\pi}\right)+2\mathrm{erf}\left(4\sqrt{M}\sqrt{\pi}\right)\right)\right)$
diagonal	
$\frac{1}{\mu_{1,1}}$	$\frac{1}{4M^2\pi^2}\left(1+e^{-4M\pi}-2e^{-M\pi}-2\sqrt{M}\pi\left(\mathrm{erf}\left(\sqrt{M}\sqrt{\pi}\right)-\mathrm{erf}\left(2\sqrt{M}\sqrt{\pi}\right)\right)\right)^2$
$\frac{1}{\mu_{2,2}}$	$\frac{1}{4M^2\pi^2}\left(e^{-9M\pi}-2e^{-4M\pi}+e^{-M\pi}+\sqrt{M}\pi\left(\mathrm{erf}\left(\sqrt{M}\sqrt{\pi}\right)-4\mathrm{erf}\left(2\sqrt{M}\sqrt{\pi}\right)+3\mathrm{erf}\left(3\sqrt{M}\sqrt{\pi}\right)\right)\right)^2$
$\frac{1}{\mu_{3,3}}$	$\frac{1}{4M^2\pi^2}\left(e^{-16M\pi}-2e^{-9M\pi}+e^{-4M\pi}+2\sqrt{M}\pi\left(\mathrm{erf}\left(2\sqrt{M}\sqrt{\pi}\right)-3\mathrm{erf}\left(3\sqrt{M}\sqrt{\pi}\right)+2\mathrm{erf}\left(4\sqrt{M}\sqrt{\pi}\right)\right)\right)^2$
knight	
$\frac{1}{\mu_{2,1}}$	$\frac{1}{4M^2\pi^2}\left(1+e^{-4M\pi}-2e^{-M\pi}-2\sqrt{M}\pi\left(\mathrm{erf}\left(\sqrt{M}\sqrt{\pi}\right)-\mathrm{erf}\left(2\sqrt{M}\sqrt{\pi}\right)\right)\right)\left(e^{-9M\pi}-2e^{-4M\pi}+e^{-M\pi}+\sqrt{M}\pi\left(\mathrm{erf}\left(\sqrt{M}\sqrt{\pi}\right)-4\mathrm{erf}\left(2\sqrt{M}\sqrt{\pi}\right)+3\mathrm{erf}\left(3\sqrt{M}\sqrt{\pi}\right)\right)\right)$
$\frac{1}{\mu_{3,1}}$	$\frac{1}{4M^2\pi^2}\left(1+e^{-4M\pi}-2e^{-M\pi}-2\sqrt{M}\pi\left(\mathrm{erf}\left(\sqrt{M}\sqrt{\pi}\right)-\mathrm{erf}\left(2\sqrt{M}\sqrt{\pi}\right)\right)\right)\left(e^{-16M\pi}-2e^{-9M\pi}+e^{-4M\pi}+2\sqrt{M}\pi\left(\mathrm{erf}\left(2\sqrt{M}\sqrt{\pi}\right)-3\mathrm{erf}\left(3\sqrt{M}\sqrt{\pi}\right)+2\mathrm{erf}\left(4\sqrt{M}\sqrt{\pi}\right)\right)\right)$

$\frac{1}{\mu_{3,2}}$	$\frac{1}{4M^2\pi^2}\Big(e^{-9M\pi} - 2e^{-4M\pi} + e^{-M\pi} + \sqrt{M}\pi\left(\mathrm{erf}\left(\sqrt{M}\sqrt{\pi}\right) - 4\mathrm{erf}\left(2\sqrt{M}\sqrt{\pi}\right) + 3\mathrm{erf}\left(3\sqrt{M}\sqrt{\pi}\right)\right)\Big)\Big(e^{-16M\pi} - 2e^{-9M\pi} + e^{-4M\pi} + 2\sqrt{M}\pi\left(\mathrm{erf}\left(2\sqrt{M}\sqrt{\pi}\right) - 3\mathrm{erf}\left(3\sqrt{M}\sqrt{\pi}\right) + 2\mathrm{erf}\left(4\sqrt{M}\sqrt{\pi}\right)\right)\Big)$

Numerical solution

We integrated equation (7) numerically using Mathematica 11 and compared the resultant solution to the analytical solution in equation (10). A good agreement between the analytic and numerical solution is observed (Figure 2).

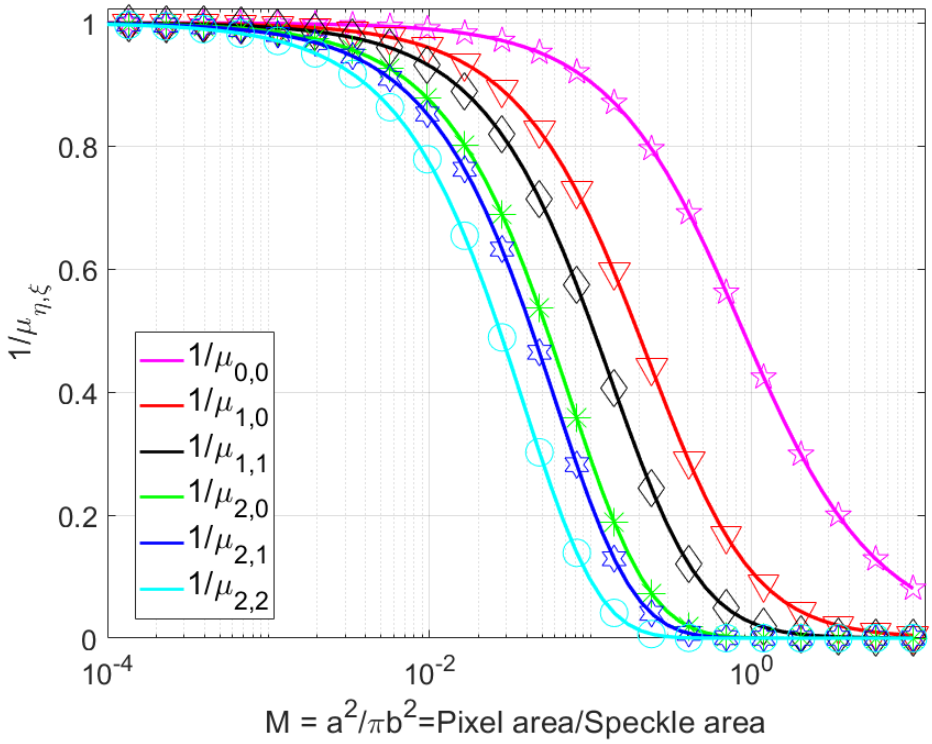

Figure 2. Comparison between the analytical expression (solid lines) using equation (10) and a numerical solution (symbols) of equation (7) using Mathematica 11.

The parameters $1/\mu_{0,0}$, $1/\mu_{1,0}$, $1/\mu_{1,1}$ are sufficient to calculate the contrast K for a spatial correlation subregion of 3×3 pixels [36]. For a subregion of 5×5 pixels, we also should include the terms $1/\mu_{2,0}$, $1/\mu_{2,1}$, $1/\mu_{2,2}$ [37]. Now it is possible to calculate the speckle contrast using equation (10) for any arbitrary odd size of sliding window ($\sqrt{N}$) and subregion ($2p + 1$).

Figure 3 shows the plots of the analytical (solid lines) and numerical (symbols) contrast for a correlation subregion of 1×1 (i.e., no spatial correlation), 3×3, and 5×5 pixels using equation (6). When the speckle size is larger than the pixel size ($i.e., M < 1$), each speckle grain spans multiple pixels, resulting in spatial correlation among adjacent pixels within the sliding window. Due

to this correlation, the standard deviation σ of intensity values within the sliding window decreases for $M < 1$, resulting in an associated decrease in K. When the speckle size is smaller than the pixel size (i.e., $M > 1$), each pixel contains intensity contributions from multiple speckle grains, leading to a lack of spatial correlation among adjacent pixels within the sliding window. In addition, the integration of multiple grains per pixel leads to a reduction in intensity variance in the speckle pattern.

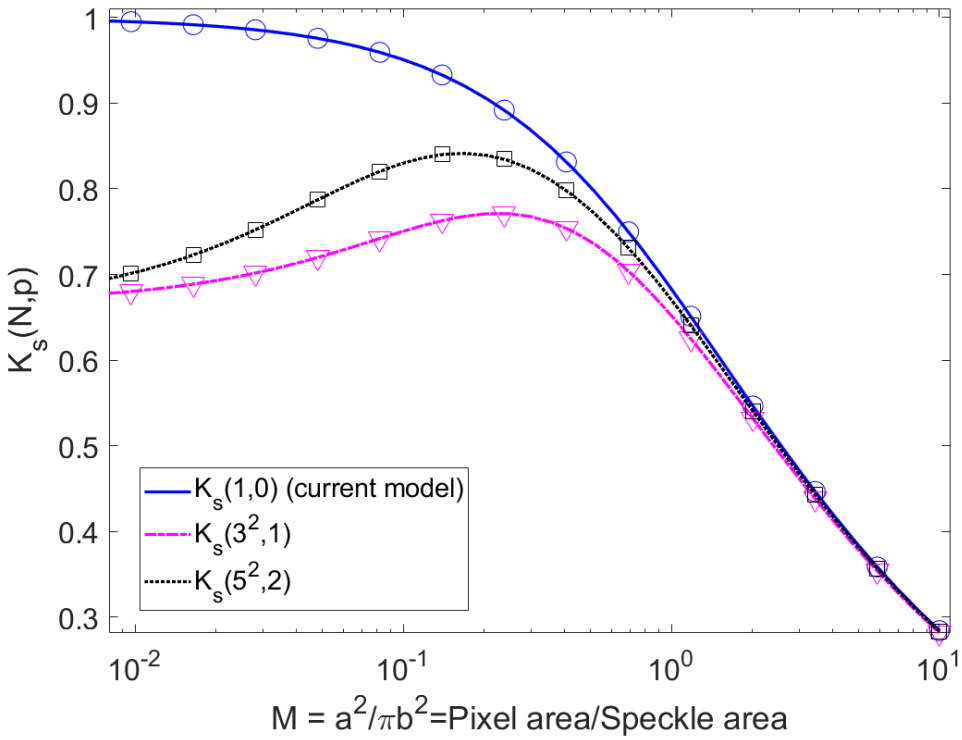

Figure 3. Solid lines show the contrast calculated using equation (6) for a correlation subregion of 1×1 (no spatial correlation), 3×3, 5×5 pixels, in blue, pink, and black respectively. The circle, triangle and square marks show the numerical solution using Mathematica 11 for spatial correlation sub-matrices of 1×1, 3×3, and 5×5 pixels. Good agreement is observed between the numerical and analytical expressions.

In Figure 3 it is show that for each size of sliding window, there is a different maximum contrast, hence, in order to maximize the contrast range, it is possible to choose the sliding window size for a given pixel and speckle area and vice versa, it is possible to choose the ratio M for a given sliding window size.

Experimental validation of proposed model

Laser light from a coherent source (Verdi, Coherent Inc., $\lambda = 532\,nm$) was expanded and collimated. Then, the light passed through a diffuser to achieve a homogeneous illumination of a flow phantom, which consisted of a microfluidic slide (thinXXS Microtechnology AG) with channel diameter of $300\,\mu m$. Intralipid (1%) was delivered with a syringe-based infusion pump into the channels at flow speeds from 4 to $20\,mm/s$ in step of $2\,mm/s$. Raw speckle were recorded with a CCD camera (Retiga 2000R) ($7.4\,\mu m \times 7.4\,\mu m$ pixel area). The camera was equipped with a macro

lens with a variable aperture (Figure 4). See reference [38] for a detailed explanation of the experimental setup.

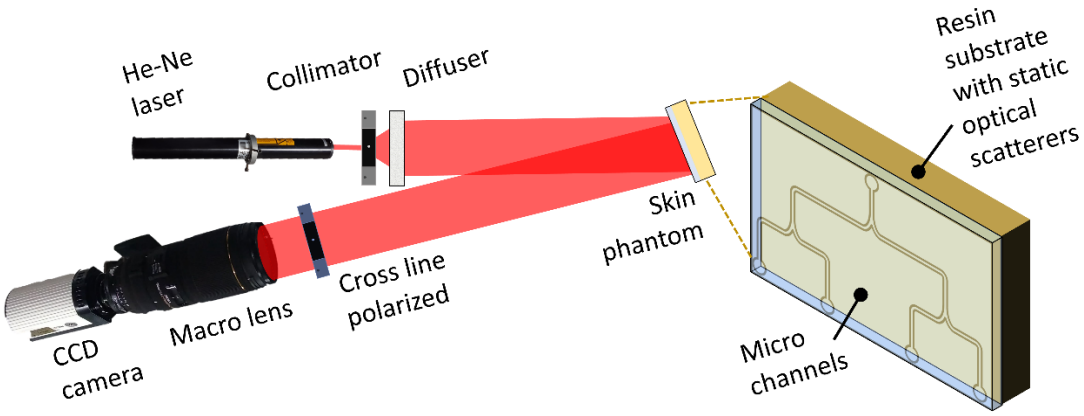

Figure 4. Experimental setup used to test the spatial speckle correlation model. An expanded and collimated 532 nm laser illuminated the skin phantom. A Retiga CCD camera equipped with a variable-aperture macro acquired speckle images. A linear polarizer was placed in front of the lens to mitigate specular reflectance contributions to the images.

We modified the speckle size by changing the $f\#$ of the lens attached to the CCD camera:

$$speckle\ size = 2.44(Mag + 1)\lambda\ f\#, \tag{12}$$

where Mag is the magnification of the lens. The spatial speckle contrast was calculated from the experimental data using a sliding window of $N = 3^2, 7^2\ and\ 15^2$.

Figure 5 shows the mathematical prediction of speckle contrast using equation (6) and the experimental data. The curves generated with equation (7) overlap when $M \geq 1$ but diverge when $M < 1$. Considering no correlation between neighboring pixels, the speckle contrast K_0 calculated by the model approaches 1 when M approaches zero (black continuous line) which is a contradiction, as the standard deviation should approach zero in that scenario and therefore the speckle contrast approaches zero, as observed experimentally. The speckle contrast must be less than one when M is less than one. When correlation subregions (i.e., 3×3, 5×5) are considered, speckle contrast reduces for lower values of M as expected.

The relationship between the pixel and the speckle grain size has an important effect on the speckle contrast [39]. Figure 5 shows spatial contrast calculated using a standard spatial contrast algorithm ($K_s(1,0)$), which does not consider the potential spatial correlation of adjacent pixels, and calculations with our analytic model considering a sliding window of 3×3, 7×7, and 15×15 pixels. For different window sizes, the curves have a different maximum contrast at different values of M. Therefore, with our model, knowledge of M is sufficient to choose the appropriate sliding window and correlation subregion sizes to achieve the maximum speckle contrast.

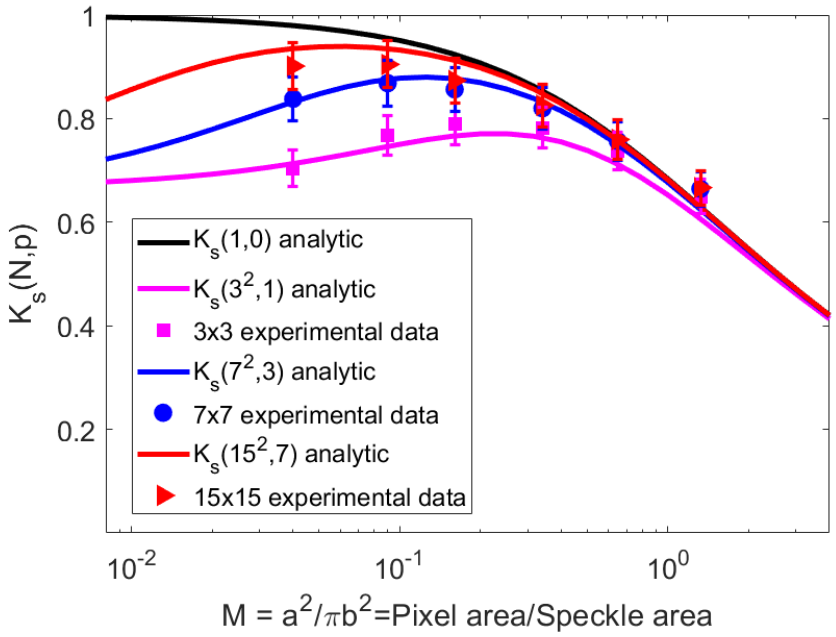

Figure 5. Solid lines show the contrast $K_S(3^2,1)$, $K_S(7^2,3)$ and $K_S(15^2,)$ calculated using equation (6) and (10) for spatial correlation sub-matrix of 3×3, 7×7 and 15×15 pixels in pink, blue and red respectively. Dots show the experimental data for 3×3, 7×7 and 15×15 pixels, in pink, blue and red respectively.

We note that the experimental data in Figure 5 agrees with calculations using our analytic model for all interrogated values of M. For $M \ll 1$ (the speckle grain size is larger than the pixel), choosing a sub-matrix at least as large as the speckle size to minimize loss of potential correlation between pixels is recommended.

Given a particular experimental setup and a sliding window size, M, N and p are defined. Therefore, the correction factor $\beta = K_s\,(N,p)$ (equation (6)) should be utilized to determine the perfusion index ($PI = 1/\tau_c$) from the contrast (K) obtained with the sliding window, and given by equations (2) or (4). Considering $T \gg \tau_c$, the PI is given by [34]: $PI = \beta/TK^2$.

In Figure 5, we use these window sizes merely as an example. However, the size of the sliding window is at the user's discretion based on the characteristics of the speckle image they are analyzing. It should be noted that the larger the sliding window size, the greater the loss of spatial resolution.

Figure 6 illustrates the impact of the correction factor $\beta = K_s\,(N,p)$ on the PI image (for $T \gg \tau_c$), for two sliding window sizes (first row: 3×3 and second row: 7×7 pixels) and a fixed value of $M = 0.0338$. The first column, (a) and (d), shows the PI without considering the correlation between pixels (equation (5)), resulting in $\beta = K_s(1,0) = 0.9827$. The second column, (b) and (e), shows the corrected PI (equation (6)) by considering all the potential correlations within the sliding window. In this case, the correction factors are $K_s\,(3^2,1) = 0.7073$ and $K_s\,(7^2,3) = 0.8198$ respectively. The third column, (c) and (f), is the difference between the first two columns. As shown, when $N = 3^2$, the error in PI calculation is nearly 30% and when $N = 7^2$, the error is approximately 20% with $M = 0.0338$. The PI images shown in Figure 6 represent the average PI over 30 frames.

From Figure 6, we can observe that the difference between the first two columns is only the scalar multiplication by the correction factor, thus preventing the overestimation of the PI.

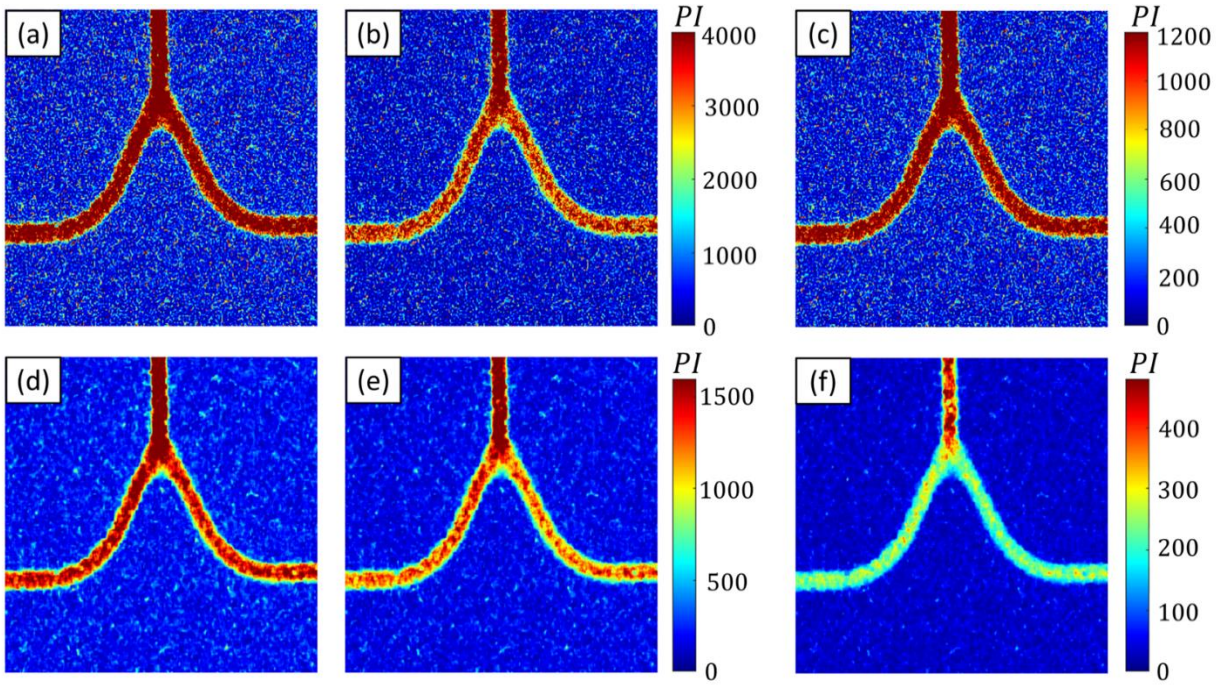

Figure 6. Accounting for the spatial correlation among pixels is required to calculate an accurate Perfusion Index (PI). In the first row, images (a), (b), (c) correspond to the $PI = \beta/TK^2$ calculated using a sliding window of 3×3. In the second row, (d), (e), (f) correspond to a sliding window of 7×7 pixel, with $M = 0.0338$. The first column, (a), (d), shows the PI without considering the correlation between pixels, i.e., $\beta = K_s(1,0) = 0.9827$. The second column, (b), (e), shows the corrected PI, $\beta = K_s\,(3^2, 1) = 0.7073$ and $\beta = K_s\,(7^2, 3) = 0.8198$, respectively. The third column, (c), (f), is the difference between the first two columns.

Conclusions

We present a more accurate estimation of the constant β and therefore of the contrast speckle contrast value by considering the effects of spatial correlation among the neighboring pixels. For a wide range of ratios of speckle grain size to pixel size, our model estimates the theoretical value of contrast more accurately than the standard model that does not consider the potential spatial correlation among adjacent pixels [35]. For the special case of Gaussian illumination, we present an analytical solution for the spatial speckle contrast of any spatial correlation sub-matrix size. The resultant impact of our new model is a more accurate estimation of speckle contrast, which in turn should lead to improved estimations of tissue blood flow.

Acknowledgments

J. C. Juarez-Ramirez expresses gratitude to CONAHCYT for the scholarship (grant number 629327).

Code, Data, and Materials Availability

Implementation of equation (6) and (10) as functions in MATLAB and Mathematica are available at the GitHub repository: SpatialSpeckle

References

[1] J. Chen, Y. Kong, D. Zhang, Y. Fu and S. Zhuang, "Two-dimensional phase unwrapping based on U^2-Net in complex noise environment," *Optics Express,* vol. 31, no. 18, pp. 29792-29812, 2023.

[2] M. Ihmeida and M. Shahzad, "Enhanced Change Detection Performance Based on Deep Despeckling of Synthetic Aperture Radar Images," *IEEE Access,* vol. 11, pp. 1-14, 2023.

[3] K. Zhuo, Y. Wang, Y. Ma, S. An, Z. Zalevsky, J. Zheng and P. Gao, "Quantitative Phase Contrast Microscopy with Optimized Partially Coherent Illumination," *Photonics,* vol. 10, no. 391, pp. 1-9, 2023.

[4] J. Zhao, B. Liang, E. Dobo, M. J. Khan, E. Yang and D. Kang, "Speckle and Shadow Artifacts Reduction in Scattering-Based Light Sheet Microscopy," in *Biophotonics Congress: Optics in the Life Sciences 2023 (OMA, NTM, BODA, OMP, BRAIN),* , 2023.

[5] S. Morawiec, P. Stremplewski, A. Ajduk, B. F. Kennedy and M. Szkulmowski, "Dynamic full-field optical coherence microscopy of early mammalian oocytes," in *Multiscale Imaging and Spectroscopy IV;*, San Francisco, 2023.

[6] W. Thompson, C. Marois, C. R. Do Ó, Q. Konopacky, J.-B. Ruffio, J. Wang, A. J. Skemer, R. J. De Rosa and B. Macintosh, "Deep Orbital Search for Additional Planets in the HR 8799 System," *The astronomical journal,* vol. 165, no. 1, p. 29, 2023.

[7] A. Tokovinin, "Exploring Thousands of Nearby Hierarchical Systems with Gaia and Speckle Interferometry," *The Astronomical Journal,* vol. 165, no. 4, p. 180, 2023.

[8] J. Kammerer, C. C. Stark, K. J. Ludwick, R. Juanola-Parramon and Bijan Nemati, "Simulating Reflected Light Coronagraphy of Earth-like Exoplanets with a Large IR/O/UV Space Telescope: Impact and Calibration of Smooth Exozodiacal Dust," *The Astronomical Journal,* vol. 164, no. 6, p. 235, 2022.

[9] Y. Zhou and Y. Fang, "Diagnosis of breast cancer lesion using ultrasound images, elastography, and Ki-67 protein cell proliferation index: Ultrasound images, elastography, and Ki-67 protein in breast cancer," *Cellular and molecular biology,* vol. 69, no. 4, pp. 16-23, 2023.

[10] D. C. P. a. D. W. Park, "Ultrasound Speckle Decorrelation-Based Blood Flow Measurements," *Ultrasound in Medicine & Biology,* vol. 49, no. 7, pp. 1491-1498, 2023.

[11] T. Sato, M. Miyazaki, A. Rikuta and K. Kobayashi, "Application of the Laser Speckle-Correlation Method for Determining the Shrinkage Vector of a Light-cured Resin," *Denntal Materials Journal,* vol. 23, no. 3, pp. 284-290, 2004.

[12] C. Stoianovici, P. Wilder-Smith and B. Choi, "Assessment of Pulpal Vitality Using Laser Speckle Imaging," *Laser in Surgery and Medicine,* vol. 43, no. 8, pp. 833-837, 2011.

[13] D. D. Patel and D. M. Lipinski, "Validating a low-cost laser speckle contrast imaging system as a quantitative tool for assessing retinal vascular function," *Scientific Reports,* pp. 1-11, 2020.

[14] A. I. Srienc, Z. L. Kurth-Nelson and E. A. Newman, "Imaging retinal blood flow with laer speckle flowmetry," *Frontiers in Neuroenergetics,* vol. 2, pp. 128-1 - 128-10, 2010.

[15] B. Choi, N. M. Kang and J. S. Nelson, "Laser speckle imaging for monitoring blood flow dynamics in the in vivo rodent dorsal skin fold model," *Microvascular Research,* vol. 68, pp. 143-146, 2004.

[16] J. Cracowski, F. Gaillard-Bigot, C. Cracowski, M. Roustit and C. Millet, "Skin microdualysis coupled with laser Speckle Contrast Imaging to assess microvascular reactivity," *Microvascular Research,* vol. 82, no. 3, pp. 333-338, 2011.

[17] A. K. Dunn, "Laser Speckle Contrast Imaging of Cerebral Blood Flow," *Annals of Biomedical Engineering,* vol. 40, pp. 367-377, 2012.

[18] G. A. Armitage, K. G. Todd, A. Shuaib and I. R. Winship, "Laser speckle contrast imaging of collateral blood flow during acute ischemic stroke," *Journal of Cerebral Blood Flow & Metabolism,* vol. 30, pp. 1432-1436, 2010.

[19] D. A. Boas and A. K. Dunn, "Laser speckle contrast imaging in biomedical optics," *Journal of biomedical optics,* vol. 15, no. 1, p. 011109, 2010.

[20] J. Senarathna, A. Rege, N. Li and N. V. Thakor, "Laser Speckle Contrast Imaging: Theory, Instrumentation and Applications," *IEEE Reviews in Biomedical Engineering,* vol. 6, pp. 99-110, 2013.

[21] J. D. Briers and S. Webster, "Laser Speckle Contrast Analysis (LASCA): A Nonscanning, Full-field Technique For Monitoring Capillary Blood Flow," *Journal of Biomedical Optics,* vol. 1, no. 2, pp. 174-179, 1996.

[22] J. D. Briers, "Laser speckle contrast imaging for measuring blood flow," *Optica Applicata,* vol. 37, no. 1-2, pp. 139-152, 2007.

[23] E. A. Mannoh, G. Thomas, C. C. Solórzano and A. Mahadevan-Jansen, "Intraoperative assessment of parathyroid viability using laser speckle contrast imaging," *Scientific reports,* vol. 7, pp. 1-11, 2017.

[24] A. F. Fercher and J. D. Briers, "Flow visualization by means of single-exposure speckle photography," *Optics Communications,* vol. 37, no. 5, pp. 326 - 330, 1981.

[25] P.-A. Lemieux and D. J. Durian, "Investigating non-Gaussian scattering processes by using nth-order intensity correlation functions," *Journal of the Optical Society of America A,* vol. 16, no. 7, pp. 1651-1664, 1999.

[26] D. Briers, D. D. Duncan, E. R. Hirst, S. J. Kirkpatrick, M. Larsson, W. Steenbergen, T. Stromberg and O. B. Thompson, "Laser speckle contrast imaging: theoretical and practical limitations," *Journal of Biomedical Optics,* vol. 18, no. 6, pp. 1 - 10, 2013.

[27] R. Bandyopadhyay, A. S. Gittings, S. S. Suh, P. K. Dixon and D. J. Durian, "Speckle-visibility spectroscopy: A tool to study time-varying dynamics," *Review of Scientific Instruments,* vol. 76, no. 9, p. 093110, 2005.

[28] A. B. Parthasarathy, W. J. Tom, A. Gopal, X. Zhang and A. K. Dunn, "Robust flow measurement with multi-exposure speckle imaging," *Optics Express,* vol. 16, no. 3, pp. 1975-1989, 2008.

[29] J. C. Ramírez San Juan, R. Ramos García, G. Martínez Niconoff and B. Choi, "Simple correction factor for laser speckle imaging of flow dynamics," *Optics Letters,* vol. 39, no. 3, pp. 678-681, 2014.

[30] J. C. Ramirez San Juan, C. Regan, B. Coyotl Ocelotl and B. Choi, "Spatial versus temporal laser speckle contrast analyses in the presence of static optical scatterers," *Journal of Biomedical Optics,* vol. 19, no. 10, pp. 106009-1-5, 2014.

[31] M. Draijer, E. Hondebrink, T. van Leeuwen and W. Steenbergen, "Review of laser speckle contrast techniques for visualizing tissue perfusion," *Lasers in Medical Science,* vol. 24, pp. 639-651, 2009.

[32] J. W. Goodman, Statistical Optics, Wiley-Interscience, 2000.

[33] S. E. Skipetrov, J. Peuser, R. Cerbino, P. Zakharov, B. Weber and F. Scheffold, "Noise in laser speckle correlation and imaging techniques," *Optics Express,* vol. 18, no. 14, pp. 14519-14534, 2010.

[34] J. C. Ramírez San Juan, R. Ramos García, I. Guizar Iturbide, G. Martinez Niconoff and B. Choi, "Impact of velocity distribution assumption on simplified laser speckle imaging equation," *Optics Express,* vol. 16, no. 5, pp. 3197-3203, 2008.

[35] J. W. Goodman, Speckle Phenomena in Optics: Theory and Applications, Robert & Company, 2007.

[36] J. C. Juárez Ramírez, B. Coyotl Ocelotl, R. Ramos García, R. Chiu Zarate, T. Spezzia Mazzocco, J. P. Padilla Martínez and J. C. Ramírez San Juan, "Speckle Contrast Calculation and Pixel

Correlation," in *Proceedings of the 1st International Conference on Optics, Photonics and Lasers (OPAL' 2018)*, Barcelona, 2018.

[37] B. Coyotl Ocelotl, J. C. Juárez Ramírez, R. Ramos García, R. Chiu, T. Spezzia Mazzocco and J. C. Ramírez San Juan, "Speckle contrast calculation based on pixels correlation: spatial analysis," in *Interferometry XIX*, San Diego, 2018.

[38] J. C. Ramirez-San-Juan, E. Mendez-Aguilar, N. Salazar-Hermenegildo, A. Fuentes-Garcia, R. Ramos-Garcia and B. Choi, "Effects of speckle/pixel size ratio on temporal and spatial speckle-contrast analysis o dynamic scattering systems: Implication for measurements of blood-flow dynamics," *Biomedical Optics Express,* vol. 4, no. 10, p. 1883, 2013.

[39] S. J. Kirkpatrick, D. D. Duncan and E. M. Wells-Gray, "Detrimental effects of speckle-pixel size matching in laser speckle contrast imaging," *Optics Letters,* vol. 33, no. 24, pp. 2886-2888, 2008.

Improved temporal speckle contrast model for slow and fast dynamic samples: effect of temporal correlation among neighboring camera pixels

Abstract

Significance: Speckle contrast analysis (spatial or temporal) is a valuable optical technique that is widely used in medical and engineering fields due to its simplicity, affordability, and non-invasive attributes. It is based on the statistical analysis of the dynamic speckle pattern emanating from the sample under study, which provides information about the dynamics and/or health of the sample. Despite its advantages, challenges remain in accurately measuring temporal speckle contrast, especially for slow dynamic samples. In such cases, existing mathematical models fail to accurately reflect the experimental data, potentially leading to misinterpretation of the analyzed results.

Aim: To address these limitations, a novel mathematical model that considers the correlation between neighboring pixels is introduced. As the second part of our proposed model, in this work, we focus on temporal correlation (i.e. neighboring frames) for the calculation of the temporal speckle contrast.

Approach: We theoretically reproduce the statistical analysis normally performed to compute temporal speckle contrast in a set of sequentially raw speckle images. In this case, our calculations consider the likely correlation between neighboring pixels over time (neighbor frames), which has been neglected in previous models. To test this model, Escherichia coli ATCC 25922 colonies were analyzed using the proposed model.

Results: Considering the likely temporal correlation between neighboring pixels, the proposed model significantly improves the accuracy of temporal speckle contrast measurements for slow dynamic samples. Analytical expressions for the contrast are obtained considering both Gaussian and Lorentzian correlation functions, which show excellent agreement with experimental results done in E. coli colonies. For fast dynamic samples where neighboring pixels are not correlated, our model recovers the results of the current model.

Conclusions: The proposed model is suitable for the calculation of temporal contrast for both slow and fast dynamics, which makes this tool suitable for application in biological and industrial systems.

This chapter has been send to the Journal of Biomedical Optics with the title; Improved temporal speckle contrast model for slow and fast dynamic samples: effect of temporal correlation among neighboring camera pixels.

Introduction

Laser speckle is a random interference pattern created when coherent laser light illuminates a rough or scattering surface. It's worth noting that laser speckle can be observed not only on rough surfaces but also in media with scattering particles, such as biological tissues. In such cases, the interaction between coherent laser light and static and/or moving scatterers (for instance, tissue and red blood cells) within the tissue generates static and/or dynamic speckle pattern.

Analyzing the intensity fluctuations within the speckle pattern, whether in the spatial, temporal, or combined domains, presents a significant challenge to extract valuable information about the dynamics of the sample. Dynamic speckle analysis has found applications in diverse fields, for instance, in the industrial context, it has provided insights into the degradation processes of metal surfaces due to corrosion [1, 2] and the characterization of drying dynamics during paint application [3, 4]. In the bio-arena, it has enabled the non-invasive assessment of blood flow dynamics [5, 6, 7], the evaluation of seed viability for agricultural purposes [8, 9, 10], the dynamic behavior of microorganism [9, 11, 12], among others.
To analyze dynamic speckle, various contrast analysis techniques have been developed. In reference [13], the authors provide a comprehensive overview of these techniques, highlighting their individual strengths and applications. Some of these techniques include Generalized Differences [14], Weighted Generalized Differences [14], Fuji's Method [15], Time History of the Speckle Pattern (THSP) [16], Speckle Contrast Imaging (both spatial and temporal), among others. Since the dynamics of a sample can originate from different sources, each technique yields different results, and their interpretation depends on the specific experiment, sample characteristics, and the expertise of the analyst.
Laser Speckle Contrasts Imaging (LSCI) is commonly used to study objects with fast dynamics, where the exposure time (T) is on the order or greater than the correlation time (τ_c) of the backscattering light coming from the sample such as blood vessels. LSCI finds direct applications in various medical areas, including the analysis of the skin [17, 18], retina [19, 20], brain [21, 22, 23, 24], among others.
LSCI offers two possible approaches: the spatial regimen, which analyzes the spatial variations of the grains on a single raw speckle image [13, 21, 25], and the temporal regimen, which analyzes its temporal variations [13, 21, 26]. One of its main advantages is that the experimental methods for calculating the contrast match reasonably well with the theoretical model for high dynamics (i.e., blood flow), which has allowed establishing an inverse proportionality relationship between τ_c and blood flow speed.

Regrettably, the existing theory of LSCI falls short in capturing the dynamics of slow-moving objects (where $\tau_c > T$) such as bacterial colonies. This discrepancy becomes apparent when comparing the experimental results to the predictions of the current LSCI models [25, 26, 27, 28, 29] For instance, if we examine a series of consecutive speckle images acquired within the correlation time, the images exhibit high correlation, suggesting that the temporal contrast should approach zero. However, according to the current LSCI models, the contrast is expected to be close to one. This discrepancy arises because the current models assume the correlation between frames is zero, which is only valid for fast dynamics when the frames are acquired during times greater than the correlation time. Many researchers focused on the fast dynamics' scenario, and the mathematical model works reasonably well. The likely correlation between frames plays a crucial role in accurately calculating the temporal speckle contrast for both fast and slow dynamics scenarios.

In this study, we address this limitation by incorporating the correlation between neighboring frames into the calculation of the temporal speckle contrast. By considering this additional factor, we propose an improved theoretical model that yields more accurate results for slow dynamic samples. Notably, our theoretical predictions align remarkably well with the corresponding experimental results, providing a significant advancement in understanding and characterizing slow dynamic phenomena.

Furthermore, our approach ensures compatibility with the well-established results for highly dynamic samples, maintaining the consistency and applicability of LSCI across a wide dynamic range. By accounting for

the correlation between neighboring frames, we achieve a more comprehensive and reliable analysis of speckle contrast in various scenarios, including both slow and fast dynamics.

Theory

Temporal LSCI

Fercher and Bries [25] developed a method called single-exposure speckle photography, which enables full-field monitoring of flow fields by exploiting the relationship between the spatial contrast of a time-integrated speckle pattern and the speed of the scatterers responsible for the speckle formation. Their technique involves the temporal integration of the backscattered light at a single pixel. By integrating the temporal variations of the speckle pattern at a specific pixel, Fercher and Bries derived an expression to calculate the speckle contrast considering Lorentzian correlation. This expression allows for quantifying the level of contrast in the speckle pattern in the following way;

$$K = \frac{\sigma}{\langle I \rangle} = \left(\frac{\tau_c}{2T}\left\{1 - e^{-\frac{2T}{\tau_c}}\right\}\right)^{1/2}, \tag{1}$$

where T is the exposure time and τ_c is the correlation time of the backscattered light, σ is the standard deviation, and $\langle I \rangle$ the mean intensity of one point over all the frames, respectively. To enhance the spatial resolution of the contrast image, a minimum of fifteen frames are averaged, with thirty frames been the most employed practice.

Fercher and Bries' model does not account for the physical size of the pixel, neglecting both spatial and temporal correlations between neighboring pixels and frames, respectively. It is only valid for exposure times greater than the correlation time (fast dynamics). For instance, it is suitable for measuring blood vessels but not applicable for slow dynamics such as seed growing.
Several researchers [26, 27, 28, 29] have been improving the model until the equation;

$$K = \alpha^{1/2}\beta^{1/2}(M)\left[\rho^2\frac{e^{-2x} - 1 + 2x}{2x^2} + 4\rho(1-\rho)\frac{e^{-x} - 1 + x}{x^2} + (1-\rho)^2\right]^{1/2} + C_n, \tag{2}$$

where, $x = T/\tau_c$, M is the ratio between the pixel area over the correlation area, ρ is the fraction of the total light attributed to dynamical scatterers, C_n is a constant term accounting for experimental noise [26], α is a normalization (proportionality) term that accounts for effects that reduce speckle contrast such as the light polarization and β corresponds to the spatial component of the contrast [30]. For no spatial correlation, it is given by [27, 30]; $\beta^{1/2}(M) = \sqrt{1/M}\,\mathrm{erf}\left(\sqrt{\pi M}\right) - (1/(\pi M))(1 - e^{-\pi M})$.

Equation (2) describes the temporal contrast for Lorentzian correlation by considering factors including the physical size and geometry of the camera pixel, the contributions of both stationary and dynamical scatterers, noise resulting from external factors. However, it is important to remark that equations (2) do not consider the temporal correlation between neighboring frames. Equation (2) represent the state of the art, this model serves as the basis for other works aiming to model the speckle contrast.

Various computational algorithms can be employed to measure the speckle contrast using one or a set of raw speckle images, for instances, Photothermal LSI [31], Physicochemical Tissue Optical Clearing (PCTOC) [32], Light Speckle Imaging Integrated with Spatial Frequency Domain Imaging (LSI-SFDI) [33], Gradient Analysis and LSI [34], use of Kurtosis [5], among others . One such algorithm is the temporal algorithm [35], which requires a set of consecutive L frames. The contrast K is obtained by calculating the ratio of de standard deviation σ

and the mean intensity $\langle I \rangle$ for each one pixel across the sliding temporal window, which contains L frames. The spatial resolution of the contrast image is identical to the spatial resolution of the original frames. However, the temporal resolution of the contrast image is reduced compared to the temporal resolution of each individual frame because the information from the frames within the sliding temporal window is combined to create the contrast image.

While the theory mentioned above and the temporal algorithm align well for $T > \tau_c$ [36, 37], a well-known problem arises when the set of frames is acquired within the correlation time. In this case, the acquired frames are correlated with each other, resulting in a standard deviation (σ) approaching zero and, consequently, K must approach to zero as well ($K = \sigma/\langle I \rangle \to 0$). However, the present mathematical model without correlation—equation (2)—predict a K value approaching 1 (when $\alpha, \beta, \rho = 1$). This discrepancy is due to the lack of consideration for the temporal correlation between neighboring pixels within the sliding temporal window.

In this work, we solve this disagreement considering the temporal correlation between neighboring pixels for a best estimation of K and, therefore, a more accurate measurement of the speed of the dynamic scatterers. It is shown that the proposed mathematical model has an excellent agreement with experimental data for both regimes: $T > \tau_c$ and $T \leq \tau_c$. In an experiment, the correlation time τ_c is not known a priori. One way to determine it is to solve for x equation (2) numerically.

2.2 Novel proposal for a temporal correlation model

Let us consider a sequence of L raw speckle images taken one after another indexed by $\psi \in \{0,1,2, \dots, L-1\}$ (Figure 1 a) with the same exposure time T and temporal delay δ between the end and the beginning of two consecutive frames (Figure 1 b). The minimal value for δ is the death time of the system, which represents the time required for the system to process the current frame before capturing the next one. However, this value may be greater depending on the specific requirements of the experiment.

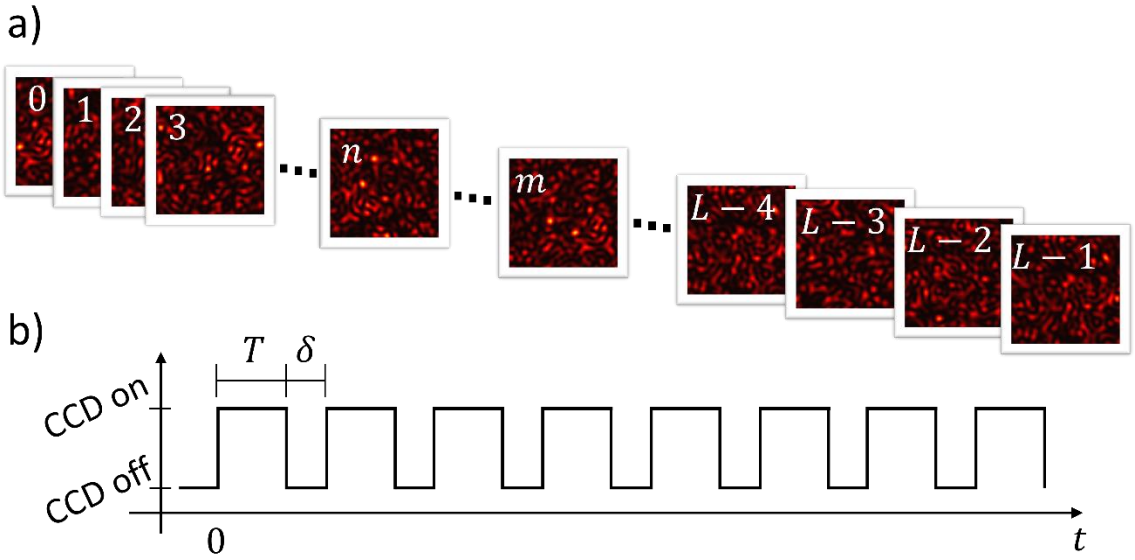

Figure 1. a) Schematic representation of the set of frames. b) Schematic representation of the time the camera is acquiring a frame.

Let us define S as the number of frames acquired within the correlation time. When $S = 0$ it implies that no frame is correlated with any other, and only the autocorrelation within a single frame is meaningful. Conversely, when $S = L - 1$, all L frames exhibit some degree of correlation with each other.

Let us define the ψ-type correlation as the correlation between two frames separated by exactly ψ frames, i.e., the correlation between the $n - th$ frame and the $m - th$ frame, such that, $|m - n| = \psi$. Following this definition, the correlation 0-type corresponds to the autocorrelation. Each frame has one correlation 0-type, see Figure 2. The correlation 1-type represents the correlation between a frame and its adjacent frame (either

the next one or the previous one). Almost every frame has two correlation 1-type —one with the frame that follows and one with the frame that precedes it—except for the first and last frames, which have only one correlation 1-type each. And so on, the correlation $(L-1)$-type represents the correlation between the first and the last frame of the sequence. There are only these two correlations $(L-1)$-type.

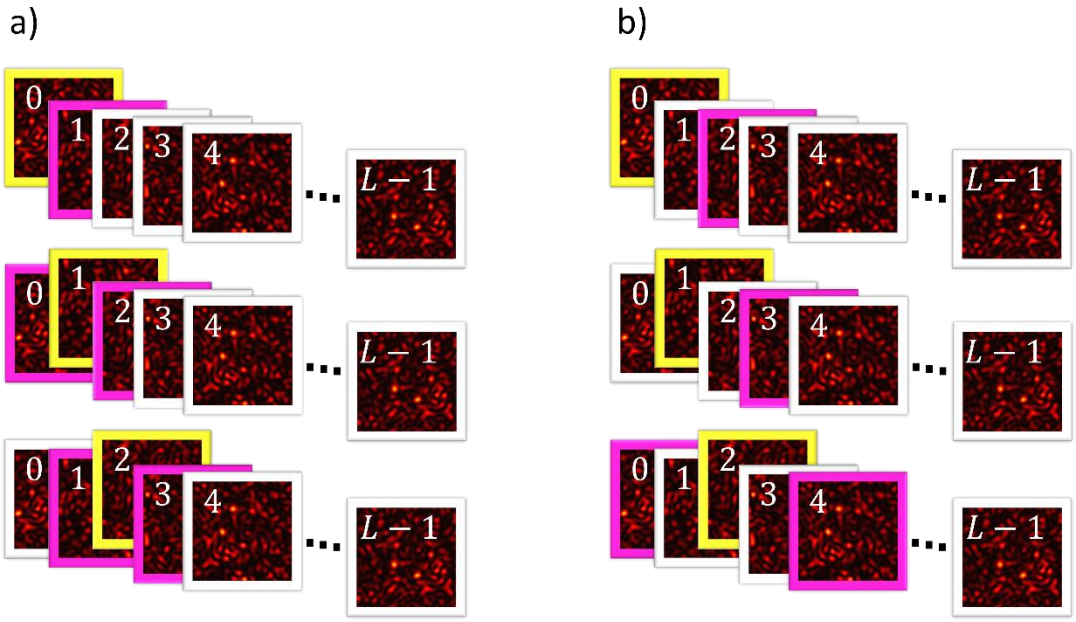

Figure 2. a) Schematic representation of the frame 1-type, the selected frame (yellow frame), and the 1-type in magenta. The first and last frame only has one 1-type correlation, and any other frame has two 1-type correlations b) Schematic representation of the frame 2-type, the selected frame (yellow frame), and the 2-type in magenta. The first two and the last two frames only have one 2-type correlation, and any other frame has two 2-type correlations.

It is evident that there are exactly L autocorrelations in total, i.e., there are L number of 0-type correlation, one for each frame in the sequence. For any other $\psi > 0$, with the limitation $\psi \leq L-1$, each frame may exhibit one or two correlations of ψ-type, depending on the presence of sufficient frames before or after it (see Figure 2). However, it can be proved that the number of correlations of ψ-type denoted by β_ψ is;

$$\beta_\psi = \begin{cases} L & \psi = 0 \\ 2(L-\psi) & 0 < \psi \leq L-1. \end{cases} \quad (3)$$

Considering these likely temporal correlations between neighboring pixels in a set of speckle images acquired with exposure time T, a delay between frames of δ. In the process of calculating the contrast, see the Appendix for full details, it is necessary to compute the correlation for all possible combination of frames, $\frac{1}{L^2}\sum_{\psi=0}^{L-1}\sum_{\psi'=0}^{L-1}\langle I_0, I_\psi\rangle$. All these combinations can be expressed as the sum of three different types of correlations; auto correlations $\sum_{central}\langle I_0, I_\psi\rangle$ when $(\psi = 0)$, correlation between preceding and subsequent frames $\sum_{lateral}\langle I_0, I_\psi\rangle$ when $(\psi \leq S)$, and correlation with frames outside the temporal window of correlation $\sum_{outsiders}\langle I_0, I_\psi\rangle$ when $(\psi > S)$. These correlations are referred to as central, lateral and outsiders respectively, following the notation of our spatial contrast model [30]. For simplicity, previous models have neglected all the correlations except for autocorrelations.
Following the mathematics described in Appendix 1, the temporal contrast may be written as;

$$K_t^2(x,L,S) = \frac{1}{\nu_0} - \frac{2}{L(L-1)}\sum_{\psi=1}^{S}(L-\psi)\frac{1}{\nu_\psi}, \tag{4}$$

where the parameter ν_ψ accounts for the temporal correlation between frames separated by ψ number of frames and is given by;

$$\frac{1}{\nu_\psi} = \frac{1}{T^2}\int_0^T \int_{\psi(T+\delta)}^{(\psi+1)T+\psi\delta} g_1^2(t-t')dt'\,dt, \tag{5}$$

where $g_1(t-t')$ is the temporal field correlation (first-order correlation).

The summation on equation (4) stands for all types of correlation from 1-type to S-type. Let us define those correlations as lateral correlations; as mentioned before, equation (4) is valid for $S \geq 1$. For the case of $S = 0$, there is only autocorrelation, i.e., no lateral correlation; therefore, no summation, then equation (4) is reduced to;

$$K_t^2(x,L,0) = \frac{1}{\nu_0}, \tag{6}$$

where, ν_0 represents only the contribution of the autocorrelation. Henceforth $S \geq 1$ is considered to be consistent with the summation index.

Gaussian correlation function

One of the most frequently used distributions in LSCI is the Gaussian correlation function, which describes laminar (ordered) flow [38, 39]. For instance, the blood flow on blood vessels away from bifurcations may be considered laminar flow and its can be modeled with the Gaussian correlation function. Due to the simpler mathematics, equations (1) and (2) consider Lorentzian correlation instead of Gaussian correlation.

Analytical solutions for Gaussian correlation.

It is possible to solve equation (5) analytically, assuming a Gaussian correlation [37], which is defined to satisfied Mandel´s definition of correlation time (see Appendix 1 for more details);

$$g_1(\tau) = \exp\left[-\frac{\pi}{2}\frac{\tau^2}{{\tau_c}^2}\right]. \tag{7}$$

As before, τ_c represents the correlation time of the backscattered light from the sample.

Substituting equation (7) into (5), we obtain;

$$\begin{aligned}\frac{1}{\nu_\psi} = \frac{1}{2x}\{&\left(\mathrm{erf}\left[\sqrt{\pi}(\psi+\psi\Delta)x\right] - \mathrm{erf}\left[\sqrt{\pi}(\psi-1+\psi\Delta)x\right]\right)(1-\psi-\psi\Delta)\\ &+\left(\mathrm{erf}\left[\sqrt{\pi}(\psi+1+\psi\Delta)x\right] - \mathrm{erf}\left[\sqrt{\pi}(\psi+\psi\Delta)x\right]\right)(1+\psi+\psi\Delta)\}\\ &+\frac{1}{2\pi x^2}(\exp[-\pi(\psi-1+\psi\Delta)^2x^2] - 2\exp[-\pi(\psi+\psi\Delta)^2x^2]\\ &+\exp[-\pi(\psi+1+\psi\Delta)^2x^2]),\end{aligned} \tag{8}$$

where $\Delta = \delta/T$ and $x = T/\tau_c$. In Figure 3, the first seven ($\psi = 0,1,\ldots,7$) different correlation factors $1/\nu_\psi$ are plotted for a) $\Delta = 0$ and b) $\Delta = 5$.

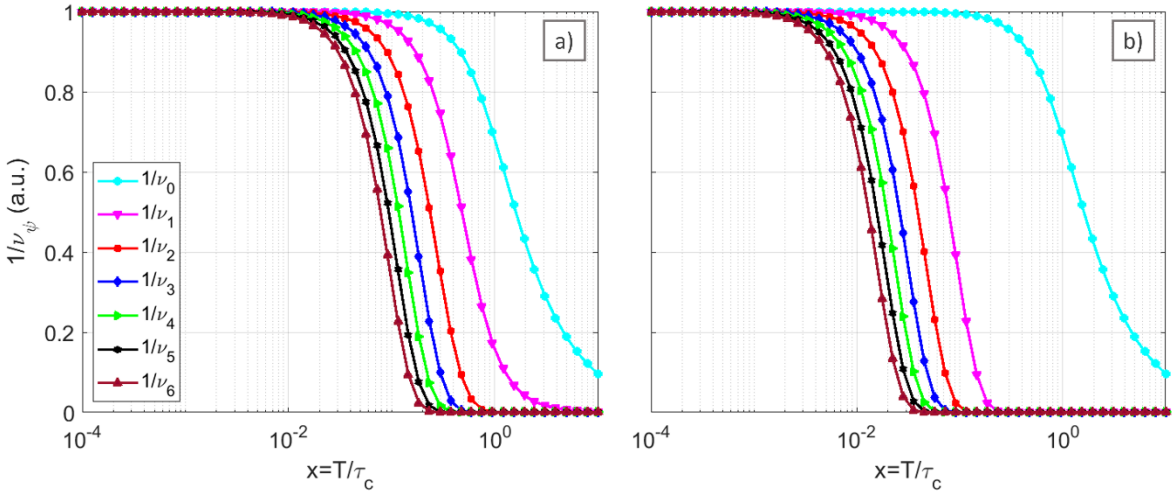

Figure 3. First seven gaussian correlation factors for $\psi = 0$ to $\psi = 7$ considering a) $\Delta = 0$ and b) $\Delta = 5$.

Let us note that for the simplest case ($\psi = 0$), our analytical solution for $1/\nu_\psi$, equations (6) and (8), recovers the well-known expression for the temporal contrast reported in [37], which does not consider the correlation between neighbors pixels;

$$K_t^2(x, L, S) = \frac{1}{\nu_0} = \frac{\mathrm{erf}\left[\sqrt{\pi}x\right]}{x} + \frac{\exp[-\pi x^2] - 1}{\pi x^2}. \tag{9}$$

It is important to note that equation (9) does not depend on Δ, as expected, since only autocorrelation is considered; therefore, the delay between frames does not matter.

Figure 4 shows the temporal contrast as a function of x for $L = 1, 15, 30,\ 40$, and $S = L - 1$, using equations (4) and (8) for (a) $\Delta = 0$ and (b) $\Delta = 5$. The cyan line corresponds to the current models (equations (1) and (2) when $\alpha, \beta, \rho = 1$), i.e., stationary scatterers are not considered. It predicts a monotonically decreasing contrast as a function of x, starting from one and decaying to zero.

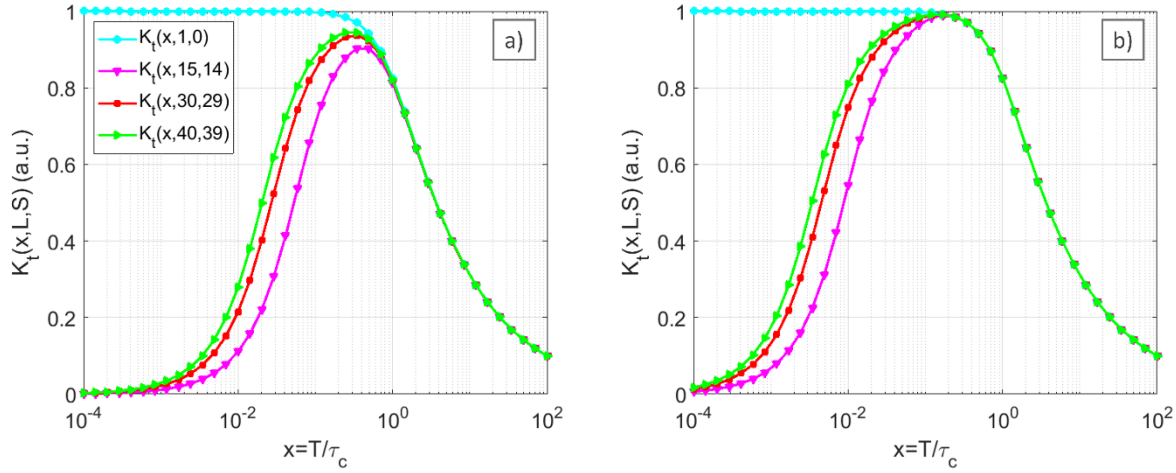

Figure 4. Contrast (equation (4) and (8)) for gaussian correlation and $L = 1, 15, 30,\ 40$ a) considering $\Delta = 0$ and b) $\Delta = 5$.

On the other hand, when the correlation is taken into account between neighbor frames, each contrast curve exhibits a distinct local maximum, which is not predicted by equations (1) or (2), occurring at different values of x. The frames are highly correlated for small x values (close to zero), and therefore, the temporal contrast

should be close to zero, as predicted correctly by our model. In contrast, equations (1) or (2) predicts a temporal contrast value close to 1 for this scenario. On the other hand, for $x \approx 1$ or greater, both models match.

Lorentzian correlation function

Brownian motion is more accurately described by the Lorentzian correlation function [38, 39]. This correlation function is commonly employed in LSCI due to its simplicity, for instance, equations (1) and (2), consider the Lorentzian distribution.

Analytical solutions for Lorentzian distribution

It is possible to solve equation (5) analytically, assuming a Lorentzian distribution [37], which is defined to satisfied Mandel´s definition of correlation time (see Appendix 1 for more details);

$$g_1(\tau) = \exp\left[-\frac{|\tau|}{\tau_c}\right]. \tag{10}$$

Due to the presence of the absolute value in equation (10), the solution is calculated in two cases, for $\psi = 0$ and $\psi > 0$. For $\psi = 0$;

$$\frac{1}{\nu_0} = \frac{1}{2x^2}(2x + \exp[-2x] - 1), \tag{11}$$

for $\psi > 0$;

$$\frac{1}{\nu_\psi} = \frac{1}{4x^2}\left(-2\exp[-2(\psi + \psi\Delta)x] + \exp[-2\big((\psi - 1) + \psi\Delta\big)x] + \exp[-2\big((\psi + 1) + \psi\Delta\big)x]\right), \tag{12}$$

as before, $\Delta = \delta/T$ and $x = T/\tau_c$. In Figure 5, the first seven ($\psi = 0,1, \ldots ,7$) different correlation factors $1/\nu_\psi$ are plotted for a) $\Delta = 0$ and b) $\Delta = 5$.

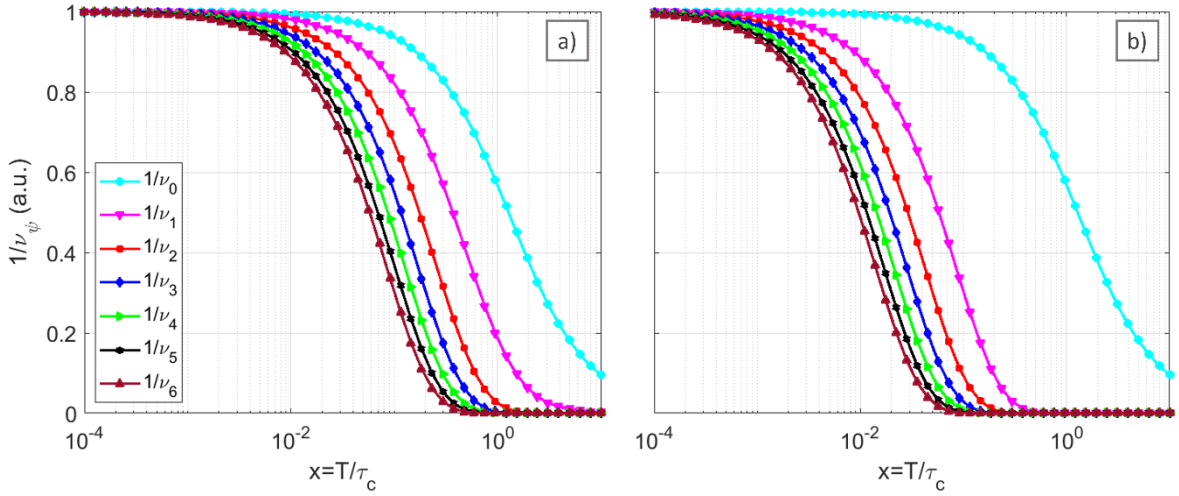

Figure 5. First seven lorentzian correlation factors for $\psi = 0$ to $\psi = 7$ considering a) $\Delta = 0$ and b) $\Delta = 5$.

For the simplest case $\psi = 0$, our analytical solution for $1/\nu_\psi$, equation (11), recover the well-known expression for temporal contrast reported in the literature [36, 38, 28, 37, 40];

$$K_t^2(x,L,S) = \frac{1}{\nu_0} = \frac{1}{2x^2}(2x + \exp[-2x] - 1). \quad (13)$$

Let us note that, similar to Gaussian correlation, equation (13) does not depend on Δ, as expected, since only autocorrelation is considered; therefore, the delay between frames does not matter in this case.

The implementation on MATLAB and Mathematica of temporal contrast K_t (eq. (4)) and $1/\nu_\psi$ for Gaussian and Lorentzian correlation (equations (8), (11) and (12)) for any ψ are programmed and available in MATLAB and Mathematica, see Code, Data, and Materials Availability section.

Figure 6 shows the contrast for $L = 1, 15, 30,\ 40$, and $S = L - 1$, using equations (4), (8) (11) and (12) for $\Delta = 0$ and $\Delta = 5$. Once again, the cyan line corresponds to the current model where the correlation between neighbor frames is not considered.

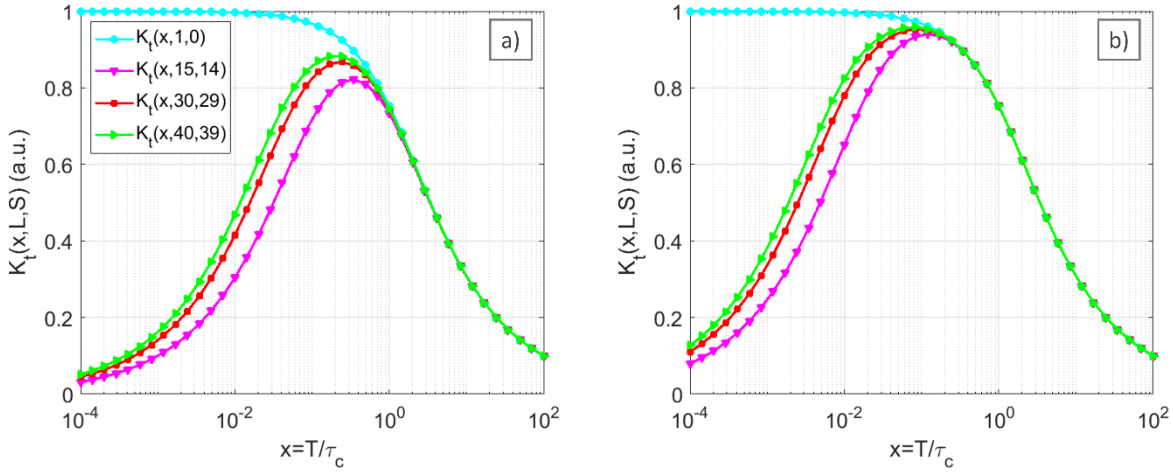

Figure 6 Contrast (equation (4) and (8)) for Lorentzian correlation and $L = 1, 15, 30,\ 40$,, a) considering $\Delta = 0$ and b) $\Delta = 5$.

When the correlation between neighbor frames is considered, each contrast curve has a different local maximum (not predicted by the current model) at different values of x; moreover, all the maximums were shifted to the left compared with $\Delta = 0$. The frames are highly correlated for small x values (close to zero). Therefore, the temporal contrast should be close to zero which aligns with our model. In contrast, equations (1) and (2) when $\alpha, \beta, \rho = 1$ predicts a temporal contrast value close to 1 for this case. However, for x around 1 or x greater than 1 both models match.

Experimental verification

Experimental setup

We conducted an experiment using a slow enough dynamics sample (Escherichia coli colony) to verify our theoretical model. This allowed us to acquire images within the correlation time using a standard CCD camera Retiga 2000R, $7.4\ \mu m \times 7.4\ \mu m$ pixel area.

The experimental setup is shown in Figure 7. A He-Ne laser (Melles Griot, 20 mW, 632 nm wavelength) illuminates an engineered diffuser, which in turn, homogeneously illuminates the sample. The CCD camera was placed 20° out of the laser beam's axis to avoid ballistic light. No lens was used on the CCD camera.

Biological sample

As mentioned before, we used a colony of the strain E. coli ATCC 25922 as a sample. The colony was grown on soy dextrose agar (BD Bioxon) for 24 h at 37°C. The growth obtained was collected in a 1X phosphate-buffered saline solution (PBS) (Omnichem). The necessary dilutions were made to obtain a final 5 x 103 cells/ml concentration. Consecutively, 50 μl from this solution were inoculated in a $60 \times 15\ mm$ Petri dish by the spread plate technique and incubated at 37°C for 24 h expecting to find a growth of isolated colonies on the agar. Under these conditions, the dynamics of the sample are slow, with a correlation time around five minutes, as shown in Figure 8, which is considerably slower compared to blood flow.

After E. coli colonies were grown, the Petri dishes were placed on the experimental setup mentioned before over a floating table, and an isolated colony was chosen for images acquisition. The image acquisition was carried out at room temperature ($20 - 25°C$). A set of 901 frames was captured with an exposure time of $T = 1\ s$. The delay between frames is $\delta = 347\ ms$. For these parameters, $\Delta = \delta/T = 347$ respectively.

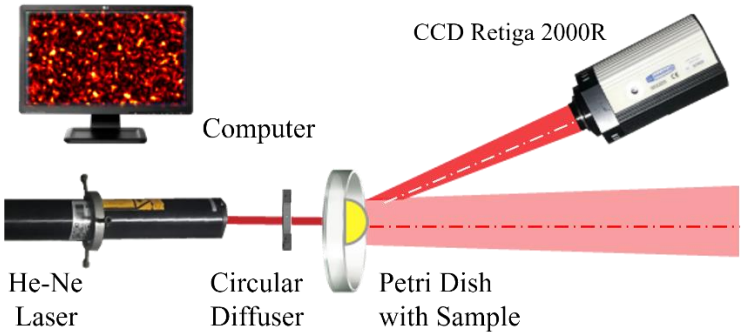

Figure 7 Setup scheme, a He-Ne laser illuminated an E. coli *sample in transillumination. The camera is out of axis to avoid saturation due to ballistic light with little interaction with the sample, so its direction is almost unchanged, so it contains little information about the sample.*

Experimental results

For each exposure time (T), the correlation time τ_c from the corresponding set of images (Figure 8 for $T = 1\ s$) was calculated by fitting the correlation of the first frame against all the subsequent frames (magenta triangles). The correlation is fitted using both Lorentzian and Gaussian correlation functions, represented by the red and blue lines respectively.

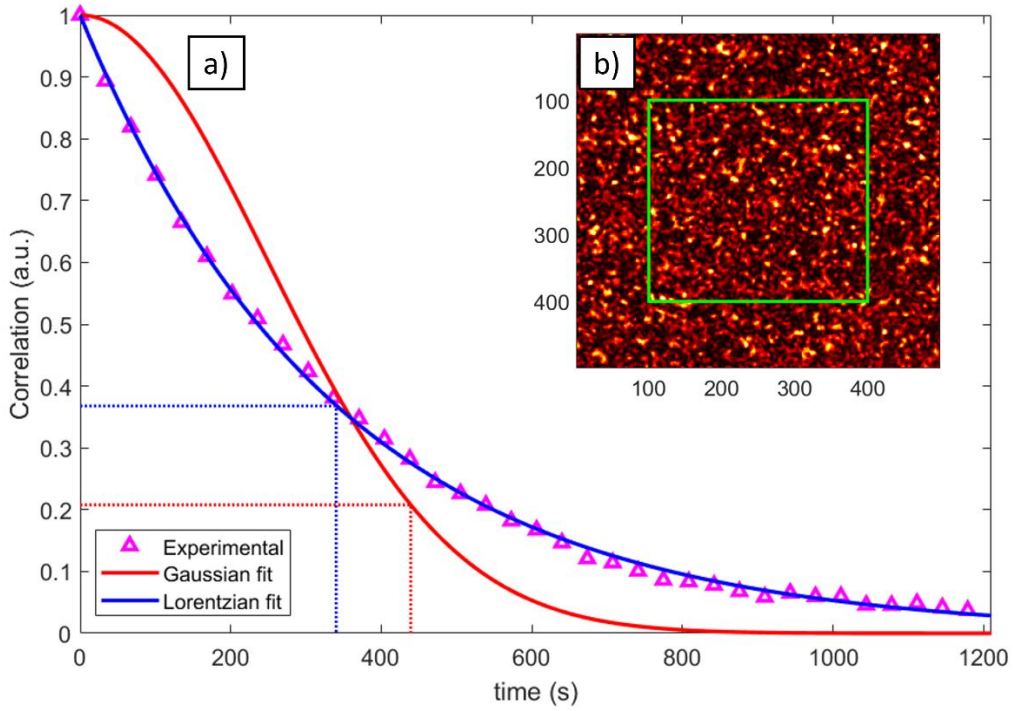

Figure 8 a) Correlation between the first frame versus the rest (magenta triangles), Lorentzian, and Gaussian fit (blue and red lines, respectively). The Lorentzian correlation time for this set of frames is $\tau_{cl} = 340.76\ s$ (blue dashed line) and for Gaussian correlation time $\tau_{cg} = 439.01\ s$ (red dashed line) b) Typical speckle frame and the interest region (green square) of 300×300 pixels. The exposure time is $T = 1\ s$.

All calculations were made for Gaussian and Lorentzian models; nevertheless, only the Lorentzian results are presented in this work because, as shown in Figure 8, the Lorentzian fit adjusts better than the Gaussian fit. Therefore, the dynamic behavior of the E. coli colony is similar to Brownian motion [38, 39] .

Since the sample is a living E. coli colony, its dynamic may change considerably meanwhile the frames are acquired due to various factors as the temperature, the laser light, the colony age, the amount of nutrients in the Petri dish, among others. In order to compare the same dynamic (correlation time) with different exposure time, we captured experimental data with exposure time $T = 1\ s$. Using these frames, we integrated ω consecutively frames, to simulated experimental data with exposure time greater than one second. The Lorentzian correlation time is measured as $\tau_{cl} = 340.76\ s$. We considered ω values ranging from 1 to 30. Figure 9 illustrates the temporal contrast plotted against x, calculated using 30 frames ($L = 30$). In Figure 9 a), the experimental data is presented in a logarithmic plot, while Figure 9 b) provides a zoomed-out view with a logarithmic scale on the x-axis. The region of interest is highlighted within a red rectangle.

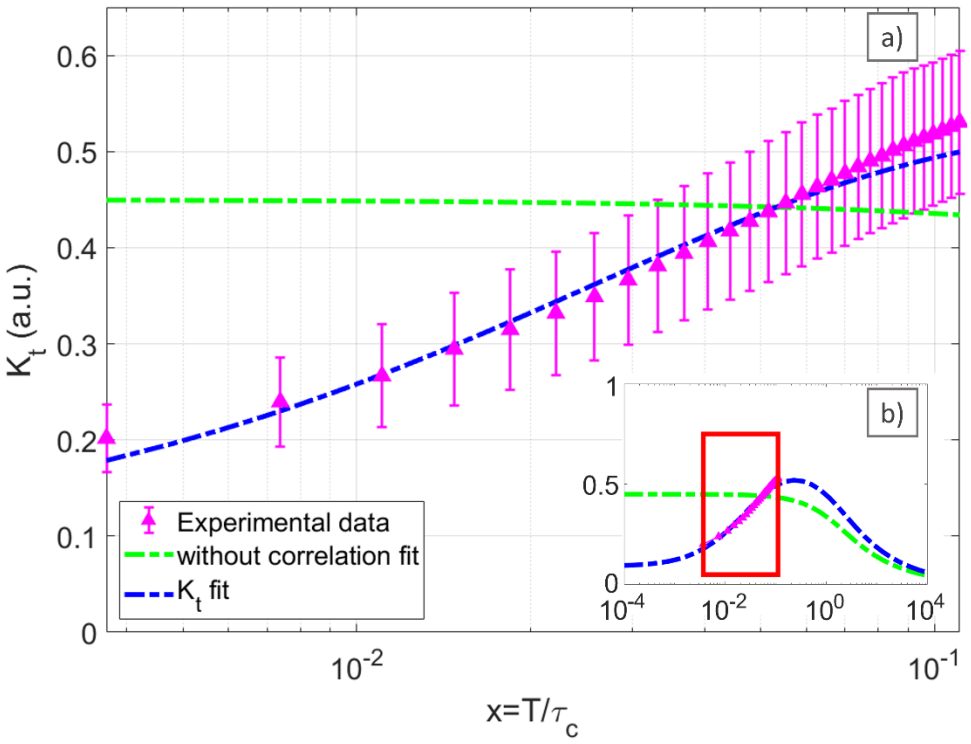

Figure 9 Experimental data obtained from averaging ω consecutive frames of the frames of $T = 1\ s$, considering $\omega = 1,2,3,\ldots,30$ (magenta triangle), current model (green dashed line) and our proposal (blue dashed line). Both models were fitted to the experimental data. a) Logarithmic plot of the experimental data. b) Zoomed-out view on a logarithmic scale along the x-axis.

Let us note the excellent agreement between our proposal (blue dashed line) and the experimental data (magenta triangle), when ($x < 1$), as expected. Furthermore, unlike the experimental data, which increases as x increases, the contrast without correlation (green dashed line) decreases with x.

Spatial-temporal analysis

Until now, we do not consider spatial temporal correlation, however, the electric field E depends not only on space but time, i.e. $E(\vec{r},t)$. It is well known [41] that for the superposition of static E_s and fluctuating E_f electric field, i.e, $E(\vec{r},t) = E_f(\vec{r},t)e^{-i\omega t} + E_s(\vec{r})e^{-i\omega t}$ the intensity autocorrelation of the fluctuating field $g_{1,f}(\Delta\vec{r},\tau)$ is;

$$\left|g_{1,f}(\Delta\vec{r},\tau)\right| = \left|g_{1,s}(\Delta\vec{r})\right|\left|g_{1,f}(\tau)\right|, \tag{14}$$

where, $g_{1,f}$, $g_{1,s}$ are the intensity autocorrelation of the fluctuating and static fields, respectively, i.e., $g_{1,f}(\Delta\vec{r},\tau)$ is separable in space and time.

Analogous to the factor $1/\nu$ in the temporal correlation, the factor $1/\mu_{\eta,\xi}$ corresponds to the spatial correlations [30], and due to the separability of the temporal and spatial variables in the autocorrelation (equation (14)), the contrast can be rewritten as:

$$K^2(N,p,x,L,S) = \alpha\, K_s^2(N,p) \times K_t^2(x,L,S)$$
$$= \left(\frac{1}{\mu_{0,0}} \right.$$
$$- \frac{1}{N(N-1)} \left(4 \sum_{\eta=1}^{p} \left(\sqrt{N}-\eta\right)\sqrt{N} \frac{1}{\mu_{\eta,0}} + 4 \sum_{\eta=1}^{p} \left(\sqrt{N}-\eta\right)^2 \frac{1}{\mu_{\eta,\eta}} \right. \quad (15)$$
$$\left. \left. + 8 \sum_{\xi=1}^{p-1} \sum_{\eta=\xi+1}^{p} \left(\sqrt{N}-\eta\right)\left(\sqrt{N}-\xi\right) \frac{1}{\mu_{\eta,\xi}} \right) \right) \times K_t^2(x,L,S) + C_n,$$

the contrast K^2 considering the effect of space-time correlation have three factors, the first one α, take into account factors such as polarization and coherence properties of the light source. The second corresponds to the spatial correlation (K_s^2 , [30]), and the third one corresponds to the temporal correlation (K_t^2). Equation (15) is a general expression for the contrast, considering both spatial and temporal correlation. $K_t^2(x,L,S)$ will correspond to equation (8) for Gaussian correlation or equations (11) or (12) for Lorentzian correlation.

It is worth to note that considering no spatial correlation, the size of the subregion where the pixels may be correlated, denoted by p [30], is equal to zero ($p = 0$), equation (15) reduces to;

$$K^2(N,0,x,L,S) = K_s^2(N,0) \times K_t^2(x,L,S) = \frac{1}{\mu_{0,0}} \times K_t^2(x,L,S)$$
$$= \frac{1}{\pi^2 M^2} \left(-1 + e^{-\pi M} + \pi\sqrt{M}\, Erf\left[\sqrt{\pi M}\right]\right)^2 \times K_t^2(x,L,S), \quad (16)$$

which is the well-known contrast equation considering the physical size of the pixel [30, 42].

To satisfy the Nyquist-Shannon criterion, ensuring that the speckle grain size is at least twice the size of a pixel ($M \leq 1/2$), the correction factor $\beta^{1/2}$ depends on the size of sliding window (N) and the size of the subregion (p) where the pixels may be correlated [30]. The values for $\beta^{1/2}$ for sliding window of 3×3, 5×5, 7×7 and 9×9 pixels, with $p = 1, 2, 3, 4$ respectively (i.e., considering all the pixels in the sliding window may be correlated), for Gaussian and Lorentzian correlation are given in Table 1. The values in Table 1 are calculated with $M = 0.5$.

Table 1. The value of $\beta^{1/2}$ which satisfies the Nyquist-Shannon criterion ($M = 0.5$), for sliding windows of 3×3, 5×5, 7×7 and 9×9 pixels, considering that all the sliding windows may be correlated.

$\beta^{1/2}$ for Nyquist-Shannon criterion	Gaussian correlation	Lorentzian correlation
$N = 3^2, \quad p = 1$	0.73853	0.59253
$N = 5^2, \quad p = 2$	0.77525	0.62463
$N = 7^2, \quad p = 3$	0.78748	0.63846
$N = 9^2, \quad p = 4$	0.7929	0.64521

5 Conclusions

In this study, we have addressed the significant challenges associated with accurate measurement of temporal speckle contrast, particularly for slow dynamic samples, by introducing a novel mathematical model that takes into account the correlation between neighboring pixels over time. Our results and the implications of this work can be summarized as follows:

1.- Improving accuracy for slow dynamic samples: The primary goal of this study was to improve the accuracy of temporal speckle contrast measurements, especially for slow dynamic samples. Our proposed mathematical model, has shown remarkable success in achieving this goal. This improvement is a critical advancement in the field, as it can prevent the potential misinterpretation of experimental results that has been prevalent with existing models.

2. Validation through experimental data: We validated the effectiveness of our model by analyzing E. coli ATCC 25922 colonies using the proposed approach. The results showed that our model is in good agreement with the experimental data, providing further confidence in its practical utility.

3. Versatility and applicability: our model can be applied not only to slow dynamic samples, but also to fast dynamic samples where neighboring pixels are not correlated. This adaptability is advantageous because it allows researchers to apply the same model to a wide range of dynamic scenarios, making it a valuable tool for applications in both biological and industrial systems.

4. Mathematical expressions for different correlation functions: To accommodate different scenarios, we have developed analytical expressions for contrast based on both Gaussian and Lorentzian correlation functions. This flexibility ensures that researchers can choose the appropriate model based on the characteristics of their specific samples, thereby improving the accuracy of their measurements.

In summary, we believe that our results pave the way for more accurate and reliable speckle contrast analysis in various applications.

Acknowledgments

J. C. Juarez-Ramirez expresses gratitude to CONAHCYT for the scholarship (grant number 629327).

D. I. Loaiza-Toscuento expresses gratitude to CONAHCYT for the scholarship (grant number 863172).

Code, Data, and Materials Availability

Implementation of equation (4), (8), (11) and (12) as function in Mathematica and MATLAB are available at the GitHub repository: TemporalSpeckle.

References

[1] F. Nirwana, P. Prajitno and S. Kusama Wijaya, "Correlation of Laser Speckle Image with Metal Surface Changes due to Corrosion Process," *2019 International Conference on Electrical, Electronics and Information Engineering (ICEEIE),* vol. 6, pp. 244-249, 2019.

[2] P. C. da Silva, C. F. L. Junior, J. A. O. Huguenin, E. A. Ferreira, L. da Silva and S. A. Carvalho, "Investigation of copper and zinc alloy surface exposed to corrosion environment by digital image processing," *Journal of materials research and technology,* vol. 24, pp. 9743-9753, 2023.

[3] G. Dwivedi, V. Kumari, N. Barak, A. Anand, A. K. Sharma and G. Sheoran, "Multimodal optical device to study dynamics of drying process," *Optics and Lasers in Engineering,* vol. 169, p. 107726, 2023.

[4] S. Szalai, B. F. Szívós, D. Kurhan, A. Németh, M. Sysyn and S. Fischer, "Optimization of Surface Preparation and Painting Processes for Railway and Automotive Steel Sheets," *Infrastructures,* vol. 8, no. 2, pp. 1-26, 2023.

[5] H. Peregrina Barreto, C. E. Perez Corona, J. Rangel Magdaleno, R. Ramos García, R. Chiu Zarate and J. C. Ramírez San Juan, "Use of kurtosis for locating deep blood vessels in raw speckle imaging using a homogeneity representation," *Journal of Biomedical Optics,* vol. 22, no. 6, p. 066004, 2017.

[6] A. Garrett, B. Kim, E. J. Sie, N. Z. Gurel, F. Marsili, D. A. Boas and D. Roblyer, "Simultaneous photoplethysmography and blood flow measurements towards the estimation of blood pressure using speckle contrast optical spectroscopy," *Biomedical Optics Express,* vol. 14, no. 4, pp. 1594-1607, 2023.

[7] Y. Z. Liu, S. K. Shah, C. M. Sanders, C. Nwaiwu, A. F. Dechert, S. Mehrotra, S. D. Schwaitzberg, P. C. W. Kim and E. B. Wilson, "Utility and usability of laser speckle contrast imaging (LSCI) for displaying real-time tissue perfusion/blood flow in robot-assisted surgery (RAS): comparison to indocyanine green (ICG) and use in laparoscopic surgery," *Surgical Endoscopy,* vol. 37, pp. 4803-4811, 2023.

[8] E. W. N. Contado, M. Pasqual, J. Dória, R. J. Gnzalez-Peña, L. X. Dupuy and A. Braga Jr., "Assessment of the use of infrared laser for dynamic laser speckle (DLS) technique," *Agriculture,* vol. 13, no. 546, pp. 1-15, 2023.

[9] N. Kaler, V. Bhatia and A. K. Mishra, "Deep Learning-Based Robust Analysis of Laser Bio-Speckle Data for Detection of Fungal-Infected Soybean Seeds," *IEEEAccess,* vol. 11, pp. 112814-112829, 2023.

[10] T. G. Porch, J. C. Rosas, K. Cichy, G. G. Lutz, I. Rodriguez, R. W. Colbert, G. Demosthene, J. C. Hernández, D. M. Winham and J. S. Beaver, "Release of tepary bean cultivar 'USDA Fortuna' with improved disease and insect resistance, seed size, and culinary quality," *Journal of Plant Registrations,* pp. 1-10, 2023.

[11] I. Balmages, J. Liepins, E. T. Auzins, D. Bliznuks, E. Baranovics, I. Lihacova and A. Lihachev, "Use of the speckle imaging sub-pixel correlation analysis in revealing a mechanism of microbial colony growth," *Scientific Reports,* vol. 13, no. 2613, 2023.

[12] I. Balmages, A. Reinis, S. Kistkins, D. Bliznuks, E. V. Plorina, A. Lihachev and I. Lihacova, "Corrigendum: Laser speckle imaging for visualization of hidden effects for early detection of antibacterial susceptibility in disc diffusion tests," *Frontiers in microbiology,* vol. 14, no. 1266723, 2023.

[13] H. J. Rabal and R. A. Braga Jr., Dynamic Laser Speckle and Applications, CRC Press, 2009.

[14] R. A. Arizaga, N. L. Cap, H. J. Rabal and M. Trivi, "Display of local activity using dynamical spekle patterns," *Optical Engineering,* vol. 41, no. 2, 2002.

[15] A. Chatterjee, R. Disawal and S. Prakash, "Biospeckle Assessment of Bread Spoilage by Fungus Contamination Using Alternative Fujii Technique," *Advances in Optical Science and Engineering,* vol. 194, pp. 395-401, 2017.

[16] V. Farzam Rad, M. Panahi , R. Jamali, A. Darudi and A.-R. Moradi, "Non-invasive in situ monitoring of bone scaffold activity by speckle pattern analysis," *Biomedical Optics Express,* vol. 11, pp. 6324-6336, 2020.

[17] B. Choi, N. M. Kang and J. S. Nelson, "Laser speckle imaging for monitoring blood flow dynamics in the in vivo rodent dorsal skin fold model," *Microvascular Research,* vol. 68, pp. 143-146, 2004.

[18] J. Cracowski, F. Gaillard-Bigot, C. Cracowski, M. Roustit and C. Millet, "Skin microdualysis coupled with laser Speckle Contrast Imaging to assess microvascular reactivity," *Microvascular Research,* vol. 82, no. 3, pp. 333-338, 2011.

[19] D. D. Patel and D. M. Lipinski, "Validating a low-cost laser speckle contrast imaging system as a quantitative tool for assessing retinal vascular function," *Scientific Reports,* pp. 1-11, 2020.

[20] A. I. Srienc, Z. L. Kurth-Nelson and E. A. Newman, "Imaging retinal blood flow with laer speckle flowmetry," *Frontiers in Neuroenergetics,* vol. 2, pp. 128-1 - 128-10, 2010.

[21] D. A. Boas and A. K. Dunn, "Laser speckle contrast imaging in biomedical optics," *Journal of biomedical optics,* vol. 15, no. 1, p. 011109, 2010.

[22] A. K. Dunn, "Laser Speckle Contrast Imaging of Cerebral Blood Flow," *Annals of Biomedical Engineering,* vol. 40, pp. 367-377, 2012.

[23] G. A. Armitage, K. G. Todd, A. Shuaib and I. R. Winship, "Laser speckle contrast imaging of collateral blood flow during acute ischemic stroke," *Journal of Cerebral Blood Flow & Metabolism,* vol. 30, pp. 1432-1436, 2010.

[24] J. Senarathna, A. Rege, N. Li and N. V. Thakor, "Laser Speckle Contrast Imaging: Theory, Instrumentation and Applications," *IEEE Reviews in Biomedical Engineering,* vol. 6, pp. 99-110, 2013.

[25] A. F. Fercher and J. D. Briers, "Flow visualization by means of single-exposure speckle photography," *Optics Communications,* vol. 37, no. 5, pp. 326 - 330, 1981.

[26] A. B. Parthasarathy, W. J. Tom, A. Gopal, X. Zhang and A. K. Dunn, "Robust flow measurement with multi-exposure speckle imaging," *Optics Express,* vol. 16, no. 3, pp. 1975-1989, 2008.

[27] J. C. Ramírez San Juan, R. Ramos García, G. Martínez Niconoff and B. Choi, "Simple correction factor for laser speckle imaging of flow dynamics," *Optics Letters,* vol. 39, no. 3, pp. 678-681, 2014.

[28] R. Bandyopadhyay, A. S. Gittings, S. S. Suh, P. K. Dixon and D. J. Durian, "Speckle-visibility spectroscopy: A tool to study time-varying dynamics," *Review of Scientific Instruments,* vol. 76, no. 9, p. 093110, 2005.

[29] P.-A. Lemieux and D. J. Durian, "Investigating non-Gaussian scattering processes by using nth-order intensity correlation functions," *Journal of the Optical Society of America A,* vol. 16, no. 7, pp. 1651-1664, 1999.

[30] J. C. Juarez-Ramirez, B. Coyotl-Ocelotl, B. Choi, R. Ramos-Garcia, T. Spezzia-Mazzocco and J. C. Ramirez-San-Juan, "Improved spatial speckle contrast model for tissue blood flow imaging: effects of spatial correlation among neighboring camera pixels," *Journal of Biomedical Optics,* vol. 28, no. 12, pp. 1-15, 2023.

[31] C. Regan, J. C. Ramirez-San-Juan and B. Choi, "Phototermal laser speckle imaging," *Optics letters,* vol. 39, no. 17, pp. 5006-5009, 2014.

[32] T. Son, J. Lee and B. Jung, "Contrast enhancement of laser speckle contrast image in deep vasculature by reduction of tissue scattering," *Journal of the Optical Society of Korea,* vol. 17, no. 1, pp. 86-90, 2013.

[33] A. Mazhar, D. J. Cuccia, T. B. Rice, S. A. Carp, A. J. Durkin, D. A. Boas, B. Choi and B. J. Tromberg, "Laser speckle imaging in the spatial frequency domain," *Biomedical Optics Express,* vol. 2, no. 6, pp. 1553-1563, 2011.

[34] D. D. Postnov, V. V. Tuchin and O. Sosnovtseva, "Estimation of vessel diameter and blood flow dynamics from laser speckle images," *Biomedical Optics Express,* vol. 7, no. 7, pp. 2759-2768, 2016.

[35] H. Cheng, Q. Luo, S. Zeng, S. Chen, J. Cen and H. Gong, "Modified laser speckle imaging method with improved spatial resolution," *Journal of Biomedical Optics,* vol. 8, no. 3, pp. 559-564, 2003.

[36] D. Briers, D. D. Duncan, E. R. Hirst, S. J. Kirkpatrick, M. Larsson, W. Steenbergen, T. Stromberg and O. B. Thompson, "Laser speckle contrast imaging: theoretical and practical limitations," *Journal of Biomedical Optics,* vol. 18, no. 6, pp. 1 - 10, 2013.

[37] J. C. Ramírez San Juan, R. Ramos García, I. Guizar Iturbide, G. Martinez Niconoff and B. Choi, "Impact of velocity distribution assumption on simplified laser speckle imaging equation," *Optics Express,* vol. 16, no. 5, pp. 3197-3203, 2008.

[38] D. D. Duncan, S. J. Kirkpatrick and J. C. Gladish, "What is the proper statistical model for laser speckle flowmetry?," in *Complex Dynamics and Fluctuations in Biomedical Photonics V*, San Jose, 2008.

[39] P. G. Vaz, A. Humeau-Heurtier, E. Figueiras, C. Correia and J. Cardoso, "Laser speckle imaging to monitor microvascular blood flow: a review," *IEEE REVIEWS IN BIOMEDICAL ENGINEERING,* vol. 9, pp. 106-120, 2016.

[40] P. Zakharov, "Ergodic and non-ergodic regimes in temporal laser speckle imaging," *Optics Letters,* vol. 42, no. 12, pp. 2299-2301, 2017.

[41] Photon, Photon Correlation and Light Beating Spectroscopy, E. R. P. H. Z. Cummins, Ed., NY: Springer New York, 1974.

[42] J. C. Juárez Ramírez, B. Coyotl Ocelotl, R. Ramos García, R. Chiu Zarate, T. Spezzia Mazzocco, J. P. Padilla Martínez and J. C. Ramírez San Juan, "Speckle Contrast Calculation and Pixel Correlation," in *Proceedings of the 1st International Conference on Optics, Photonics and Lasers (OPAL' 2018)*, Barcelona, 2018.

Conclusion and summary

In this thesis, we have conducted a study on speckle contrast and developed a new mathematical model to describe it across a wider range of conditions.

The speckle pattern is an interferometric pattern that emerges when light interacts with surfaces possessing roughness comparable in size to the wavelength. Examples include skin, leaves, walls, etc., except for highly reflective materials like metals.

The speckle pattern is highly dependent on the microscopic distribution of the material. Even a minor change in the illuminated area or distribution can completely alter the speckle pattern [1, 2, 3].

Speckle patterns are often considered undesirable effects during imaging and are treated as noise. Extensive research has been dedicated to developing methods for minimizing speckle[4, 5, 6, 7, 8, 9, 10]. However, as mentioned earlier, speckle patterns carry valuable information about the sample. It is possible to either recover this information or enhance the image resolution by utilizing speckle [11, 12, 13, 14, 15, 16, 17, 18, 19, 20].

Due to the high sensitivity of the speckle pattern to the sample, akin to a fingerprint, it encodes valuable information about the sample. Specifically, the dynamics of the sample are reflected in the speckle pattern. When the sample is dynamic, the speckle pattern also exhibits dynamism.

Therefore, the analysis of speckle patterns finds application in various scientific and engineering domains. These include characterizing drying patterns during paint application [21, 22], studying metal corrosion [19, 20], analyzing astronomy images [11]. In Biological and medical fields, speckle pattern are also utilized in areas, such as; ophthalmology [13, 14], dermatology [15, 16] , neurobiology [17, 18], measuring blood flow [23, 24], neuroscience [25, 26], intraoperative assessment [27], dentistry [28, 29], monitoring capillary blood flow [30],among others.

For any research employing speckle contrast, it is imperative to align theoretical models with experimental conditions. The existing mathematical model does not account for correlations between neighboring pixels or frames, making it valid only under specific conditions. These conditions include a speckle grain size smaller than the camera pixel (not adhering to the Nyquist-Shannon sampling theorem) and a correlation time shorter than the exposure time. While these criteria are met in areas studying fast dynamics, such as blood flow, they do not align with research in slow dynamics, like bacterial growth or paint applications.

In this work, detailed in Chapter 3, we present a refined calculation of the spatial contrast factor, $\beta = K_S^2(N, p)$,which takes into account the influence of spatial correlation among neighboring pixels. This consideration is applicable when the speckle grain size is larger, equal to, or smaller than the pixel size. Notably, our mathematical model reverts to the previous model when the speckle grain size is smaller than the pixel size. Our model provides a more accurate theoretical estimation of spatial contrast compared to the previous model by accounting for spatial correlation effects. Additionally, we introduce an analytical solution for the spatial speckle contrast, applicable to any spatial correlation sub-matrix size, considering Gaussian illumination.

In Chapter 4, we introduced a novel mathematical model to address the challenges associated with accurately measuring temporal speckle contrast, considering the correlation between neighboring pixels over time. Our temporal contrast model was validated using experimental data (analyzing *E. coli* ATCC 25922 colonies) and demonstrated improved accuracy in temporal speckle contrast measurements, particularly for slow dynamics. However, for fast dynamics, our model aligns with the previous model and the experimental data.

To accommodate different scenarios, we have developed analytical models considering both Gaussian and Lorentzian correlation functions. This flexibility ensures that researchers can choose the appropriate model based on the characteristics of their specific samples and goals, thereby improving the accuracy of their measurements.

In summary, by considering both spatial and temporal correlations, our results pave the way for a more accurate and reliable speckle contrast analysis across a diverse range of applications.

The necessary code to calculate the contrast considering temporal or spatial correlation is available on the GitHub repository; *TemmporalSpeckle* and *SpatialSpeckle* respectively.

Scientific production:

As a result of this work, we had the opportunity to present our findings at the 1st International Conference on Optics.;

1. J. C. Juarez-Ramirez, B. Coyotl-Ocelotl, R. Ramos-Garcia, R. Chiu-Zarate, T. Spezzia-Mazzocco, J. P. Padilla-Martinez, J. C. Ramirez-San-Juan, “Speckle contrast calculation and pixel correlation”, 1st International Conference on Optics, Photonics and Lasers, OPAL (2018).

The following proceedings were accepted in conjunction with an oral participation;

2. Beatriz Coyotl-Ocelotl, Julio César Juárez Ramírez, Rubén Ramos-García, Roger Chiu, Teresita Spezzia-Mazzocco, Julio-Cesar Ramirez-San-Juan, “Speckle contrast calculation based on pixels correlation: spatial analysis”, Proceedings of SPIE Vol. 10749, 1074903 (2018).
3. Contrast temporal analysis using correlation between frames. Julio César Juárez Ramírez, Beatriz Coyotl-Ocelotl, Rubén Ramos-García, Roger Chiu, Teresita Spezzia-Mazzocco, Julio-Cesar Ramirez-San-Juan, Proceedings of SPIE Vol. 10749, 1074904 (2018).

The next article was published in the journal of biomedical optics;

4. Julio Cesar Juarez-Ramirez, Beatriz Coyotl-Ocelotl,a Bernard Choi ,b, Ruben Ramos-Garcia , Teresita Spezzia-Mazzocco, and Julio C. Ramirez-San-Juan, “Improved spatial speckle contrast model for tissue blood flow imaging: effects of spatial correlation among neighboring camera pixels”, Journal of Biomedical Optics, Vol. 28(12) (2023).

The next paper has been submitted to the Journal of Biomedical Optics, and we are currently awaiting review comments;

5. “Improved temporal speckle contrast model for slow and fast dynamic samples: effect of temporal correlation among neighboring camera pixels.”

References

[1] S. Feng, C. Kane, P. A. Lee y A. D. Stone, «Correlations and Fluctuations of Coherent Wave Transmission through Disordered Media,» *Physical Review Letters,* vol. 61, nº 7, pp. 834-837, 1988.

[2] I. Freund, M. Rosenbluh y S. Feng, «Memory Effects in Propagation of Optical Waves through Disordered Media,» *Physical Review Letters,* vol. 61, nº 20, pp. 2328-2332, 1988.

[3] A. P. Mosk, A. Lagendijk, G. Lerosey y M. Fink, «Controlling waves in space and time for imaging and focusing in complex media,» *Nature Photonics,* vol. 6, nº 5, pp. 283-292, 2012.

[4] J. Chen, Y. Kong, D. Zhang, Y. Fu y S. Zhuang, «Two-dimensional phase unwrapping based on U^2-Net in complex noise environment,» *Optics Express,* vol. 31, nº 18, pp. 29792-29812, 2023.

[5] M. Ihmeida y M. Shahzad, «Enhanced Change Detection Performance Based on Deep Despeckling of Synthetic Aperture Radar Images,» *IEEE Access,* vol. 11, pp. 1-14, 2023.

[6] V. Kumar, A. Kumar Dubey, M. Gupta, V. Singh, A. Butola y D. Singh Mehta, «Speckle noise reduction strategies in laser-based projection imaging, fluorescence microscopy, and digital holography with uniform illumination, improved image sharpness, and resolution,» *Optics & laser technology,* vol. 141, 2021.

[7] V. Bianco, P. Memmolo, M. Leo, S. Montresor, C. Distante, M. Paturzo, P. Picart, B. Javidi y P. Ferraro, «Strategies for reducing speckle noise in digital holography,» *Light science & applications,* vol. 7, nº 48, pp. 1-16, 2018.

[8] K. Zhuo, Y. Wang, Y. Ma, S. An, Z. Zalevsky, J. Zheng y P. Gao, «Quantitative Phase Contrast Microscopy with Optimized Partially Coherent Illumination,» *Photonics,* vol. 10, nº 391, pp. 1-9, 2023.

[9] J. Zhao, B. Liang, E. Dobo, M. J. Khan, E. Yang y D. Kang, «Speckle and Shadow Artifacts Reduction in Scattering-Based Light Sheet Microscopy,» de *Biophotonics Congress: Optics in the Life Sciences 2023 (OMA, NTM, BODA, OMP, BRAIN),* , 2023.

[10] W. Thompson, C. Marois, C. R. Do Ó, Q. Konopacky, J.-B. Ruffio, J. Wang, A. J. Skemer, R. J. De Rosa y B. Macintosh, «Deep Orbital Search for Additional Planets in the HR 8799 System,» *The astronomical journal,* vol. 165, nº 1, p. 29, 2023.

[11] A. Tokovinin, «Exploring Thousands of Nearby Hierarchical Systems with Gaia and Speckle Interferometry,» *The Astronomical Journal,* vol. 165, nº 4, p. 180, 2023.

[12] D. C. P. a. D. W. Park, «Ultrasound Speckle Decorrelation-Based Blood Flow Measurements,» *Ultrasound in Medicine & Biology,* vol. 49, nº 7, pp. 1491-1498, 2023.

[13] D. D. Patel y D. M. Lipinski, «Validating a low-cost laser speckle contrast imaging system as a quantitative tool for assessing retinal vascular function,» *Scientific Reports,* pp. 1-11, 2020.

[14] A. I. Srienc, Z. L. Kurth-Nelson y E. A. Newman, «Imaging retinal blood flow with laer speckle flowmetry,» *Frontiers in Neuroenergetics,* vol. 2, pp. 128-1 - 128-10, 2010.

[15] B. Choi, N. M. Kang y J. S. Nelson, «Laser speckle imaging for monitoring blood flow dynamics in the in vivo rodent dorsal skin fold model,» *Microvascular Research,* vol. 68, pp. 143-146, 2004.

[16] J. Cracowski, F. Gaillard-Bigot, C. Cracowski, M. Roustit y C. Millet, «Skin microdualysis coupled with laser Speckle Contrast Imaging to assess microvascular reactivity,» *Microvascular Research,* vol. 82, nº 3, pp. 333-338, 2011.

[17] A. K. Dunn, «Laser Speckle Contrast Imaging of Cerebral Blood Flow,» *Annals of Biomedical Engineering,* vol. 40, pp. 367-377, 2012.

[18] G. A. Armitage, K. G. Todd, A. Shuaib y I. R. Winship, «Laser speckle contrast imaging of collateral blood flow during acute ischemic stroke,» *Journal of Cerebral Blood Flow & Metabolism,* vol. 30, pp. 1432-1436, 2010.

[19] F. Nirwana, P. Prajitno y S. Kusama Wijaya, «Correlation of Laser Speckle Image with Metal Surface Changes due to Corrosion Process,» *2019 International Conference on Electrical, Electronics and Information Engineering (ICEEIE),* vol. 6, pp. 244-249, 2019.

[20] P. C. da Silva, C. F. L. Junior, J. A. O. Huguenin, E. A. Ferreira, L. da Silva y S. A. Carvalho, «Investigation of copper and zinc alloy surface exposed to corrosion environment by digital image processing,» *Journal of materials research and technology,* vol. 24, pp. 9743-9753, 2023.

[21] G. Dwivedi, V. Kumari, N. Barak, A. Anand, A. K. Sharma y G. Sheoran, «Multimodal optical device to study dynamics of drying process,» *Optics and Lasers in Engineering,* vol. 169, p. 107726, 2023.

[22] S. Szalai, B. F. Szívós, D. Kurhan, A. Németh, M. Sysyn y S. Fischer, «Optimization of Surface Preparation and Painting Processes for Railway and Automotive Steel Sheets,» *Infrastructures,* vol. 8, nº 2, pp. 1-26, 2023.

[23] J. D. Briers y S. Webster, «Laser Speckle Contrast Analysis (LASCA): A Nonscanning, Full-field Technique For Monitoring Capillary Blood Flow,» *Journal of Biomedical Optics,* vol. 1, nº 2, pp. 174-179, 1996.

[24] J. D. Briers, «Laser speckle contrast imaging for measuring blood flow,» *Optica Applicata,* vol. 37, nº 1-2, pp. 139-152, 2007.

[25] D. A. Boas y A. K. Dunn, «Laser speckle contrast imaging in biomedical optics,» *Journal of biomedical optics,* vol. 15, nº 1, p. 011109, 2010.

[26] J. Senarathna, A. Rege, N. Li y N. V. Thakor, «Laser Speckle Contrast Imaging: Theory, Instrumentation and Applications,» *IEEE Reviews in Biomedical Engineering,* vol. 6, pp. 99-110, 2013.

[27] E. A. Mannoh, G. Thomas, C. C. Solórzano y A. Mahadevan-Jansen, «Intraoperative assessment of parathyroid viability using laser speckle contrast imaging,» *Scientific reports,* vol. 7, pp. 1-11, 2017.

[28] T. Sato, M. Miyazaki, A. Rikuta y K. Kobayashi, «Application of the Laser Speckle-Correlation Method for Determining the Shrinkage Vector of a Light-cured Resin,» *Denntal Materials Journal,* vol. 23, nº 3, pp. 284-290, 2004.

[29] C. Stoianovici, P. Wilder-Smith y B. Choi, «Assessment of Pulpal Vitality Using Laser Speckle Imaging,» *Laser in Surgery and Medicine,* vol. 43, nº 8, pp. 833-837, 2011.

[30] J. D. Briers y S. Webster, «Laser Speckle Contrast Analysis (LASCA): A Nonscanning, Full-field Technique For Monitoring Capillary Blood Flow,» *JOURNAL OF BIOMEDICAL OPTICS,* vol. 1, nº 2, pp. 174-179, 1996.

Appendix 1: Code

Synthetic speckle

MATLAB 2022b:

The necessary code to generate the synthetic speckle pattern in *MATLAB R2022b* is provided in Code 1. The function receives the desire size tam of the speckle size and the radius r of the circular mask, which is inversely proportional to the speckle grain size as parameters. It returns an image of $tam \times tam$ pixels of a synthetic speckle pattern, normalized in intensity.

```
1   %tam is the x size of the speckle image
2   %r is the radius of the circular filter, the size of
    the speckle grain is
3   %proportional inversely of r
4   function Return=StaticSpeckle(tam,r)
5   phase = rand(tam);%random phase
6   X=-tam/2:tam/2-1;Y=X';xc=0;yc=0;radio=r;%to create a
7   disk filter
    temp=(X-xc).^2+(Y-yc).^2<radio.^2;%create a disk filter
8   E1 = exp(i*2*pi* phase);%complex field
9   FFT1 = fft2(E1);%fourier transform
10  FF1 = fftshift(FFT1);%shift
11  FF1=FF1.*temp;%apply the disk filter
12  FF1=ifft2(FF1);%inverse fourier transform
13  in1=FF1.*conj(FF1);%get the intensity
14  in1=(in1-min(in1(:)))/(max(in1(:))-
    min(in1(:)));%normalize
15  Return=in1;%return the field with the desire size
16  end
```

Code 1. StaticSpeckle in MATLAB R2022b*; receive the image size* tam *and the radius of the circular mask* r*, which is inversely proportional to the speckle grain size. Returns synthetic speckle pattern normalized in intensity.*

Mathematica 11

The necessary code to generate the synthetic speckle pattern in *Mathematica 11* is provided in Code 2. The function receives the desire size tam of the speckle size and the radius r of the circular mask, which is inversely proportional to the speckle grain size as parameters. It returns an image of $tam \times tam$ pixels of a synthetic speckle pattern, normalized in intensity.

```
1   (*tam is the x size of the speckle image
    r is the radius of the circular filter, the size of the
    speckle grain is
    proportional inversely  of r *)
2   staticSpeckle[tam_, r_] := Module[{return, phase, temp,
    i, j, E1, FFT1, FF1, in1},
3     phase = RandomReal[2 Pi, {tam, tam}];(*random phase
    between 0, 2 Pi*)
4     temp = ConstantArray[0, {tam, tam}];
5     (*to create a disk filter*)
6     For[i = 1, i <= tam, i++,
7      For[j = 1, j <= tam, j++,
8       If[(i - tam/2)^2 + (j - tam/2)^2 <= r^2,
9        temp[[i, j]] = 1](*end if*)
10      ](*end for j*)
11     ];(*end for i*)
12    E1 = Exp[I 2 Pi*phase];(*complex field*)
13    FFT1 = Fourier[E1];(*fourier transform*)
14    FF1 = FFT1*temp;(*apply the disk filter*)
15    FF1 = InverseFourier[FF1];(*inverse fourier
    transform*)
16    in1 = FF1*Conjugate[FF1];(*get the intensity*)
17    in1 = (in1 - Min[in1])/(Max[in1] -
    Min[in1]);(*normalize*)
18    return = in1(*return the field with the desire size*)
19    ]
```

Code 2. StaticSpeckle in Mathematica 11; *receive the image size* tam *and the radius of the circular mask* r, *which is inversely proportional to the speckle grain size. Returns synthetic speckle pattern normalized in intensity.*

Spatial contrast algorithm

MATLAB 2022b:

The necessary code to calculate the spatial contrast in *MATLAB R2022b* is provided in Code 3. The function receives the speckle image I, the window size w, and the number of rows and columns er removed from the edges to avoid edge noise as parameters. It returns the spatial contrast image of the given speckle image.

```
1   %main function,
2   % l  are the frames
3   % w is the size of the window
4   %er is the number of rows and columns that will be
    remove it
5
6   %returns SC; the contrast image
7   function SC = SpatialContrast(I,w,er);
8   % compute the speckle contrast for a bxb region for all
    files
9   SC=zeros(size(I));% initializing variables
10  SC=colfilt(I,[w w],'sliding',@speckle_contrast);
11  %sliding window uses function speckle_contrast(v)
12  SC = double(SC);% change to double data type
13  SC=SC(er+1:end-er,er+1:end-er);%%remove the edges of
    "erase" pixels
14  end
15
16  %internal function that calculate the speckle contrast
    of a vector
17  %this function is used by the main function
18  %return the contrast as a double
19  function sc=speckle_contrast(v)
20  x=double(v);% change to double data type
21  sc=std(x)./mean(x);%compute the contrast
22  end
```

Code 3. Spatial Contrast code in MATLAB R2022b, using MATLAB functions. Receive one speckle frame in the variable I*, the size of the sliding window in pixels in the variable* w *and the number of rows and columns that will be remove it from the contrast image in the variable* er*. Return the spatial contrast image.*

Mathematica 11:

The necessary code to calculate the spatial contrast in *Mathematica 11* is provided in Code 4. The function receives the speckle image $frame$, the width and height of the window size n and m respectively as parameters. It returns the spatial contrast image of the given speckle image.

In this implementation, edge noise is not removed, but it is possible to use a non-square sliding window.

```
(*spatial contrast Long
n and m should be ODD numbers
frame is the picture (speckle)
n is the width of the sliding window
m is the height of the sliding window
returns the contrast image*)
SpatialContrast[frame_, n_, m_] :=
 Module[{p, q, xTam, yTam, X, Y, x, y, w, vectorW,
return, std, avg},
  (*initializing variables that will help in the
sliding part*)
  p = (n - 1)/2;
  q = (m - 1)/2;
  {yTam, xTam} = Dimensions[frame];
  return = ConstantArray[0, {yTam - (m - 1), xTam - (n
- 1)}];
  X = Y = 1;
  (*double for cycle to slide all the pixels*)
  For[x = p + 1, x <= xTam - p, x++,
   For[y = q + 1, y <= yTam - q, y++,
    w = frame[[y - q ;; y + q, x - p ;; x +
p]];(*sliding window*)
    vectorW = Flatten[w];
    std = StandardDeviation[vectorW];(*compute the
standard deviation*)
    avg = Mean[vectorW];(*compute the average*)
    return[[Y, X]] = std/avg;(*compute the contrast*)
    Y = Y + 1;
    ];(*end for y*)
   X = X + 1;
   Y = 1;
   ];(*end for x*)
  return(*return variable "return"*)
  ](*end module*)
```

Code 4. Spatial Contrast code version in Mathematica 11. Receive one speckle frame in the variable frame*, the height and width of the sliding window in pixels in the variables* m *and* n *respectively. Return the contrast image.*

Temporal contrast algorithm

MATLAB 2022b:

The necessary code to calculate the spatial contrast in *MATLAB R2022b* is provided in Code 3. The function receives the speckle image I, the window size w, and the number of rows and columns er removed from the edges to avoid edge noise as parameters. It returns the spatial contrast image of the given speckle image.

```
1   %temporal contrast
2   %frames a set of frames (3d matrix)
3
4   %returns the contrast image
5   function salida=TemporalContrast(frames)
6   temp=permute(frames,[3,1,2]);%change the order of the
    pages in the 3D matrix
7   standard=squeeze(std(temp));%compute the standard
    deviation of one row (same pixel of all the frames) in
    the 3D matrix
8   avg=squeeze(mean(temp));%compute the average of one row
    (same pixel of all the frames) in the 3D matrix
9   salida=standard./avg;%compute the contrast
10  end
```

Code 5 . Temporal Contrast code long version in MATLAB R2022b, using MATLAB function. Receive a set of speckle frames in the variable frames. Return the contrast image.

Mathematica 11:

The necessary code to calculate the spatial contrast in *Mathematica 11* is provided in Code 4. The function receives the speckle image $frame$, the width and height of the window size n and m respectively as parameters. It returns the spatial contrast image of the given speckle image.

In this implementation, edge noise is not removed, but it is possible to use a non-square sliding window.

```
(*temporal contrast
frames a set of frames (3d matrix)

returns the contrast image*)
TemporalContrast[frames_] := Module[{x, y, z, return,
contx, conty, temp, std, avg},
  (*initializing variables of size of the frames and
number of the frames*)
  {y, x, z} = Dimensions[frames];
  return = ConstantArray[0, {y, x}];
  (*double for cycle to slide all the pixels*)
  For[contx = 1, contx <= x, contx++,
   For[conty = 1, conty <= y, conty++,
    temp = frames[[conty, contx,1 ;; z]];(*select same
pixel in all the frames*)
    std = StandardDeviation[temp];(*compute the
standard deviation*)
    avg = Mean[temp];(*compute the average*)
    return[[conty, contx]] = std/avg;(*compute the
contrast*)
    ];(*end for conty*)
   ];(*end for contx*)
  return(*return variable "return"*)
  ](*end module*)
```

Code 6 . Temporal Contrast code long version in Mathematica 11. Receive a set of speckle frames in the variable frames. Return the contrast image.

Appendix 2: Developing spatial contrast equations

The integrated intensity $I_{\eta,\xi}$ over the physical area a^2 of the pixel (η, ξ) is given by:

$$I_{\eta,\xi} = \frac{1}{a^2} \int\limits_{pixel\ \eta,\xi} I(\vec{r}) d^2\vec{r}, \tag{1}$$

The mean intensity over the sliding window is:

$$i = \frac{1}{N} \sum_{\eta,\xi} I_{\eta,\xi}, \tag{2}$$

and the corresponding unbiased variance is:

$$c = \frac{1}{N-1} \sum_{\eta,\xi} (I_{\eta,\xi} - i)^2. \tag{3}$$

The expected value of the variance is:

$$\langle c \rangle = \frac{1}{N-1} \left(-\langle i^2 \rangle N + \sum_{\eta,\xi} \langle {I_{\eta,\xi}}^2 \rangle \right). \tag{4}$$

where ⟨⟩ denotes the ensemble average.

Given two pixels within the sliding window with coordinates (η', ξ') and (η'', ξ'') respectively, the parameter $1/\mu_{\eta''-\eta',\xi''-\xi'}$ depends on the spatial correlation between the given pixels and M the ratio between the pixel and speckle spot size. Due to it is not important the actual pixel coordinates (η', ξ') and (η'', ξ'') but the distance between them $\eta = \eta'' - \eta'$, and $\xi = \xi'' - \xi'$. Therefore, the correlation factor $1/\mu_{\eta,\xi}$ of the pixels $(0,0)$ and (η, ξ) it is identical to $1/\mu_{\eta''-\eta',\xi''-\xi'}$. The correlation factor is given by the expression:

$$\begin{aligned} \frac{1}{\mu_{\eta,\xi}} &= \frac{1}{a^4} \int\limits_{pixel 0,0} \int\limits_{pixel \eta,\xi} (g_2(\vec{r} - \vec{r}') - 1) d^2\vec{r}' d^2\vec{r} \\ &= \frac{1}{a^4} \int\limits_{pixel 0,0} \int\limits_{pixel \eta,\xi} {g_1}^2(\vec{r} - \vec{r}') d^2\vec{r}' d^2\vec{r}, \end{aligned} \tag{5}$$

using equations (1) and (5) we can rewrite $\langle I_{0,0} I_{\eta,\xi} \rangle$ as:

This chapter has been published as the appendix of: Julio Cesar Juarez-Ramirez, Beatriz Coyotl-Ocelotl, Bernard Choi, Ruben Ramos-Garcia, Teresita Spezzia-Mazzocco, Julio C. Ramirez-San-Juan, "Improved spatial speckle contrast model for tissue blood flow imaging: effects of spatial correlation among neighboring camera pixels," J. Biomed. Opt. 28(12) 125002 (5 December 2023) https://doi.org/10.1117/1.JBO.28.12.125002

$$\langle I_{0,0} I_{\eta,\xi} \rangle = \langle I \rangle^2 \left(1 + \frac{1}{\mu_{\eta,\xi}} \right). \tag{6}$$

Computing $\langle i^2 \rangle$ from equation (2), where $\langle\rangle$ denotes the ensemble average, and the summation spans all pixels within the sliding window of $\sqrt{N} \times \sqrt{N}$ pixels. Using the following notation:

$$\langle i^2 \rangle = \frac{1}{N^2} \sum_{\eta=-\sqrt{N}}^{\sqrt{N}} \sum_{\xi=-\sqrt{N}}^{\sqrt{N}} \sum_{\eta'''=-\sqrt{N}}^{\sqrt{N}} \sum_{\xi'''=-\sqrt{N}}^{\sqrt{N}} \langle I_{0,0}, I_{\eta,\xi} \rangle. \tag{7}$$

It is possible to separate the summation into two sets of pixels 1) CW, where $(\eta, \xi) \in (2p+1) \times (2p+1)$; and 2) OW, where $(\eta, \xi) \notin (2p+1) \times (2p+1)$.

For set CW, we focus on particular cases. When $\eta = \xi = 0$, we call this a central correlation (see Figure 3 in Chapter 3). When $\eta = \xi \neq 0$, we call this a diagonal correlation. When $\eta \neq \xi = 0$ or $\xi \neq \eta = 0$, we call this a lateral correlation. Finally, when $(\eta, \xi) \in (2p+1) \times (2p+1)$ and are not central, diagonal, or lateral correlations, we call these knight correlations due to the resemblance of the shape to the knight's movement in chess. The other correlation when the index $(\eta, \xi) \in OW$ it be called outsiders. Then, equation (7) it may rewritten as the sum of each type of correlations, i.e.:

$$\begin{aligned} \langle i^2 \rangle = \frac{1}{N^2} \Bigg(& \sum_{(\eta,\xi) \in central} \langle I_{0,0} I_{\eta,\xi} \rangle + \sum_{(\eta,\xi) \in diagonal} \langle I_{0,0} I_{\eta,\xi} \rangle + \sum_{(\eta,\xi) \in lateral} \langle I_{0,0} I_{\eta,\xi} \rangle \\ & + \sum_{(\eta,\xi) \in knight} \langle I_{0,0} I_{\eta,\xi} \rangle + \sum_{(\eta,\xi) \in outsiders} \langle I_{0,0} I_{\eta,\xi} \rangle \Bigg). \end{aligned} \tag{8}$$

For $p = 0$, only the central correlation exists; hence, only the first summation in equation (8) is nonzero. Due to the symmetry in the correlation, some factors $1/\mu_{\eta,\xi}$ are equivalent. For example, $1/\mu_{\eta,\xi}$ is equivalent to $1/\mu_{\xi,\eta}$, as well as any paired combination of $(\pm\eta, \pm\xi)$. Approximately only the half of the pixels in one quadrant of the correlation sub-window are not equivalent to each other, without loss of generality, the fist quadrant is considered to classified/study these correlations, as it may see in Figure 1 in Chapter 3 (b) of the third chapter. In this work, it has been classified the four different types of correlations: central, lateral, diagonal and knight.

For this reason, it is unnecessary to compute the correlation of all pixels. Instead, it is sufficient to compute the correlation of the pixels that are not equivalent and to weight their contributions appropriately.

Identifying the existence of N central correlations, one for each pixel in the correlation subregion, is straightforward. The other types of correlation are not so straightforward, but it can be demonstrated that for the diagonal correlation type, $\eta = \xi \geq 1$, there are $4\left(\sqrt{N} - \eta\right)^2$ equivalent correlations. For lateral type, $\eta > \xi = 0$, there are $4\sqrt{N}\left(\sqrt{N} - \eta\right)$ equivalent correlations. For the knight type, $1 \leq \xi \neq \eta \geq 2$, there are $8\left(\sqrt{N} - \eta\right)\left(\sqrt{N} - \xi\right)$ equivalent correlations and let $B(p)$ the number of outsider correlations.

For $p = 0$, the correlation sub-window is only 1×1 pixel, i.e., only the autocorrelation is considered (central correlations), and equation (8) reduces to $\langle i^2 \rangle = \frac{1}{N^2} N \langle I_{0,0} I_{0,0} \rangle$. For $p = 1$, the correlation

sub-window is 3×3 pixels, with only one central, one diagonal, and one lateral correlation. Therefore, equation (8) reduces to $\langle i^2 \rangle = \frac{1}{N^2}\Big(N\langle I_{0,0}I_{0,0}\rangle + 4\big(\sqrt{N}-1\big)^2\langle I_{0,0}I_{1,1}\rangle + 4\sqrt{N}\big(\sqrt{N}-1\big)\langle I_{0,0}I_{1,0}\rangle\Big)$, which is the exact case analyzed by Skipetrov et. al. [1]. The 1×1 pixels correlations sub-window ($p = 0$) only has central correlation type, 3×3 is the first sub-window ($p = 1$) with lateral and diagonal correlations type, and the 5×5 pixels correlation sub-window ($p = 2$) it is the first one that has one knight type correlation, equation (8) reduce to:

$$\begin{aligned}\langle i^2 \rangle = \tfrac{1}{N^2}\Big(N\langle I_{0,0}I_{0,0}\rangle + 4\Big(\big(\sqrt{N}-1\big)^2\langle I_{0,0}I_{1,1}\rangle + \big(\sqrt{N}-2\big)^2\langle I_{0,0}I_{2,2}\rangle\Big) + \\ 4\sqrt{N}\Big(\big(\sqrt{N}-1\big)\langle I_{0,0}I_{1,0}\rangle + \big(\sqrt{N}-2\big)\langle I_{0,0}I_{2,0}\rangle\Big) + 8\big(\sqrt{N}-2\big)\big(\sqrt{N}-1\big)\langle I_{0,0}I_{2,1}\rangle\Big),\end{aligned} \tag{9}$$

Coyotl-Ocelotl analyzed this case [2].

Henceforth $p \geq 2$, the first subregion with all types of correlation (diagonal, lateral and knight) to avoid potential problems with missing terms in the summation. Then equation (8) is rewritten to:

$$\begin{aligned}\langle i^2 \rangle = \frac{1}{N^2}\Bigg(N\langle I_{0,0}I_{0,0}\rangle + \sum_{\eta=\xi=1}^{p} 4\big(\sqrt{N}-\eta\big)^2\langle I_{0,0}I_{\eta,\eta}\rangle + \sum_{\eta=1}^{p} 4\sqrt{N}\big(\sqrt{N}-\eta\big)\langle I_{0,0}I_{\eta,0}\rangle \\ + \sum_{\xi=1}^{p-1}\sum_{\eta=\xi+1}^{p} 8\big(\sqrt{N}-\eta\big)\big(\sqrt{N}-\xi\big)\langle I_{0,0}I_{\eta,\xi}\rangle + B(p)\langle I_{0,0}I_{\eta,\xi}\rangle\Bigg).\end{aligned} \tag{10}$$

Another possible correlation is what we call outsider correlations, which expand beyond the total number of central, diagonal, lateral, and knight correlations within the correlation subregion $(2p+1) \times (2p+1)$:

$$\begin{aligned}B(p) = N^2 - \Bigg(N + \sum_{\eta=\xi=1}^{p} 4\big(\sqrt{N}-\eta\big)^2 + \sum_{\eta=1}^{p} 4\sqrt{N}\big(\sqrt{N}-\eta\big) \\ + \sum_{\xi=1}^{p-1}\sum_{\eta=\xi+1}^{p} 8\big(\sqrt{N}-\eta\big)\big(\sqrt{N}-\xi\big)\Bigg),\end{aligned} \tag{11}$$

Solving the summations, we obtain:

$$\begin{aligned}B(p) = N^2 - \Bigg(N + \Big(\frac{2p}{3} - 4\sqrt{N}p + 4Np + 2p^2 - 4\sqrt{N}p^2 + \frac{4p^3}{3}\Big) \\ + \big(-2\sqrt{N}p + 4Np - 2\sqrt{N}p^2\big) \\ + \Big(-\frac{2p}{3} + 4\sqrt{N}p - 4Np - p^2 + 4Np^2 + \frac{2p^3}{3} - 4\sqrt{N}p^3 + p^4\Big)\Bigg).\end{aligned} \tag{12}$$

Simplifying equation (12), we obtain:

$$B(p) = N^2 - \Big(p(1+p) - \sqrt{N}(1+2p)\Big)^2. \tag{13}$$

Here, we assume that the outsider correlations are negligible by assuming that spatial correlations beyond the correlation subregion size are zero. For those pixels, $\langle I_{0,0}, I_{\eta,\xi}\rangle = \langle I_{0,0}\rangle\langle I_{\eta,\xi}\rangle = \langle I\rangle^2$, and using equation (6), we obtain:

$$\begin{aligned}\langle i^2\rangle = \frac{1}{N^2}\Bigg(& N\langle I\rangle^2\left(1+\frac{1}{\mu_{0,0}}\right) + \sum_{\eta=1}^{p} 4\big(\sqrt{N}-\eta\big)^2\langle I\rangle^2\left(1+\frac{1}{\mu_{\eta,\eta}}\right) \\ & + \sum_{\eta=1}^{p} 4\sqrt{N}\big(\sqrt{N}-\eta\big)\langle I\rangle^2\left(1+\frac{1}{\mu_{\eta,0}}\right) \\ & + \sum_{\xi=1}^{p-1}\sum_{\eta=\xi+1}^{p} 8\big(\sqrt{N}-\eta\big)\big(\sqrt{N}-\xi\big)\langle I\rangle^2\left(1+\frac{1}{\mu_{\eta,\xi}}\right) + B(p)\langle I\rangle^2\Bigg),\end{aligned} \tag{14}$$

factorizing $\langle I\rangle^2$ and regrouping:

$$\begin{aligned}\langle i^2\rangle = \frac{\langle I\rangle^2}{N^2}\Bigg(& \Bigg(N\frac{1}{\mu_{0,0}} + \sum_{\eta=1}^{p} 4\big(\sqrt{N}-\eta\big)^2\frac{1}{\mu_{\eta,\eta}} + \sum_{\eta=1}^{p} 4\sqrt{N}\big(\sqrt{N}-\eta\big)\frac{1}{\mu_{\eta,0}} \\ & + \sum_{\xi=1}^{p-1}\sum_{\eta=\xi+1}^{p} 8\big(\sqrt{N}-\eta\big)\big(\sqrt{N}-\xi\big)\frac{1}{\mu_{\eta,\xi}}\Bigg) \\ & + \Bigg(N + \sum_{\eta=1}^{p} 4\big(\sqrt{N}-\eta\big)^2 + \sum_{\eta=1}^{p} 4\sqrt{N}\big(\sqrt{N}-\eta\big) \\ & + \sum_{\xi=1}^{p-1}\sum_{\eta=\xi+1}^{p} 8\big(\sqrt{N}-\eta\big)\big(\sqrt{N}-\xi\big)\Bigg) + B(p)\Bigg).\end{aligned} \tag{15}$$

Using equation (11), some summation terms are eliminated with $B(p)$, and equation (15) becomes:

$$\begin{aligned}\langle i^2\rangle = \frac{\langle I\rangle^2}{N^2}\Bigg(& \Bigg(N\frac{1}{\mu_{0,0}} + \sum_{\eta=1}^{p} 4\big(\sqrt{N}-\eta\big)^2\frac{1}{\mu_{\eta,\eta}} + \sum_{\eta=1}^{p} 4\sqrt{N}\big(\sqrt{N}-\eta\big)\frac{1}{\mu_{\eta,0}} \\ & + \sum_{\xi=1}^{p-1}\sum_{\eta=\xi+1}^{p} 8\big(\sqrt{N}-\eta\big)\big(\sqrt{N}-\xi\big)\frac{1}{\mu_{\eta,\xi}}\Bigg) + N^2\Bigg).\end{aligned} \tag{16}$$

Similarly, to compute $\langle c\rangle$ (equation (4)), the term $\langle {I_{\eta,\xi}}^2\rangle = \langle I_{\eta,\xi} I_{\eta,\xi}\rangle$ is equivalent to $\langle I_{\eta,\xi} I_{\eta,\xi}\rangle = \langle I_{0,0} I_{0,0}\rangle$. Using equation (6), equation (4) is rewritten to:

$$\langle c\rangle = \frac{1}{N-1}\left(-\langle i^2\rangle N + \sum_{\eta,\xi}\langle I\rangle^2\left(1+\frac{1}{\mu_{0,0}}\right)\right), \tag{17}$$

solving the summation:

$$\langle c\rangle = \frac{1}{N-1}\left(-\langle i^2\rangle N + \langle I\rangle^2\left(1+\frac{1}{\mu_{0,0}}\right)N\right), \tag{18}$$

substituting equation (16) and factorizing $\langle I\rangle^2$:

$$\begin{aligned}\langle c\rangle = \frac{\langle I\rangle^2}{N-1}\Bigg(-\frac{1}{N^2}\Bigg(\Bigg(N\frac{1}{\mu_{0,0}} + \sum_{\eta=1}^{p} 4\left(\sqrt{N}-\eta\right)^2\frac{1}{\mu_{\eta,\eta}} + \sum_{\eta=1}^{p} 4\sqrt{N}\left(\sqrt{N}-\eta\right)\frac{1}{\mu_{\eta,0}} \\ + \sum_{\xi=1}^{p-1}\sum_{\eta=\xi+1}^{p} 8\left(\sqrt{N}-\eta\right)\left(\sqrt{N}-\xi\right)\frac{1}{\mu_{\eta,\xi}}\Bigg) + N^2\Bigg)N + \left(1+\frac{1}{\mu_{0,0}}\right)N\Bigg).\end{aligned} \tag{19}$$

After simplification:

$$\begin{aligned}\langle c\rangle = \frac{\langle I\rangle^2}{N(N-1)}\Bigg(N(N-1)\frac{1}{\mu_{0,0}} - \sum_{\eta=1}^{p} 4\left(\sqrt{N}-\eta\right)^2\frac{1}{\mu_{\eta,\eta}} - \sum_{\eta=1}^{p} 4\sqrt{N}\left(\sqrt{N}-\eta\right)\frac{1}{\mu_{\eta,0}} \\ - \sum_{\xi=1}^{p-1}\sum_{\eta=\xi+1}^{p} 8\left(\sqrt{N}-\eta\right)\left(\sqrt{N}-\xi\right)\frac{1}{\mu_{\eta,\xi}}\Bigg).\end{aligned} \tag{20}$$

Finally, dividing $\langle c\rangle$ by $\langle I\rangle^2$ results in the calculation of the spatial contrast:

$$\begin{aligned}K_s^2(N,p) = \frac{1}{\mu_{0,0}} \\ - \frac{1}{N(N-1)}\Bigg(4\sum_{\eta=1}^{p}\left(\sqrt{N}-\eta\right)\sqrt{N}\frac{1}{\mu_{\eta,0}} + 4\sum_{\eta=1}^{p}\left(\sqrt{N}-\eta\right)^2\frac{1}{\mu_{\eta,\eta}} \\ + 8\sum_{\xi=1}^{p-1}\sum_{\eta=\xi+1}^{p}\left(\sqrt{N}-\eta\right)\left(\sqrt{N}-\xi\right)\frac{1}{\mu_{\eta,\xi}}\Bigg).\end{aligned} \tag{21}$$

Equation (21) is an analytic expression for speckle contrast that assumes both an arbitrary sliding window size and an arbitrary correlation subregion of pixels ($p \geq 2$). At this time, we do not consider any heterogeneity in illumination intensity $\left({g_1}^2(\vec{r}-\vec{r}')\right)$; this should be the subject of future work.

Equation (21) is expressed in terms of the factors $1/\mu_{\eta,\xi}$. Those factors are given by equation (5), which may be simplified using the following changes of variable $w = x - x'$, $\bar{w} = (x+x')/2$, $u = y - y'$, $\bar{u} = (y+y')/2$ equivalent to the triangular weight reported in the literature after Bandyopadhyay et. al. [3]. Equation (5) can thus be rewritten as:

$$\frac{1}{\mu_{\eta,\xi}} = \frac{1}{a^4} \int_{-a(1+\xi)}^{-a\xi} (a(\xi + 1) \left\{ \int_{-a(1+\eta)}^{-a\eta} g_1^2(w,u)(a(\eta+1)+w)dw - \int_{-a\eta}^{a(1-\eta)} g_1^2(w,u)(a(\eta-1)+w)dw \right\} du - \int_{-a\xi}^{a(1-\xi)} (a(\xi-1)+u) \left\{ \int_{-a(1+\eta)}^{-a\eta} g_1^2(w,u)(a(\eta+1)+w)dw - \int_{-a\eta}^{a(1-\eta)} g_1^2(w,u)(a(\eta-1)+w)dw \right\} du. \quad (22)$$

To this point, we have not made any assumptions about the shape of the correlation function $g_1^2(w,u)$. We now assume a Gaussian correlation shape:

$$g_1^2(w,u) = \left(\exp\left[-\frac{\pi}{2} \frac{(w^2+u^2)}{\pi\, b^2} \right] \right)^2 = \exp[-(w^2+u^2)/b^2], \quad (23)$$

where A_c is the correlation area and has been approximated to a circle of radius b.

Substituting equation (23) into equation (22), we arrive at the following expression for the factors $1/\mu_{\eta,\xi}$, which is equation (10) in the main texto of chapter 2:

$$\frac{1}{\mu_{\eta,\xi}} = \frac{1}{4\pi^2 M^2} \times \left(e^{-\pi M(\eta-1)^2} - 2e^{-\pi M\eta^2} + e^{-\pi M(\eta+1)^2} + \pi\sqrt{M}\left((\eta-1)Erf\left[\sqrt{\pi M}(\eta-1)\right] - 2\eta Erf\left[\sqrt{\pi M}\eta\right] + (\eta+1)Erf\left[\sqrt{\pi M}(\eta+1)\right]\right)\right) \times \left(e^{-\pi M(\xi-1)^2} - 2e^{-\pi M\xi^2} + e^{-\pi M(\xi+1)^2} + \pi\sqrt{M}\left((\xi-1)Erf\left[\sqrt{\pi M}(\xi-1)\right] - 2\xi Erf(\sqrt{\pi M}\xi) + (\xi+1)Erf\left[\sqrt{\pi M}(\xi+1)\right]\right)\right). \quad (24)$$

References

[1] S. E. Skipetrov, J. Peuser, R. Cerbino, P. Zakharov, B. Weber and F. Scheffold, "Noise in laser speckle correlation and imaging techniques," *Optics Express,* vol. 18, no. 14, pp. 14519-14534, 2010.

[2] B. Coyotl Ocelotl, J. C. Juárez Ramírez, R. Ramos García, R. Chiu, T. Spezzia Mazzocco and J. C. Ramírez San Juan, "Speckle contrast calculation based on pixels correlation: spatial analysis," in *Interferometry XIX*, San Diego, 2018.

[3] R. Bandyopadhyay, A. S. Gittings, S. S. Suh, P. K. Dixon and D. J. Durian, "Speckle-visibility spectroscopy: A tool to study time-varying dynamics," *Review of Scientific Instruments,* vol. 76, no. 9, p. 093110, 2005.

Appendix 3. Developing temporal contrast equations.

Let us consider a set of L frames with exposure time T and a delay δ in time between frames (Figure 1 in Chapter 4). As mentioned previously in this work, two frames will be considered correlated if there are no more than S frames between them.

The integrated intensity I_ψ over the exposure time T of the camera;

$$I_\psi = \frac{1}{T} \int_{\psi(T+\delta)}^{(\psi+1)T+\psi\delta} I(t)dt, \tag{1}$$

then, the mean intensity over the L frames considering $L > 0$, is;

$$i = \frac{1}{L}\sum_{\psi} I_\psi. \tag{2}$$

Let us note that when $L = 0$, there is only one frame and the calculation of the temporal contrast does not make any sense. The corresponding unbiased variance is written as;

$$c = \frac{1}{L-1}\sum_{\psi=0}^{L-1}(I_\psi - i)^2 = \frac{1}{L-1}\left(-i^2 L + \sum_{\psi=0}^{L-1} {I_\psi}^2\right). \tag{3}$$

Equation (3) is not defined for $L = 1$. Henceforth $L > 1$ is considered. Normally, at least 15 frames are used ($L = 14$).

The expected value of the variance is;

$$\langle c\rangle = \frac{1}{L-1}\left(-\langle i^2\rangle L + \sum_{\psi}\langle {I_\psi}^2\rangle\right), \tag{4}$$

where $\langle\rangle$ denotes the ensemble average. The parameter v_ψ depends on the ratio of the exposition time T and correlation time t_c and the temporal correlation between the frames 0 and ψ.

The correlation factor between two frames separated by ψ frames, denoted by $1/v_\psi$, is given by the expression;

This chapter has been send to the Journal of Biomedical Optics as the appendix of; Improved temporal speckle contrast model for slow and fast dynamic samples: effect of temporal correlation among neighboring camera pixels.

$$\frac{1}{\nu_\psi} = \frac{1}{T^2}\int_0^T \int_{\psi(T+\delta)}^{(\psi+1)T+\psi\delta} (g_2(t-t')-1)dt'\,dt = \frac{1}{T^2}\int_0^T \int_{\psi(T+\delta)}^{(\psi+1)T+\psi\delta} g_1^2(t-t')dt'\,dt. \quad (5)$$

Using equations (1) and (5) we can write $\langle I_0 I_\psi \rangle$ as;

$$\langle I_0 I_\psi \rangle = \langle I \rangle^2 \left(1 + \frac{1}{\nu_\psi}\right). \quad (6)$$

Calculating $\langle i^2 \rangle$ from equation (2) an the summation goes over the L frames considerate. Using the notation of equation (6);

$$\langle i^2 \rangle = \frac{1}{L^2}\sum_{\psi=0}^{L-1}\sum_{\psi\prime=0}^{L-1} \langle I_0, I_\psi \rangle, \quad (7)$$

In temporal correlation, there are three types of correlation. Following the notation from our previous work on the first part of our contrast model [1], we refer to them as, *central* (autocorrelation), *lateral* (in time, correlation between neighbors frames closer than S frames), and the *outsiders* (correlation between frames which are farther than S frames between the two frames considered. Then, equation (7) it may rewrite as the sum of each type of correlations, i.e.;

$$\langle i^2 \rangle = \frac{1}{L^2}\left(\sum_{central} \langle I_0, I_\psi \rangle + \sum_{lateral} \langle I_0, I_\psi \rangle + \sum_{outsiders} \langle I_0, I_\psi \rangle\right). \quad (8)$$

Let us note that, if $S = 0$, there are no lateral type correlations, only central correlation, therefore, only the first summation in (8) is not zero. Henceforth $S \geq 1$ is considerated to avoid problems with the summation index.

It is easy to see that there are L central correlation, one for each pixel of the frames considered. The lateral correlation is not so straight forward, but properly counted, it can be proved that there are $2(L-\psi)$ equivalent correlations and let $B(S)$ the number of outsider correlations;

$$\langle i^2\rangle = \frac{1}{L^2}\left(L\langle I_0 I_0\rangle + \sum_{\psi=1}^{S} 2(L-\psi)\langle I_0 I_\psi\rangle + B(S)\langle I_0 I_\psi\rangle \right). \tag{9}$$

It is possible to calculate, but it is not necessary, the number of *outsider* correlations. This can be obtained by subtracting from the total number of correlations, L^2, the total number of the other types of correlations (central and lateral), i.e;

$$\begin{aligned} B(S) &= L^2 - \left(L + \sum_{\psi=1}^{S} 2(L-\psi) \right) = L^2 - L - 2SL + S(S+1) \\ &= (L-S-1)(L-S). \end{aligned} \tag{10}$$

All of these pixels are considered uncorrelated due to the there are more than s frames between the frames, then for those pixels, $\langle \mathrm{I}_0, \mathrm{I}_\psi \rangle = \langle \mathrm{I}_0 \rangle \langle \mathrm{I}_\psi \rangle = \langle \mathrm{I} \rangle^2$ and using equation (6) and (10);

$$\langle i^2\rangle = \frac{1}{L^2}\left(L\langle I\rangle^2 \left(1+\frac{1}{\nu_0}\right) + \sum_{\psi=1}^{S} 2(L-\psi)\langle I\rangle^2 \left(1+\frac{1}{\nu_\psi}\right) + B(S)\langle I\rangle^2 \right), \tag{11}$$

factorizing $\langle I\rangle^2$ and regrouping;

$$\langle i^2\rangle = \frac{\langle I\rangle^2}{L^2}\left(L\frac{1}{\nu_0} + \sum_{\psi=1}^{S} 2(L-\psi)\frac{1}{\nu_\psi} + \left(L + \sum_{\psi=1}^{S} 2(L-\psi) \right) + B(S) \right), \tag{12}$$

cancelling the inner parenthesis with $B(S)$ using equation (10), equation (12) become;

$$\langle i^2\rangle = \frac{\langle I\rangle^2}{L^2}\left(L\frac{1}{\nu_0} + \sum_{\psi=1}^{S} 2(L-\psi)\frac{1}{\nu_\psi} + L^2 \right). \tag{13}$$

In a similar way, computing $\langle c\rangle$ (equation (4)), let us note that, the term $\langle {I_\psi}^2\rangle = \langle I_\psi I_\psi\rangle$ is equivalent to $\langle I_\psi I_\psi\rangle = \langle I_0 I_0\rangle$, and then using equation (6), equation (4) is rewritten to;

$$\langle c\rangle = \frac{1}{L-1}\left(-\langle i^2\rangle L + \sum_{\psi} \langle I\rangle^2 \left(1+\frac{1}{\nu_0}\right) \right), \tag{14}$$

simplifying the summation;

$$\langle c\rangle = \frac{1}{L-1}\left(-\langle i^2\rangle L + \langle I\rangle^2 \left(1+\frac{1}{\nu_0}\right) L \right), \tag{15}$$

Substituting $\langle i^2\rangle$ from equation (13) and factorizing $\langle I\rangle^2$;

$$\langle c\rangle = \frac{\langle I\rangle^2}{L-1}\left(-\frac{1}{L^2}\left(L\frac{1}{\nu_0} + \sum_{\psi=1}^{S} 2(L-\psi)\frac{1}{\nu_\psi} + L^2 \right) L + \left(1+\frac{1}{\nu_0}\right) L \right), \tag{16}$$

simplifying equation (16);

$$\langle c\rangle = \langle I\rangle^2\left(\frac{1}{\nu_0} - \frac{2}{L(L-1)}\sum_{\psi=1}^{S}(L-\psi)\frac{1}{\nu_\psi}\right). \tag{17}$$

Henceforth $S \geq 1$ is considered to avoid problems with the summation index. For the case of $S = 0$ there are only autocorrelation, which means $\langle c\rangle = \langle I\rangle^2/\nu_0$, and therefore $K_t^2(x, L, 0) = \frac{1}{\nu_0}$. As final step, dividing $\langle c\rangle$ by $\langle I\rangle^2$ to calculate the temporal contrast $K^2 = \langle c\rangle/\langle I\rangle^2$;

$$K_t^2(x, L, S) = \frac{1}{\nu_0} - \frac{2}{L(L-1)}\sum_{\psi=1}^{S}(L-\psi)\frac{1}{\nu_\psi}. \tag{18}$$

It is important to remark that equation (18) is an analytic expression for the temporal speckle contrast considering an arbitrary number of frames L, furthermore, an arbitrary number of correlation frames S. No consideration about the illumination shape $\left({g_1}^2(t-t')\right)$ has been taken so far.

The temporal contrast (equation (18)) is in terms of the factors $1/\nu_\psi$. Those factors are given by equation (5) , which may be simplified using the change of variable $\tau = t - t'$, $\bar{\tau} = (t + t')/2$ equivalent to the triangular weight reported in the literature after Bandyopadhyay et. al. [2], equation (5) is rewrite as;

$$\frac{1}{\nu_\psi} = \frac{1}{T^2}\left(\int_{(\psi-1)T+\psi\delta}^{\psi T+\psi\delta}(T - T\psi - \delta\psi + \tau)g_1^2(\tau)d\tau + \int_{\psi T+\psi\delta}^{(\psi+1)T+\psi\delta}(T + T\psi + \delta\psi - \tau)g_1^2(\tau)d\tau\right). \tag{19}$$

Let us note that no assumptions over $g_1^2(\tau)$ have been made so far.

Gaussian correlation

$$g_1(\tau) = \exp\left[-\frac{\pi}{2}\frac{\tau^2}{{t_c}^2}\right] \tag{20}$$

The expression (20) satisfied the Mandel´s definition of the correlation time t_c (21);

$$t_c = \int_{-\infty}^{\infty}\left|g_1(\tau)\right|^2 d\tau. \tag{21}$$

The integration on equation (19) it is straight forward (but not quick) substituting equation (20);

$$\frac{1}{\nu_\psi} = \frac{1}{2x}\{\left(\mathrm{erf}\left[\sqrt{\pi}(\psi+\psi\Delta)x\right] - \mathrm{erf}\left[\sqrt{\pi}(\psi-1+\psi\Delta)x\right]\right)(1-\psi-\psi\Delta) + \left(\mathrm{erf}\left[\sqrt{\pi}(\psi+1+\psi\Delta)x\right] - \mathrm{erf}\left[\sqrt{\pi}(\psi+\psi\Delta)x\right]\right)(1+\psi+\psi\Delta)\} + \frac{1}{2\pi x^2}(\exp[-\pi(\psi-1+\psi\Delta)^2x^2] - 2\exp[-\pi(\psi+\psi\Delta)^2x^2] + \exp[-\pi(\psi+1+\psi\Delta)^2x^2]), \quad (22)$$

where $\Delta = \delta/T$ and $x = T/\tau_c$.

Lorentzian correlation

$$g_1(\tau) = \exp\left[-\frac{|\tau|}{t_c}\right] \quad (23)$$

The expression (23) satisfied the Mandel´s definition of the correlation time (21)

Due to the absolute value, it is necessary to be careful with the limits on the integrals of equation (19);

$$\begin{aligned} l_1 &= (\psi-1)T + \psi\delta, \\ l_2 &= \psi T + \psi\delta, \\ l_3 &= (\psi+1)T + \psi\delta, \end{aligned} \quad (24)$$

T and δ are times, therefore, there are always positive, and $\psi \in \mathbb{N}$, then $l_2, l_3 > 0$ for all T, δ, ψ. Only l_1 could be negative when $\psi < 1 \Rightarrow \psi = 0$. For this reason, equation (19) is solved and the solution is presented in two cases, for $\psi = 0$ and $\psi > 0$.

For $\psi = 0$;

$$\frac{1}{\nu_0} = \frac{1}{2x^2}(2x + \exp[-2x] - 1). \quad (25)$$

For $\psi > 0$;

$$\frac{1}{\nu_\psi} = \frac{1}{4x^2}\left(-2\exp[-2(\psi+\psi\Delta)x] + \exp[-2\left((\psi-1)+\psi\Delta\right)x] + \exp[-2\left((\psi+1)+\psi\Delta\right)x]\right), \quad (26)$$

where $\Delta = \delta/T$ and $x = T/\tau_c$.

References

[1] J. C. Juarez-Ramirez, B. Coyotl-Ocelotl, B. Choi, R. Ramos-Garcia, T. Spezzia-Mazzocco and J. C. Ramirez-San-Juan, "Improved spatial speckle contrast model for tissue blood flow imaging: effects of spatial correlation among neighboring camera pixels," *Journal of Biomedical Optics,* vol. 28, no. 12, pp. 1-15, 2023.

[2] R. Bandyopadhyay, A. S. Gittings, S. S. Suh, P. K. Dixon and D. J. Durian, "Speckle-visibility spectroscopy: A tool to study time-varying dynamics," *Review of Scientific Instruments,* vol. 76, no. 9, p. 093110, 2005.